# Study of High-Pressure Glow Discharges Generated by Micro-Structured Electrode (MSE) Arrays

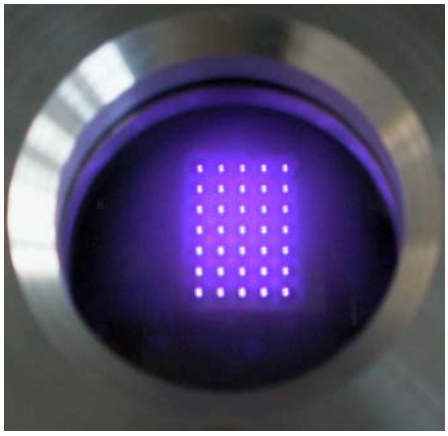

**Maria Cristina Penache**

# Study of High-Pressure Glow Discharges Generated by Micro-Structured Electrode (MSE) Arrays

Dissertation
zur Erlangung des Doktorgrades
der Naturwissenschaften

vorgelegt beim Fachbereich Physik
der Johann Wolfgang Goethe - Universität
in Frankfurt am Main

von
Maria Cristina Penache
aus Bukarest, Rumänien

Frankfurt am Main 2002

Vom Fachbereich Physik der
Johann Wolfgang Goethe - Universität als Dissertation angenommen.

Dekan: Prof. Dr. Walter Greiner
1. Gutachter: Prof. Dr. Horst Schmidt-Böcking
2. Gutachter: Prof. Dr. Karl-Heinz Gericke
Datum der Disputation: 1. März 2002

*In the memory of my father*

# Zusammenfassung

Die Erzeugung einer selbständigen Gasentladung bei Atmosphärendruck mit einem niedrigen Energieverbrauch würde einen wichtigen Fortschritt bezüglich industrieller Anwendungen der Plasmatechnologie bedeuten. Oberflächenbearbeitung, wie Aktivierung oder Veredelung, neuartige Lichtquellen, Schadstoffreinigung sind nur einige Anwendungsgebiete [Rot-01], bei denen die Mikroentladungen bei Hochdruck eingesetzt werden können.

Der innovative Ansatz dieser Arbeit ist die Plasmaerzeugung mit Hilfe von Mikrostruktur-Elektrodensysteme (MSE). Durch die Verkleinerung der Elektrodengeometrie werden hohe elektrische Felder bei relativ niedriger Spannung (wenige 100 V) erreicht und dadurch die Bedingungen für einen Zündprozeß im Gas bei hohen Drücken (dies sind Bereiche oberhalb von 100 mbar) erfüllt. Wenn die Elektrodengeometrie in der Größenordnung von einigen 100 µm liegt, wird der Betrieb einer Gasentladung bei Atmosphärendruck mit wenigen hundert Volt Spannung möglich.

Mit Hilfe moderner Technologien (LIGA-Technik, Siebdruckverfahren und laserbasierenden Mikrostrukturierung) können heute großflächige, sehr präzise Mikroelektroden-Systeme hergestellt werden. Für diese Untersuchungen wurden dreidimensionale MSE eingesetzt, die von der Detektorenbautechnik übernommen wurden.

Auf beiden Seiten eines Isolatorträgers sind jeweils metallische Elektroden aufgebracht. In dem gesamten Mehrschichtsystem befinden sich Löcher mit einem typischen Durchmesser von einigen 100 µm. Eine REM-Aufnahme und eine schematische Darstellung von einem MSE-Loch sind in Abbildung 1a und b gezeigt. Der Abstand zwischen den Elektroden ist durch die Dicke des Isolators gegeben und liegt typischerweise in der gleichen Größenordnung (etwa 100 µm). Für Folien mit mehreren Löchern wurde der Abstand von Lochmitte zu Lochmitte (pitch) zwischen 0.14 und 3 mm variiert. In den Experimenten wurden Folien mit bis zu 200 Poren, entsprechend eine aktiven Fläche von bis zu 50x50 $mm^2$, verwendet. Die Eigenschaften der in dieser Arbeit

benutzten Mikrostrukturen sind in Tabelle 1 zusammengefaßt. Die Löcher in den ersten beiden MSE Typen (Tabelle 1) wurden geätzt, während die Löcher in den Keramiken MSE mechanisch oder mit Hilfe eines Femtosekunden-Lasers erzeugt wurden.

| Substrat | Elektroden | Isolatordicke | Elektrodendicke | Lochdurchmesser |
|---|---|---|---|---|
| Glas | Al, Cr, Pt | 300 - 350 µm | 0.7 - 1 µm | 100 - 500 µm |
| Polyimid | Cu, Cu/Ni | 50 µm | 15 - 130 µm | 70 - 300 µm |
| Aluminium Oxid | Pt, Cu/Ni | 100 - 250 µm | 25 - 200 µm | 70 - 130 µm |

**Tabelle 1:** Eigenschaften der in dieser Arbeit verwendeten Mikrostrukturen.

In dieser Arbeit wurde das Verhalten von MSE-unterstützten Entladungen in verschiedenen Geometrien in Abhängigkeit von Gasart, Gasdruck und Elektrodenmaterial durch elektrische und optische Messungen untersucht. Es konnte gezeigt werden, dass stabile nicht-filamentierende Glimmentladungen bei Gasdrücken von 50 mbar bis zu 1000 mbar betrieben werden können. Die elektrische Kennlinie entspricht typischerweise der einer normalen Glimmentladung. Ein resistives Verhalten zeigt die MSE-unterstützte Entladung nur in der Townsend-Phase bei kleiner Stromdichte.

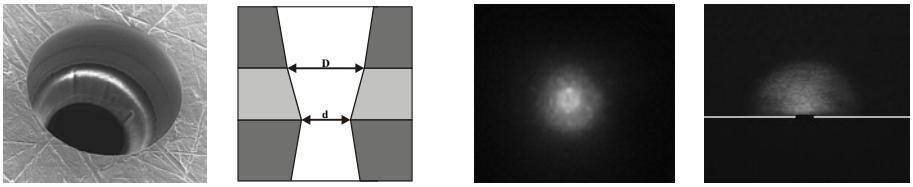


**a** **b** **c** **d**

**Abbildung 1:** REM-Aufnahme (a) und schematische Darstellung (b) von einem MSE-Loch. Optische Erscheinung einer Mikroentladung: Aufsicht (c) und Seitenansicht (d) an der Kathodenseite.

Die optische Erscheinung der Entladung ist in Abbildung 1c, Aufsicht und Abbildung 1d, Seitenansicht dargestellt. In Abbildung 1d sind die Kathodenfläche und der Lochdurchmesser eingezeichnet. Helle und dunkle Zonen wurden an der Kathodenseite beobachtet. Deren Druckabhängigkeit entspricht der einer Glimmentladung bei Niederdruck [Rai-97] in einer Hohlkathodengeometrie.

Das Plasma ist nicht nur innerhalb der Kavität der MSE konzentriert, es dehnt sich auch außerhalb des Loches aus, wie in Abbildung 1d dargestellt wird. Die Ausdehnung des Plasmas auf der Kathodenfläche nimmt mit steigendem Strom und abnehmendem Gasdruck zu und kann bis zum 10-fachen Lochdurchmesser betragen.

Die Betriebsparameter der MSE-unterstützten Entladung sind in Tabelle 2 zusammengefaßt, wobei p der Druck, $V_P$ die Plasmaspannung, I der Strom und j die Stromdichte ist. Um eine thermische Überbelastung der MSE zu verhindern, wurde der Entladungsstrom kleiner als 20 mA gehalten. Es konnte festgestellt werden, dass die Zündspannung vom Elektrodenabstand abhängt, während für den Betrieb der Entladung der Lochdurchmesser der entscheidende Parameter ist.

| Gasart | p (mbar) | $V_P$ (V) | I (mA/Loch) | j (A/cm$^2$) |
|---|---|---|---|---|
| Ar; He; Ne; Luft; Ar/Luft; Ar, He /NO; Ar, He/$N_2$; Ar/$CCl_2F_2$ | 50-1000 | 140-270 | 0.05-20 | 0.6-120 |

**Tabelle 2:** Betriebsparameter der MSE-unterstützten Entladung.

Zusammendfassend ist festzustellen, dass die MSE-unterstützte Entladung eine normale Glimmentladung darstellt, wobei Anregungs- und Ionizationsprozesse durch die spezielle verwendete Entladungsgeometrie (Hohlstruktur) sehr effizient stattfinden.

Für eine eventuelle Anwendung stellt sich die Frage, in wie weit sich diese Erkenntnisse auf mehrere parallel brennende Entladungen übertragen lassen. Das Ziel ist, mit Hilfe einer regulären Matrix von Mikroentladungen ein großflächiges stabiles Plasma zu erzeugen. Dieser Parallelbetrieb mehrerer individueller Entladungen stellt allerdings höchste Anforderungen an die Homogenität und Genauigkeit der einzelnen Löcher. Ohne elektrische Entkopplung konnten bei maximal 300 mbar in Ar und Ar-Luft Gasgemisch bis zu 200 parallel brennende Mikroentladungen betrieben werden. Bei höherem Druck ist die elektrische Entkopplung der Mikroentladungen notwendig. Die Entkopplung kann mit in der Mikrostruktur integrierten passiven Vorwiderständen erreicht werden. Basierend auf solchen Mikrostrukturen konnte der Druckbereich für den Parallelbetrieb bis zum Atmosphärendruck erweitert werden. Der Nachteil dieser Methode liegt in dem hohen

Energieverlust im Vorwiderstand. In Zukunft ist eine Entkopplung durch aktive Bauelementen (z.B. Transistoren) vorgesehen.

Der Schwerpunkt der vorliegenden Arbeit liegt in der Charakterisierung der MSE-unterstützten Entladung mittels Emission- und Absorptionsspektroskopie. Hierzu wurden Messungen zur Bestimmung der Plasmaparameter wie Gastemperatur, Elektronen-temperatur, Elektronendichte und Dichte der angeregte Atomen durchgeführt.

Emissionsspektroskopie kann zur Messung der intrinsischen Parameter der Entladung verwendet werden, vorausgesetzt die Energieverteilungen der Elektronen und der schweren Teilchen sind thermisch (Maxwell) [Hut-87]. Die Elektronentemperatur (elektronische Verteilungstemperatur) wurde in dieser Arbeit aus dem Vergleich von atomaren und ionischen Linienintensitäten bestimmt. In einem stoßdominierten Plasma kann diese Methode eingesetzt werden, auch wenn kein Gleichgewicht zwischen alle Komponenten herrscht. Die in diesem Experiment gemessene Elektronentemperatur beträgt etwa 0.8 eV bei 500 mbar. Es ist zu erwarten, dass durch die Hohlkathodengeometrie die elektronische Energieverteilung von einer thermischen (Maxwell) Verteilung abweicht und einen höheren Anteil an hochenergetischen Elektronen besitzt.

Um die Gastemperatur zu bestimmen, wurde die Populationsverteilung der Rotationszustände der Stickstoffbanden des zweiten positiven Systems, dem $N_2(C^3\Pi_u)\rightarrow N_2(B^3\Pi_g)$ Übergang, und des ersten negativen Systems, dem $N_2^+(B^2\Sigma_u^+)\rightarrow N_2^+(X^2\Sigma_g^+)$ Übergang, verwendet. Der Translation-Rotation Energietransfer ist sehr effektiv und findet sehr schnell statt, die Rotationszustände erreichen in kurzer Zeit eine Gleichgewichtverteilung bei einer Temperatur nahe der Neutralgastemperatur [Bib-87]. Infolge der sehr kurzen Relaxationszeit für Rotation (wenige Nanosekunden für den Hochdruckbereich) entspricht die Verteilung über die Rotationszustände mit hoher Wahrscheinlichkeit der kinetischen Temperatur des neutralen Gases.

Der $N_2(C^3\Pi_u)$-Zustand kann durch direkte Anregung in Stößen mit schnellen Elektronen oder durch die so genannte „Pooling-Reaktion“ zwischen zwei langlebigen $N_2$-Molekülen im metastabilen $N_2(A^3\Sigma_u^+)$-Zustand erzeugt werden, wobei die zweite Reaktion dominiert. Diese Reaktion kann im Umgebungsgas stattfinden, weil die metastabilen $N_2$-Moleküle aufgrund der langen Lebensdauer über größere Distanzen diffundieren können. Folglich entspricht die mit Hilfe des $N_2(C^3\Pi_u)\rightarrow N_2(B^3\Pi_g)$

Übergangs gemessene Temperatur im wesentlichen der Umgebungsgastemperatur und nur zu einem geringen Anteil der in der Entladungszone herrschenden Temperatur.

Die mit Hilfe des $N_2^+(B^2\Sigma_u^+) \rightarrow N_2^+(X^2\Sigma_g^+)$ Übergangs ermittelte Temperatur ist deutlich höher und entspricht der Gastemperatur der Entladung. Die Auswertung der Rotationsverteilung kann durch zwei Temperaturen beschrieben werden. Der Grund dafür kann die nicht vollendete Relaxation der hochliegenden Rotationszustände sein. Dieses Ergebnis kann auch durch den Anregungsmechanismus des höheren angeregten Zustands $N_2^+(B^2\Sigma_u^+)$ erklärt werden. Der $N_2^+(B^2\Sigma_u^+)$-Zustand kann sowohl in der inneren Entladungzone durch Stöße mit molekularen Ionen, als auch außerhalb dieser Zone durch Stöße mit metastabilen Edelgasatomen (Penningionization) angeregt werden. Es konnte festgestellt werden, dass die Temperatur des Umgebungsgases nur leicht oberhalb der Raumtemperatur liegt, während die Gastemperatur in der Entladungszone deutlich höher ist.

Die Vibrationszustände befinden sich in einer „Quasiverteilung“ bei einer charakteristischen Temperatur $T_v$. Diese Vibrationstemperatur wurde aus dem Vergleich der Intensität der Bandenköpfe gemessen und liegt im Bereich von 2000 K. Die vibronischen Relaxationszeiten liegen bei den experimentellen Bedingungen hier in der Größenordnung von 100 ns bis 1 µs, während die Lebensdauer der angeregten Zustände ns beträgt. Das bedeutet, dass die Vibration nicht völlig relaxiert ist und die gemessene Temperatur als Anregungstemperatur zu verstehen ist. Diese Temperatur ist durch die chemischen Prozesse im Plasma gegeben und entspricht weder der Gastemperatur noch der Elektronentemperatur.

Die Anwendung der Laserdioden-unterstützten Absorptionsspektroskopie [Dem-96] für die Untersuchung der MSE initiierte Entladung ist ein sehr innovativer Ansatz. Zwar gehört diese Methode zu den Standardverfahren der Plasmadiagnose für Niederdruck Gasentladungen, sie wird aber im Hochdruckbereich nur selten benutzt. Weiterhin ist die Anwendung dieses Verfahrens an Entladungen mit Abmessungen im Submillimeter-Bereich nicht trivial. Probleme sind hierbei die sehr kurze Absorptionslänge, Beugungseffekte an der Mikrostruktur und mögliche Linseneffekte aufgrund der hohen Gastemperatur in der Entladungszone. Die hohe Dichte der angeregte Atomen in der Mikroentladung ermöglichte es, diese Technik zu benutzen, trotz der sehr kleinen Absorptionslänge von weniger als 2 mm.

Die Untersuchungen wurden an Ar im Druckbereich 50-400 mbar bei einer mit konstantem Strom (0.5 mA) betriebenen Mikroentladung durchgeführt. Mit dieser Methode wurde die absolute Dichte der angeregten Atome für metastabile und resonante Zustände ($1s_i$, i = 2÷5 in Paschen Notation) gemessen, sowie auch die Gastemperatur in der Entladung und die Elektronendichte in der Kavität der Mikrostruktur. Die Verteilung der angeregten Atome außerhalb des Loches an der Kathodenseite wurde durch ortsaufgelöste Messungen parallel zu der Elektrodenoberfläche ermittelt. Es konnte gezeigt werden, dass die Atome in metastabilen Zuständen und die in resonanten Zuständen eine ähnliche Ortsverteilung zeigen, wahrscheinlich aufgrund der starken „Stoßkopplung“ der benachbarten Zustände bei hohen Drücken. Die MSE-unterstützten Entladungen zeigen eine hohe Dichte angeregter Atome, die im Bereich von $10^{13}$ $cm^{-3}$ liegt.

Aus der Messung von Linienprofilen in Plasmen kann man sehr detaillierte Information über die Plasmaeigenschaften wie Elektronen- und Ionendichte sowie die zugehörigen Temperaturen gewinnen [Gri-97]. Die in dieser Arbeit ermittelten Plasmaparameter sind in Tabelle 3 dargestellt.

| Gasart | p (mbar) | $n_{m,r}$ ($cm^{-3}$) | $n_e$ ($cm^{-3}$) | $T_e$ (eV) | $T_g$ (K) |
|---|---|---|---|---|---|
| Ar | 50 → 400 | $10^{12} \rightarrow 2 \cdot 10^{13}$ | $8 \cdot 10^{14} \rightarrow 5 \cdot 10^{15}$ | ~ 0.8 | 380 → 1100 |

**Tabelle 3:** Plasmaparameter, wobei $n_{m,r}$ die Dichte der angeregten Atome in metastabilen und resonanten Zustände, $n_e$ die Elektronendichte, $T_e$ die Elektronentemperatur und $T_g$ die Gastemperatur in der Entladungszone bedeuten.

Die Gastemperatur wurde aus der Doppler-Verbreiterung von atomaren Linien ermittelt. Da diese Methode direkt mit der translatorischen Bewegung der Emitter zusammen hängt, entspricht die gemessene Temperatur der Gastemperatur. Die Gastemperatur steigt linear mit dem Druck von ca. 380 K bei 50 mbar bis auf maximal 1100 K bei 400 mbar an. Die gemessene Gastemperatur entspricht der Temperatur in der Kavität der MSE. Die Erhöhung der Gastemperatur mit dem Gasdruck ist zu erwarten, da sich die Entladung immer mehr im Loch konzentriert und entsprechend die Leistungsdichte ansteigt. Aus den Emissions- und Absorptionsmessungen konnte gezeigt werden, dass die Temperatur lokal in der inneren Region des Loches bis zu 1000 K

steigen kann, während die Temperatur des Umgebungsgases nur leicht oberhalb der Raumtemperatur liegt.

Wegen der langreichweitigen Coulomb-Kräfte zwischen geladenen Teilchen sind Druckverbreiterung und Verschiebung der Spektrallinien groß im Plasma. Für nicht wasserstoffähnliche Atome (Ar im vorliegenden Fall) werden beide Effekte durch den quadratischen Stark-Effekt bei der Wechselwirkung zwischen den geladenen Teilchen beschrieben. Im Hochdruckbereich spielen die Stoßverbreiterung und -verschiebung auch eine wichtige Rolle und deren Einfluß auf die totale Linienbreite muss subtrahiert werden. Aufgrund des sehr hohen Auflösungsvermögens der Laserdiode (typischerweise 10 bis 100 MHz) kann die Apparatebreite vernachlässigt werden.

Die experimentell ermittelten Elektronendichten liegen zwischen $8 \cdot 10^{14}$ $cm^{-3}$ bei 50 mbar Druck und $5 \cdot 10^{15}$ $cm^{-3}$ bei 400 mbar. Bei konstantem Strom (0.5 mA) steigt die Elektronendichte mit dem Gasdruck. Die Anwendung dieser Methode bis zum Atmosphärendruck hat gezeigt, dass in MSE Plasma Elektronendichten bis zu $10^{16}$ $cm^{-3}$ erreicht werden können.

In vielen Anwendungen sind die im Plasma erzeugten freien Radikale und angeregten Atome wichtiger als die Elektronen und Ionen selbst. Aufgrund der hohen Dichte und der extrem schnellen Chemie der freien Radikale bei Hochdruck können große chemische Aufbau- und Abbauraten erreicht werden. Zudem ist eine sehr schnelle Behandlung von Oberflächen möglich. Die Reaktivität der Entladung wurde bezüglich Oberflächenmodifizierung und Gasreinigung untersucht. Die bisher erzielten Ergebnisse sind so vielversprechend, dass eine weitere Optimierung der MSE erstrebenswert ist.

Im Betrieb der MSE, vor allem bei hohen Drucken, zeigten sich Alterungsprozesse der Strukturen, die mit Hilfe von REM Aufnahmen und EDX Analysen untersucht wurden. Diese Effekte sind bei den Mikrostrukturen auf Polyimid Basis und mit Kupfer Elektroden sehr ausgeprägt. Die Alterungseffekte sind deutlich reduziert wenn man den Polyimid Isolator durch Aluminiumoxid-Keramik und die Kupfer Elektroden durch Platinum oder Wolfram ersetzt.

Die MSE-unterstützte Entladung liefert ein Nichtgleichgewichtsplasma das bei Hochdruck betrieben werden kann. Der Hauptvorteil des Hochdruckbetriebs ist die hohe Dichte an angeregten neutralen Atomen, freien Radikalen, Ionen und Elektronen. Außerdem ist eine Hochvakuumapparatur nicht notwendig. Die Eigenschaften der MSE-

unterstützten Entladung empfehlen diese Plasmaquelle für industrielle Anwendungen wie Oberflächenmodifizierung, Schadstoffreinigung oder neuartige Lichtquellen für den sichtbaren und UV Bereich. Für eine großtechnische Anwendung sind aber noch viele technologische Aspekte zu untersuchen, wie zum Beispiel die Reproduzierbarkeit und Langzeitstabilität der Entladung und schließlich die Skalierbarkeit der Mikrostrukturen zu großen Flächen.

**Literatur**


[Bib-87] L. M. Biberman, G. E. Norman, K. N. Ulyanov, *"Kinetics of non-equilibrium low-temperature plasmas"*, Consultants Bureau, New York (1987).

[Dem-96] W. Demtröder, „*Laser spectroscopy"*, Springer Verlag, Berlin (1996).

[Gri-97] H. R. Griem, *„Principles of plasma spectroscopy"*, Cambridge University Press, Cambridge (1997).

[Hut-87] I. H. Hutchinson, *„Principles of plasma diagnostics"*, Cambridge University Press, New York (1987).

[Rai-97] Yu. P. Raizer, „*Gas discharge physics"*, Springer Verlag, Berlin (1997).

[Rot-01] J. Reece Roth, "*Industrial plasma engineering: Applications to nonthermal plasma processing"*, Institute of Physics Publishing, Bristol (2001).

# ABSTRACT

This thesis is devoted to the study of Micro Structured Electrode (MSE) sustained discharges. Innovative approaches in this work are i) the implementation of MSE arrays for high-pressure plasma generation and ii) the use of diode laser atomic absorption spectroscopy for investigating sub-millimetric discharges.

By means of MSE arrays the discharge gap is scaled down to the sub-millimetric range and accordingly the working pressure could be increased up to atmospheric. It should be underlined that besides the ease of use, since expensive vacuum equipment is not required, high-pressure discharges offer also a high density of active species. A MSE consists of holes, regularly distributed in a composite sheet made of two metal layers separated by an insulator. The electrodes and insulator thickness and the diameter of the holes are in the 100 μm range. Based on these microstructures stable non-filamentary DC discharges are generated in noble gases and gas mixtures at pressures up to 1000 mbar. The MSE sustained discharge can be considered as a normal glow discharge whereby the excitation and ionization efficiency is increased by the specific electrode configuration (hollow cathode geometry). Large area high-pressure plasma can be achieved by parallel operation of a large number of microdischarges. Parallel operation of up to 200 microdischarges without individual ballast was proven for pressures up to 300 mbar. Furthermore, arrays of resistively decoupled microdischarges were operated up to atmospheric pressure. Spectral investigations have revealed the presence of highly energetic electrons (20 eV), a large density of atoms in metastable states ($10^{13}$ $cm^{-3}$) and a high electron density ($10^{15}$ $cm^{-3}$). Although the plasma confined inside the hole of the MSE may reach gas temperatures up to 1000 K, the ambient gas temperature immediately above the microstructure exceeds only slightly the room temperature. The reactivity of the MSE sustained discharge was demonstrated in respect to waste gas decomposition and surface treatment.

The MSE arrays are providing a non-equilibrium high-pressure plasma, which is very promising for surface processing, plasma chemistry and generation of UV radiation.

# CONTENTS

# CHAPTER 1
# INTRODUCTION

Plasma sources operating close to atmospheric pressure are very useful tools for atomic emission spectrometry, surface treatment, reduction of pollutants, and generation of UV radiation. Besides the ease of use, since expensive vacuum equipment is not required, high-pressure discharges offer also a high density of active species. In many applications the free radicals generated in the plasma are more important than electrons and ions.

High-pressure plasmas have been intensively studied in the last years in various configurations using different types of excitation from direct current or low frequency alternative current to radio frequency or microwave. The increased interest in DC and pulsed corona discharges [Gol-78], dielectric barrier discharges [Oka-93], [Kog-97], micro hollow cathode discharges [Fra-97], [Shi-99], radio frequency [Mil-99] and microwave discharges [Bil-00] is due to the fact that for applications on industrial scale it is very important to achieve reliable high-pressure operation employing moderate voltages. Using Micro-Structured-Electrode (MSE) arrays with discharge gap of hundreds of μm atmospheric pressure plasma can be generated at forward voltage of few hundreds volts. Based on MSE, stable homogeneous DC glow discharges can be operated in air, noble gases and mixtures containing reactive gases at pressures ranging from 50 to 1000 mbar [Ger-96], [Rot-98], [Pen-00], [Brä-00]. Intrinsic properties of this new plasma source are up to now not well known and the difficulty arises from the limitation in choosing diagnostics methods due to the small dimensions of the discharge (hundreds of μm).

This thesis is concerned with the study of MSE sustained discharges operating in a wide pressure range from 50 to 1000 mbar. Different configurations were studied, involving the electrodes material and design, the type of isolator spacer, the structure diameter, the filling gases, the static or in-flow operation and the use of one or many microstructures simultaneously.

The MSE sustained discharge was investigated from the physical point of view in respect with two main aspects: i) the electrical parameters, resulting from the well-known voltage-current characteristics, and ii) the plasma parameters like gas temperature, electron density, excited atom density, derived from spectral measurements involving emission and absorption spectroscopy.

The first chapter gives a short introduction in the field of discharges operating close to atmospheric pressure and their applications.

The second chapter describes the breakdown process at moderate and high pressures and the main mechanisms for generating a controllable, self-sustained discharge. It has to be underlined that at high pressures, additionally to the secondary electron emission by electron impact, photons, metastable atoms and UV radiation may significantly contribute to the electron multiplication and ignition of the discharge. Different MSE designs developed and improved in time are briefly described and a typical electric field distribution on a MSE is illustrated.

The generation of high-pressure DC discharges by means of MSE arrays is discussed in Chapter 3. Both the optical appearance and the current-voltage characteristic measured in various conditions are indicating a stable, non-filamentary glow discharge. An advantage of the specific discharge configuration is that the excitation and ionization efficiency increases due to the hollow cathode geometry. In the normal glow discharge operation a high current density could be sustained, which is one of the main properties of a hollow cathode discharge. The range of operation for single-hole discharges and for parallel operated microdischarges is discussed. The instabilities that may occur due to the high current density in the discharge area are also underlined in this section.

In this work the emphasis is placed on spectral diagnostics. Plasma parameters are derived from emission and absorption measurements performed on single-hole discharges operating in argon and helium as filling gases, as presented in Chapter 4 and 5. Emission spectroscopy is very useful in measuring the intrinsic parameters of the discharge as long as the results in the case of non-equilibrium plasma are correctly interpreted. The electron temperature was measured from the line intensity ratio of atoms with different stages of ionization, the electron density was estimated from the broadening of hydrogen Balmer line and the neutral gas temperature was calculated from the vibrational and rotational spectra of molecular nitrogen.

Chapter 5 is concerned with the investigation of a single-hole microdischarge by means of diode laser atomic absorption spectroscopy (DLAAS). The absolute population density of the excited $1s_5$, $1s_4$, $1s_3$, and $1s_2$ levels of Ar (Paschen notation) was measured, as well as the spatial distribution of these excited species above the cathode surface. The electron number density and the gas temperature were evaluated from the analysis of the absorption line profiles, taking into account the significant broadening mechanisms. The gas temperature inside the MSE hole was estimated from the Doppler broadening of the line profiles. The electron number density was calculated from the Stark broadening after extracting the collision broadening from the total pressure broadening. The shift of the central wavelength caused by the micro-fields in the plasma (Stark shift) was used to check the results obtained using the broadening of the line profiles. This kind of measurements was performed for the first time on a high-pressure small size discharge and the results are very useful for further applications.

The high-pressure operation of the MSE discharge in the non-filamentary glow regime makes this plasma source very attractive for surface processing. Polymer films were treated in argon-oxygen mixtures and it was demonstrated that a permanent surface modification could be induced. Due to its relatively high electron density, the discharge can be also used for waste gas treatment and this application was proved by the decomposition of $NO_x$ compounds and freon molecules.

The aim of this thesis is to point out two main aspects: first the basic physics of the MSE glow discharge operating up to atmospheric pressure and second, the potential applications recommended by its characteristics.

# CHAPTER 2
# MICRO-STRUCTURED ELECTRODE (MSE) ARRAYS

## Introduction

The main idea for using Micro-Structured Electrode (MSE) arrays is to enhance locally the electric field when a potential difference is applied on the electrodes. When the MSE is placed is a gaseous medium, in the high field regions free electrons can be amplified in an avalanche process. This is the reason why microstructures are currently used as electrode devices in position sensitive gas detectors, when a high gain is needed. They are usually operated in the regime where the output signal is proportional to the number of incoming charged particles. When the external electric field exceeds a threshold value, the charge multiplication develops exponentially and a gas discharge is ignited. Secondary electrons are released also from the cathode surface, not only in the gas volume. If the voltage is further increased, the external source of ionizing particle is not anymore necessary for the sustenance of the current and a self-sustained discharge occurs. The ignition of a discharge is avoided as much as possible in gas detectors. On the contrary, in our study the MSE arrays are used as plasma sources operated at high-pressures.

## 2.1. Gas breakdown at moderate and high pressures

The breakdown can be defined as the transformation of a non-conductive medium into a conductive one, when a sufficiently strong electric field is applied. The relation between creation and removal of charge carriers under specific conditions determines the breakdown threshold [Rai-97] and the time up to its onset. The time lag of breakdown is given by the sum of the retardation time and the formative time. The retardation time depends on the probability to have primary electrons between the electrodes that are able to start multiplication. It has a statistical spread, typical values being on the order of $10^{-5}$ - $10^{-3}$ s. The retardation time depends on the discharge geometry, e.g. in very narrow gaps it

can be up to 100 times longer that in wide gaps, at the same pressure. The formative time is the effective time to buildup the current and usually varies between $10^{-8}$ s and $10^{-4}$ s, depending on the processes responsible for electron multiplication.

In the Townsend theory of breakdown, charge carriers are produced by volume processes, described by the ionization coefficient $\alpha$, and by surface processes, characterized by the secondary emission coefficient $\gamma$. For initiating a self-sustaining discharge, one primary electron lost at the anode has to be replaced by at least one secondary electron created in the gas or at the cathode. For a homogeneous electric field the condition for self-sustenance of the discharge is given by:

$$\gamma \cdot [\exp(\alpha d) - 1] = 1 \quad \text{or} \quad \alpha d = \ln(\gamma^{-1} + 1) \tag{2.1}$$

where d is the distance between the electrodes and $\alpha$, $\gamma$ the Townsend coefficients.

The ionization coefficient $\alpha$ (first Townsend coefficient) gives the electron multiplication in the gas, i.e. the average number of ionization induced by an electron on unit length in the direction of electric field. It is a function of the reduced electric field E/p. In attachment controlled discharges the first Townsend coefficient $\alpha$ has to be replaced with $\alpha_{eff}$ given by:

$$\alpha_{eff} = \alpha - a \tag{2.2}$$

where a is the attachment coefficient also E/p dependent. This is the case for example in discharges operated in mixtures of noble gases and electronegative gases like oxygen and halogens.

The secondary emission coefficient $\gamma$ (second Townsend coefficient) describes the processes that take place at the interface gas-cathode and represent the ratio between the secondary electrons released per incident particle on the cathode surface. It depends on the material of the cathode, the gas and the reduced electric field E/p. The effective secondary electron emission coefficient covers the effect of ions ($\gamma_i$), fast neutrals especially metastable atoms ($\gamma_m$) and photons ($\gamma_p$), and can be written as [Eng-83]:

$$\gamma = \gamma_i + \gamma_m + \gamma_p \tag{2.3}$$

At low pressures the secondary electrons production is mostly caused by ions impinging the cathode surface, while at high pressures besides the secondary electron emission by ion impact, the metastable atoms and photons are playing an important role. Additionally, the space charge ($\sigma$) can enhance the electron multiplication by distorting

local the electric field. The space charge effects are described by a coefficient σ similar with the Townsend coefficients α and γ.

Taking into account that both α and γ depend on the reduced electric field E/p, the breakdown voltage (ignition potential) can be analytically deduced as [Eng-65]:

$$V_B = \frac{B \cdot pd}{\ln(pd) + \ln(A/\ln(1+\gamma^{-1}))} \tag{2.4}$$

where A and B are experimentally determined constants for a given gas.

Experimentally it was shown that Eq. 2.4 holds near and not too far above the minimum. The dependence of the breakdown voltage on the product between electrode distance and gas pressure is depicted by the so-called Paschen curves. In Fig. 2.1 are presented experimentally measured Paschen curves for some common gases.

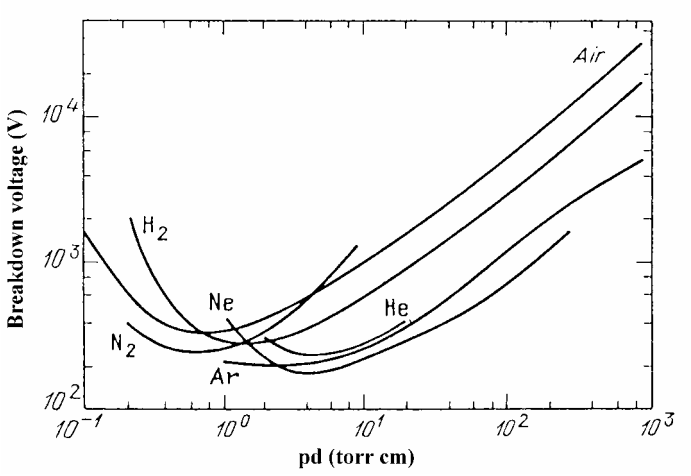


**Figure 2.1:** Paschen curves in various gases from [Rai-97].

On the right-hand side of the Paschen curve the breakdown voltage increases almost proportionally with pd. This happens because for relatively large pd (elevated pressures and large gaps) the probability that an electron produces ionization is very high, even at moderate reduced electric field E/p. On the left-hand side the breakdown voltage rises steeply as pd decreases. For small pd (low density of neutrals and short gaps) the possibilities for ionizing collisions are very limited and a very strong field is required to achieve the necessary amplification. Hence the breakdown voltage exhibits a minimum where the ionizing capability of electrons is at maximum. It can be said that around the

minimum the conditions for breakdown are the most favorable because the conditions for multiplication are optimal. Paschen curves like those presented in Fig. 2.1 are experimentally measured for planar electrode geometry, relatively low pressures and usually atomic clean electrode surface and therefore they can be used in particular situations only as a guide line.

Some aspects regarding the breakdown process and its description by a classical Paschen curve have to be further discussed. If the electrode gap is not too large and the electric field is homogeneous, the Townsend mechanism dominates even at high pressures, for pd values up to about 1000 torr·cm. For large gaps and high pressures a strongly conductive channel is formed, responsible for the breakdown being the spark mechanism [Rai-97]. For the other extreme case, i.e. very narrow gaps the required threshold voltage increase not so steeply as predicted by Eq. 2.4. The electric field can be locally enhanced in the vicinity of microscopic protrusions and electrons can be released by field emission. As well, when the cathode is sputtered by fast particles accelerated by the field the ionization takes place in the metal vapors, which requires smaller field strength.

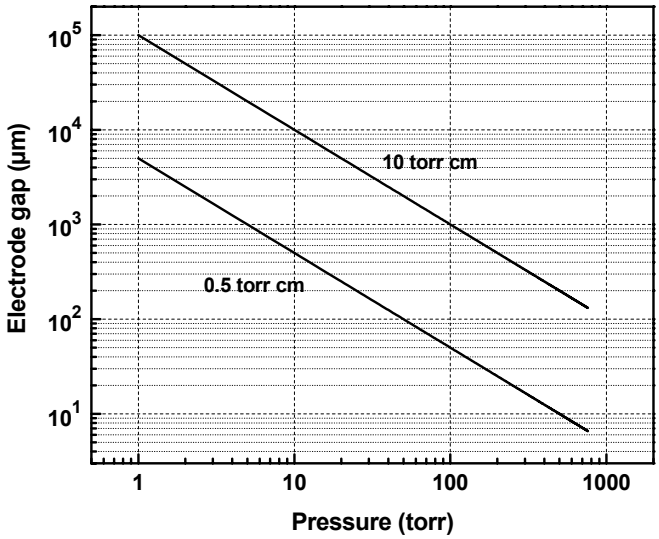


**Figure 2.2:** Electrode gap as a function of pressure at constant pd.

The values of the $V_{min}$, respectively $(pd)_{min}$ are dependent on the gas ($\alpha$) and the cathode material ($\gamma$). From Fig. 2.1 it can be concluded that in noble gases and air for

copper electrodes the voltage required for breakdown is less than 500 V at pd ranging from 0.5 to 10 torr·cm.

For high-pressure operation, the electric field necessary to induce breakdown can be achieved by increasing the applied voltage, or by reducing the dimensions between the electrodes. The use of moderate voltages will offer an advantage in respect to potential applications. Supposing a Townsend breakdown mechanism, a way to generate high-pressure plasma is to apply the scaling law *pd = constant*. This dependence is plotted in Fig. 2.2 for values of the product pd corresponding to the minimum ignition potential. In order to produce breakdown at atmospheric pressure at moderate applied voltage, the distance between the electrodes has to be about hundred of μm.

Like already said, the Townsend theory applies to homogeneous electric field and moderate pd values. For other discharge geometry is advisable to check the degree of homogeneity of the field and to investigate the role of other processes, like field emission, which are not included in this description. Therefore, the static field distribution as well the range of values for the electric field has to be known. These aspects will be discussed in the following section for the discharge geometry used in our measurements.

## 2.2. Electric field modeling

The MSE discharge geometry differs from the planar electrode geometry discussed up to now and the real electric field distribution has to be calculated. Furthermore, it is expected that due to the sub-millimeter dimensions of the MSE, very high electric field can be locally achieved. Electric field computation for diverse MSE geometry has been carried out using commercial simulation software (MAFIA 4022). MAFIA stands for Maxwell Equations by the Finite Integration Algorithm [Cst-01]. It is a complex code that simulates electromagnetic fields ranging from static up to high frequencies, but for our purpose only the static field module has been used.

In the first step a grid is created that describes the geometry in which the electric field will be applied and than the potential difference and the electrical characteristics (dielectric constant) of the medium are defined. Based on the discrete grid, the Maxwell equations are solved in each point and the solution displayed in a graphical form. An

example of static field distribution in a MSE is presented in Fig. 2.3 (cross view). A detailed description of different types of microstructures will follow in section 2.3.

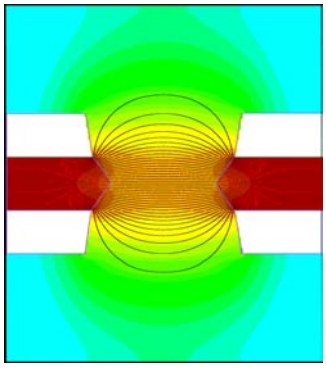

**Figure 2.3:** Transversal cross-section through a MSE and static electric field distribution.

The electric field is described by different colors (red to blue), while the black lines give the equipotential surfaces. In the middle of the hole, the static field distribution is similar to that of a plan capacitor, only the edges of the metal are enhancing locally the electric field, the maximal value being achieved at the interface insulator-electrode. The electric field is reaching maximal values up to $10^6$ V/cm in the proximity of the microelectrodes. Such high values are not necessarily indicating electron field emission as discharge mechanisms but are large enough for plasma generation at atmospheric pressure in noble gases and air.

## 2.3. Types of microstructures

Different types of Micro-Structured-Electrodes (MSE) arrays could be used: planar and three-dimensional MSE. Their designs originate in microstructures currently used in position sensitive gas detectors, and known as Gas Electron Multiplier (GEM) [Sau-96] in the case of the three dimensional MSE, respectively, Micro Strip Gas Chamber for the planar MSE (MSGC) [Oed-88]. Both have been optimized for high-pressure plasma generation. They consist either of a planar electrode system bonded to a dielectric substrate or of a regular matrix of holes perforated in a multilayer system (metal-insulator-metal). As stated before, the distance between the electrodes needs to be

around 100 µm to allow high-pressure operation. The electrodes may be identical or the dimensions of the cathode may differ from those of the anode. Both the planar and three-dimensional microstructures are schematically presented in Fig. 2.4.

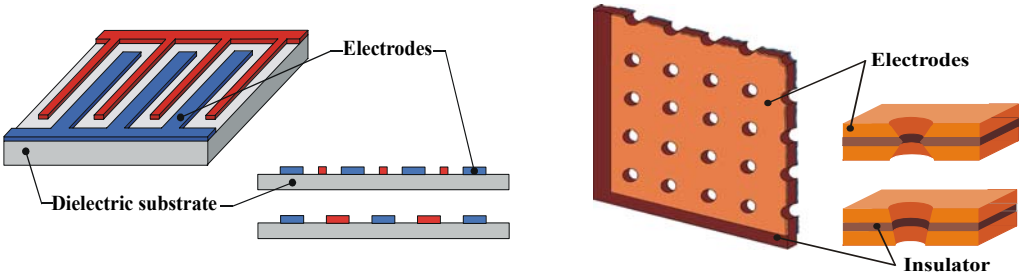


**Figure 2.4:** Planar from [Sch-01] (left) and three-dimensional (right) Micro-Structured Electrode (MSE) arrays.

This work is concerned with the investigation of the three-dimensional MSE and therefore, if not else specified the MSE notation will be further used for the three-dimensional microstructures. These structures consist of a regular matrix of holes perforated in a thin composite sheet made out of two metallic foils separated by an insulator. Each hole can be source of a microdischarge that takes place between the two metal layers representing the electrodes. The thickness of the insulator gives the distance between the electrodes. Different materials (glass, polyimide, ceramic) with thickness ranging from 50 µm to 350 µm have been used for this dielectric spacer. The electrodes are made out of diverse metals (aluminum, chromium, copper, platinum) between 0.7 µm and 200 µm thick. The opening of the holes was varied from 70 µm to 500 µm.

### 2.3.1. MSE on glass substrate

The insulator chosen for the first generation of microstructures used in our investigations was a photosensitive glass (Foturan®, Schott Glass), which enables micromachining without ablation. Foturan is a lithium-alumosilicate glass that can be structured through wet chemical etching after a suitable UV activation. The procedure will be briefly described below. By using a mask, the glass wafer is first exposed to UV

radiation (λ~300 nm). The next step in the heat treatment (T~500-600$^{o}$C), within the glass crystallizes around Ag atoms formed in the illuminated areas. The crystalline regions, when etched in a specific acid at room temperature, have an etching rate up to 20 times higher than that of the unexposed areas. The wet chemical etching can be supported by advanced etching methods (ultrasonic or spray etching) in order to obtain a high aspect ratio. Further, the metal electrodes are deposited by commonly used thin film techniques on the both sides of the structured glass wafer.

An advantage of Foturan glass is the high voltage strength. The electrical resistivity at room temperature is $8{,}1 \cdot 10^{12}$ Ω·cm and decreases with the temperature, e.g. $1{,}3 \cdot 10^{7}$ Ω·cm at 200$^{o}$C. In order to increase both the electrical resistivity and the thermal conductivity a glass ceramic can be used. This has an electrical resistivity of $5{,}6 \cdot 10^{16}$ Ω·cm at 25$^{o}$C, respectively $4{,}310^{7}$ Ω·cm at 200$^{o}$C. The thermal conductivity of the glass ceramic at room temperature is 2.73 W/mK, comparing to 1.35 W/mK for glass [Mik-01].

The manufacturing procedure allows very flexible choice of the MSE pattern. The number of the holes, their pitch and their shape can be varied.

**Figure 2.5:** Layout of MSE wafer based on glass ceramic.

For our investigations single holes and arrays of up to 200 electrically coupled holes were placed on electrically decoupled pads but on the same wafer, as it can be seen in Fig. 2.5. For reasons of mechanical stability, the smallest achievable thickness in the case of these microstructures was about 300 µm. Due to the ratio of the etching velocity in

forward to lateral direction, the minimal diameter of the holes is given by the thickness of the substrate. For the above-mentioned thickness, the diameter of the holes cannot be less than 100 μm. In our studies the opening of the holes was varied between 100 and 500 μm. The electrodes consist of thin (~0.7 μm) metal layers (Al, Cr, Pt) deposited at equal thickness on both sides of the glass foil. As shown in Fig. 2.6, holes with different geometry and shapes (here vertical walls) can be extremely precise manufactured by this method.

The measurements performed on these structures have shown that the shape of the hole has no effect either on the breakdown mechanism, or on the discharge operation. Regarding the geometry of the holes only the aspect ratio (length/diameter) plays an important role.

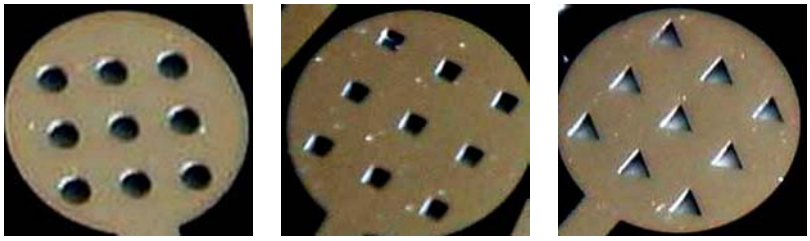

**Figure 2.6:** Microstructures based on glass substrate.

The disadvantages of this MSE type are related both to the electrodes and the substrate. The glass substrate has a relatively low thermal conductivity and there is a limitation in choosing the distance between the electrodes to at least 300 μm. The electrodes, which are very thin, are local strongly sputtered in DC operation at high-pressures, a process that in time leads to the destruction of the microstructure. For all of these reasons another insulator spacer was chosen, but still keeping the advantages offered by photolithography.

### 2.3.2. MSE on polyimide films

For this generation of microstructures the insulator is a 50 μm thick polyimide foil (Kapton® Type HN, DuPont) which can be chemically etched in a specific solvent. The polyimide foil is covered on both sides with a copper layer creating the metal-insulator-

metal system needed for our studies. A thin (0.1 μm) chromium film is used to ensure a good adhesion of copper on the insulator. In the case of Kapton, the electrical resistivity measured at 25°C and 50% relative humidity is $1.5 \cdot 10^{17}$ Ω·cm and decreases with temperature to $4.8 \cdot 10^{13}$ Ω·cm at 200°C. Its thermal conductivity at room temperature is rather poor and amounts 0.12 W/mK [Dup-01].

The holes are manufactured by chemical etching after photolithographic patterning [Hoc-98], a procedure similar to the one used for printed circuit boards. Two identical masks with the desired pattern are realized by computer assisted laser photo composer and are optically aligned with very high accuracy. The raw material (copper clad Kapton) previously coated with a thin film of photosensitive resin is inserted between the two masks and the whole system is exposed to UV light. The desired pattern (regular matrix of holes in our case) is engraved on both sides of the sheet. By using conventional acids the metal is removed. To etch the polyimide film, the sheet is immersed in a specific organic solvent, the engraved pattern in copper serving as mask. Further the foil is cleaned from all aggressive liquids and dried.

The electrode thickness (initially 5 μm) was increased up to 130 μm by copper electro-deposition. The manufacturing procedure is well established for multilayers Cu-Kapton, which implies that Cu electrodes have to be used, even if other material would offer some advantages. The spacing between holes (pitch) was varied from 0.14 to 3 mm. For most of the experiments it was chosen 3 mm in order to enable the observation of individual discharges and to reduce the thermal stress on the MSE when operating at high current densities. When needed, the manufacturing procedure allows high density of holes as well. The holes have typically diameters of 70 to 300 μm. Due to the manufacturing process described above (etching from both sides) the shape of the holes is double conical (see Fig. 2.9a). By fine-tuning of the etching parameters during the fabrication, cylindrical holes could be also obtained. A different procedure is to etch the microstructure just from one side instead of both leading, to single conical holes. Experimentally was noticed that the shape has less effect on the discharge parameters, but only regarding the lifetime of the MSE. These aspects will be discussed in detail in Chapters 3 and 7.

Single-hole structures have been studied, as well as arrays with up to 200 parallel-connected holes. The dimensions of a single-hole structure are 10x10 $mm^2$ while the active surface of a plasma module with 200 holes is 50x50 $mm^2$. For the parallel operation

of a large number of microdischarges the quality of individual holes and their reproducibility are both very important.

Microstructures with holes decoupled by individual resistors [Spi-97] have been produced using the same manufacturing technique. At a small distance from the hole, around it, the copper layer was removed up to the insulator. This channel was filled up with a resistor paste (see Fig. 2.9d). The resistor paste is basically a polymer having incorporated small metal particles. The type and amount of the resistor paste can control the value of the ballast resistor attached to each hole. The differences in the resistor value are in the range of 10%, which is good enough for parallel operation. Both the classical MSE arrays (electrically coupled holes) and the MSE with resistively decoupled holes are designed for parallel operation of large number of microdischarges and are presented in Fig. 2.7.

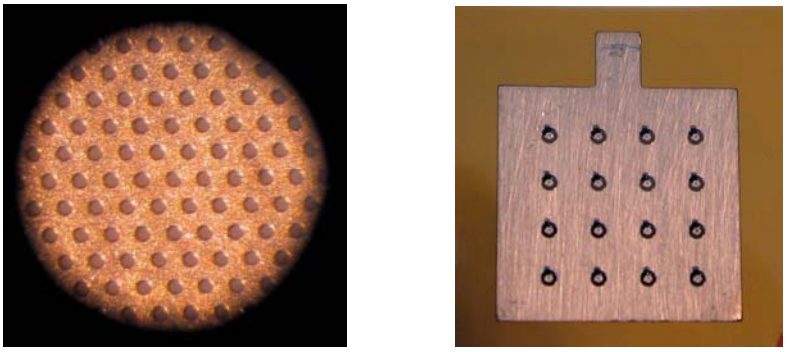

**a** **b**

**Figure 2.7:** MSE arrays of electrically coupled holes arranged at a pitch of 0.14 mm (a) and electrically decoupled holes arranged at 3 mm pitch (b).

Due to the low price and the flexibility in choosing the geometry of the array the microstructures using polyimide as dielectric spacer are appropriate for experimental studies of the discharge or for applications on laboratory scale. Industrial applications require besides the low cost also stable and reliable operation over long time. From this point of view Kapton is not the solution because does not withstand elevated temperatures and is affected by UV radiation. To this aim, the next generation of microstructures is based on ceramic as insulator.

### 2.3.3. MSE on ceramic substrate

The microstructures currently used in our investigations are based on aluminum oxide as insulator. The discharge can be successfully operated at higher pressures and current density, where both the local temperature and sputtering rates are increased. The substrate used is ceramic with 96% $Al_3O_3$ content (Rubalit®708S, CeramTec). The physical properties of interest are: electrical resistivity at room temperature of $10^{13}$ Ω·cm, decreasing slightly with the temperature ($1{,}3 \cdot 10^{12}$ Ω·cm at 200°C) and thermal conductivity of 24 W/mK at 20°C [Cer-01].

Comparing this substrate with those previously described it can be clearly seen that both the electrical resistivity and the thermal conductivity are larger, which is a clear advantage. The drawback of these structures is that the holes cannot be chemically etched, and laser or mechanical drilling is required, which implies higher costs. Basically such composite sheets can be produced either depositing a thin metal layer on a ceramic foil, or by sputtering an aluminum oxide coating on a metal foil. The commonly used deposition techniques are limited to thin films (up to about 1 μm) and therefore is difficult to have simultaneously electrodes and substrate with a thickness of about 100 μm. Using copper, the thickness of the electrodes can be increased by electro-deposition.

Diverse types of MSE using $Al_3O_3$ as insulator have been tested. The thickness of both insulator and electrodes, as well as the material of the electrodes were varied. Very robust microstructures based on Cu-$Al_3O_3$ were used, with a total thickness of 650 μm, the insulator being 250 μm thick and the electrodes 200 μm each (Fig.2.8a). The MSE is coated with a 5 μm thick Ni film for passivation. The holes are laser drilled using a high intensity ultra short pulse (fs) laser (NdYag with frequency doubling or Ti Saphire system). The diameter of the holes was chosen to be about 100 μm and their shape is usually single-conical (see Fig. 2.9c) with about 15-20% difference between the entrance and the exit side of the laser beam, but almost cylindrical holes could be also obtained when needed.

Due to its high sputtering rate, copper should be also replaced for an increased lifetime of the MSE. Materials like tantalum, tungsten or molybdenum are much stable to sputtering processes and higher temperatures. In respect to discharge operation in reactive gases, it has to be underlined that the gas mixtures commonly used for etching contain

halogens or oxygen. To operate the discharge in such gas mixture, a good choice for the electrode material would be platinum.

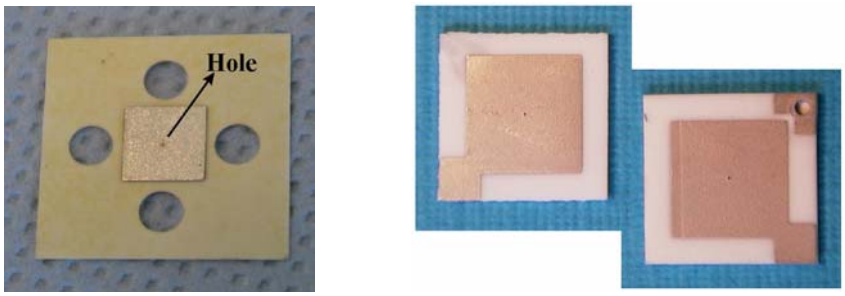


**Figure 2.8:** Single-hole MSE with ceramic substrate but different designs and material combinations: (a) Ni/Cu-$Al_3O_3$ classical multilayer and Pt-$Al_3O_3$ system with three electrodes in (b).

Microstructures based on the combination Pt-$Al_3O_3$ were already implemented. They are designed for atmospheric pressure operation and accordingly the insulator thickness and the diameter of the holes are about 100 μm. These MSE arrays are produced by a different technique. The not-sintered ceramic substrate (greentape) is first covered by a metal paste (Pt) using the so-called screen-printing technique, and then the foils are laminated at 300 K and about 3 N/mm$^2$. As the multilayer is still flexible, the holes could be mechanically drilled. Further the composite sheet is sintered at high temperature (about 1800 K), a process consisting on the burnout of the polymer binder and the sintering of the material itself. The temperature profile has to be precisely controlled in order to avoid the appearance of micro-crack and to enable an adequate densification of the material. Both the maximum thickness of the electrodes and the minimum thickness of the insulator are limited by the manufacturing procedure to about 25 μm and 100 μm, respectively.

By using this technology, composite sheets with 3 metal and 2 insulator layers could be produced, or the active surface of the electrodes could be limited by covering it with dielectric and using the so called “patch” technology to ensure electrical contact (see Fig. 2.8b right top). This makes possible the series operation of microdischarges, besides the more commonly used parallel operation.

## 2.4. Conclusions

As already discussed, different types of microstructures have been used for high-pressure plasma generation. The main characteristics of the MSE used in this study are summarized in Table 2.1.

| Substrate | Electrodes | Insulator thickness | Electrode thickness | Hole diameter |
|---|---|---|---|---|
| glass | Al, Cr, Pt | 300 - 350 µm | 0.7 - 1 µm | 100 - 500 µm |
| polyimide | Cu, Cu/Ni | 50 µm | 15 - 130 µm | 70 - 300 µm |
| alumina | Pt, Cu/Ni | 100 - 250 µm | 25 - 200 µm | 70 - 130 µm |

**Table 2.1:** Main characteristics of the microstructures used in this study.

Finally, the various types of MSE geometry used in our investigations are schematically shown in Fig. 2.9. Details about the quality of the holes, which is very important for a stable discharge operation, are obtained by means of Scanning Electron Microscopy (SEM) and are presented in Chapter 7.

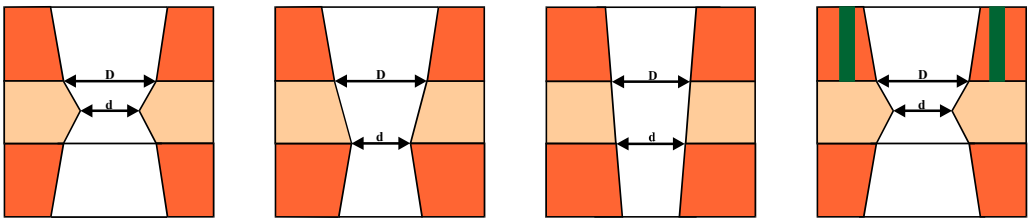


**Figure 2.9:** Schematic view of different MSE geometry.

Using MSE arrays, stable high-pressure discharges can be generated at moderate forward voltages. The pressure range investigated extends from 50 mbar to 1 bar, which corresponds to a pd of 0.2 torr·cm to 20 torr·cm in the discharge geometry used. The discharge conditions, operation parameters, optical appearance and discharge mechanisms will be discussed in the next chapter.

# CHAPTER 3
# MSE SUSTAINED DISCHARGE

## Introduction

As briefly discussed in Chapter 1, the high-pressure discharges offer real advantages upon the low-pressure plasmas. The silent discharge, which is a filamentary discharge operated at atmospheric pressure, is commonly used in industrial applications for ozone generation and production of UV radiation. The drawback of this plasma source is that the energy is concentrated in strongly conductive, statistically distributed channels (filaments). For uniform plasma treatment is desirable to have homogeneous plasma, keeping the advantage of high-pressure. The MSE are designed for high-pressure plasma generation at moderate forward voltages, but it has to be determined which kind of discharge is produced. By reducing the dimensions of the discharge gap correspondingly to the scaling law $pd = constant$ it is expected that a high-pressure glow discharge could be produced under DC excitation. This plasma should not be totally different from the low-pressure plasmas because there is now physical discontinuity from the low to moderate and high-pressure regime. The processes that sustain the ionization may be in part different or their relative importance may change with the pressure, but a Townsend mechanism for breakdown could still be valid.

Another aspect that has to be taken into account is the specific discharge geometry. The hollow cathode geometry may cause a higher excitation/ionization efficiency in respect to a conventional glow discharge with planar electrodes. The main idea for the following investigations is to understand which type of discharge is produced using MSE arrays and to define its operation range. This will be done through electrical and optical diagnostics, since the optical appearance and the electrical parameters are giving information about the mechanisms responsible for the generation and sustenance of the discharge.

## 3.1. The glow discharge

The theory of the glow discharge in the low-pressure regime was developed in the beginning of the last century and is well established. Although the high-pressure glow discharge was discovered more than 50 years ago [Eng-33] the mechanisms of its generation are still under discussion. Some aspects related to the glow discharge will be discussed in the following.

For a given discharge geometry, using a resistance in series with the discharge the current in the system can be varied and the current-voltage characteristic of an electrical discharge could be obtained. A typical U-I characteristic of a low-pressure DC discharge is given in Fig. 3.1. The operation point is the intersection between the current-voltage characteristic and the so-called "load line" given by the equation: $V=U-R_{ext}\cdot I$. The glow discharge is the region situated between the Townsend discharge and the arc discharge and presents three operation modes: the subnormal, normal and abnormal glow.

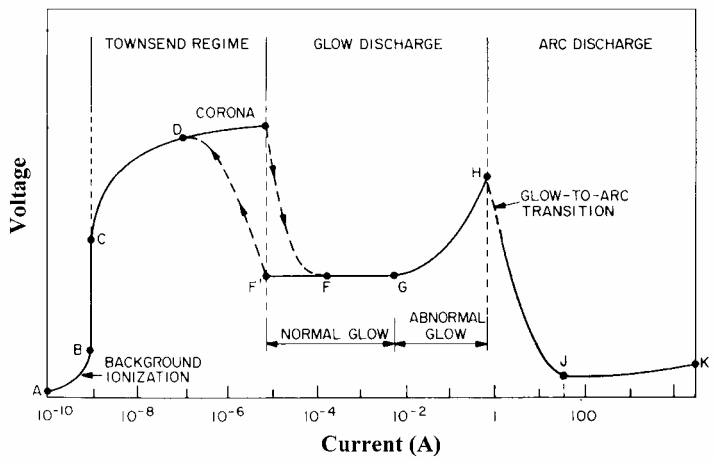


**Figure 3.1:** Typical current-voltage characteristic of a low-pressure discharge (after [Rot-95]).

The current-voltage characteristic of a high-pressure discharge it is expected to have a similar shape, as long as the mechanisms responsible for the generation of the discharge are the same as in the low-pressure range.

The transition from the Townsend discharge to the normal glow discharge results from the distortion of the external field by the space charge accumulated in front of the

electrodes. The ion mobility being much lower than that of the electrons, they accumulate close to the cathode and therefore the most pronounced space charge effects are in the vicinity of the cathode. The electric field between the electrodes becomes strongly non-uniform and most of the applied potential ($V_c$) drops over a small distance close to the cathode ($d_c$). The normal cathode fall $V_c$ and the corresponding cathode fall thickness $d_c$ define the operation of a normal glow discharge and are both experimentally measured for the low-pressure range. As an example, for Ar and Cu electrodes the normal cathode fall should be about 130 V, while the cathode fall thickness about 0.3 torr cm [Bro-59]. Using these values, at 50 mbar the cathode fall thickness should be about 80 μm, at 400 mbar about 10 μm and at 1 bar about 4 μm.

Assuming that the electrons are responsible for excitation and ionization processes, the field distribution between the electrodes should determine the optical appearance of a glow discharge. The glow discharge normally manifests stratification into dark and bright luminous layers. Very close to the cathode there should be a thin dark space (Aston dark space) followed by a luminous zone (cathode glow), these zones being visible only at low pressures. Further, the cathode glow is followed by the cathode dark space, the negative glow and the Faraday dark space. These are the so-called cathode zones of a glow discharge. The cathode fall length $d_c$ covers the distance from the cathode surface up to the cathodic limit of the negative glow. If the distance between the electrodes is high enough, the positive column (an almost field free region) is present followed by the so-called anode regions (anode dark space and anode glow). More information on this matter could be found in [Eng-65] and [Rai-97]. If the distance between the electrodes is decreased at constant pressure the positive column shortens and finally disappears, while the cathode zones remain unchanged. For a given distance between the electrodes, as the pressure increases all luminous and dark layers become thinner and move towards the cathode [Eng-83]. It has to be underlined that the cathode zones are determinant for the sustaining of the discharge because the ionization and excitation takes place mostly here. This is the reason why the negative glow is the brightest of the glowing regions. If the distance between the electrodes is smaller than the length of the cathode fall, the sustaining voltage increases. For even smaller gaps the discharge extinguishes because the electrons do not gain enough energy to produce ionization even if the electric field is high.

## 3.2. Hollow cathode discharge geometry

A hollow cathode discharge is as special form of glow discharge operated in a configuration with a planar double cathode or a cylindrical hollow cathode. The ionization efficiency in a hollow cathode discharge is higher than in a conventional glow discharge and the current density can be orders of magnitude larger for the same sustaining voltage. The diameter of the cathode opening can control the cathode fall thickness [Lit-54] and is the most important parameter of a cylindrical hollow cathode. When the distance between the opposite sides of the cathode is sufficiently small, the current density rises, as well as the light emitted, due to a higher ionization and excitation rate. The mechanisms, which can determine the better ionization efficiency in a hollow cathode configuration, are briefly described below.

In the classical hollow cathode discharge a process that leads to the rise in the discharge efficiency is the pendulum motion of the electrons between the opposites sides of the cathode, called the Pendel Effect or hollow cathode effect by Paschen in 1916. The electrons, which are accelerated in the cathode fall, are passing the negative glow where they are producing excitations and ionization and then are entering the opposite negative glow and cathode fall in a retarding field. Finally they will be accelerated again and "repelled" into the negative glow from the opposite side of the cathode. As a consequence of the motion from side to side of the cathode cavity the fast electrons are kept in the cathode zone for longer time, until they lose enough energy to be extracted towards the anode and the ionization efficiency increases. The Pendel Effect is particularly significant in low-pressure discharges where due to the large mean free path the electrons can pass the negative glow without ionizing.

The role of neutral particles (photons and excited atoms in metastable levels) in increasing the emission rate at the cathode for a hollow geometry was discussed by Sturges and Oskam [Stu-67]. In discharge geometry with plane cathodes the non-charged particles, which can produce secondary electron if they strike the cathode are lost since their motion is not affected by the electric field and they can travel towards the walls or towards the anode. In a hollow cathode configuration, due to the cylindrical geometry of the cathode, the non-charged particles will hit the opposite sides of the cathode leading to a better efficiency of the secondary electron emission. The secondary electron emission

induced by photons is a very probable process for sustaining the ionization in high-pressure discharges [Lie-94].

In a hollow cathode configuration, the higher plasma density inside the hole makes the stepwise ionization more likely, which contributes also to the rise in the discharge efficiency [Stu-67]. Like the pendulum motion of the electrons, the multistep processes become important when the two negative glows corresponding to the opposite sides of the cathode are merging.

Another mechanism contributing to the increase of the ionization efficiency in hollow cathode discharges operating in rare gases is the Penning ionization in reactions between noble gas atoms and sputtered atoms of the cathode material with lower ionization potential [Whi-59], [Mus-62]. The sputtering rate in hollow cathode discharges is larger than in normal glow discharges because of the higher current density.

The relative importance of these phenomena for the enhancement of the discharge efficiency depends on the hollow cathode geometry, the cathode material, the fill gas and the working pressure and is difficult to be determined.

Although most of the studies regarding the hollow cathode discharge have been performed at low pressures [Gün-23], [Băd-58], attempts to extend the pressure range have been also reported by White in 1959 [Whi-59]. The White-Allis similarity law $V=V(pd_{hc}, I/d_{hc})$, where V is the sustaining voltage, I is the discharge current and $d_{hc}$ the diameter of the cathode opening predicts high-pressure operation. This can be achieved at constant sustained voltage by reducing the diameter of the hollow cathode. This law considers the pendulum motion of the electrons between the opposite sides on the cathode hole to account for the hollow cathode effect. Under this condition the product $pd_{hc}$ has to be in the range 0.1-10 torr·cm for operation in noble gases [Sch-90], for molecular gases this range being shifted to smaller values [Gew-65]. The lower limit is given by the condition that the electrons mean free path for ionization must not exceed the diameter of the cathode hole. The upper limit is determined by the condition that the distance between the opposite sides of the cathode should not exceed the length of the two cathode dark spaces plus the negative glow. For atmospheric pressure operation, $d_{hc}$ has to be less than 20 μm according to the upper limit and even if a higher temperature in the discharge is taken into account, the hole diameter should be less than 100 μm [Sch-00]. Anyway, there

are also other mechanisms than the pendulum motion of the electrons that has to be considered, like photon coupling between the opposite sides of the cathode cavity.

In a hollow cathode configuration the dark and luminous spaces typical for a classical glow discharge are still present.

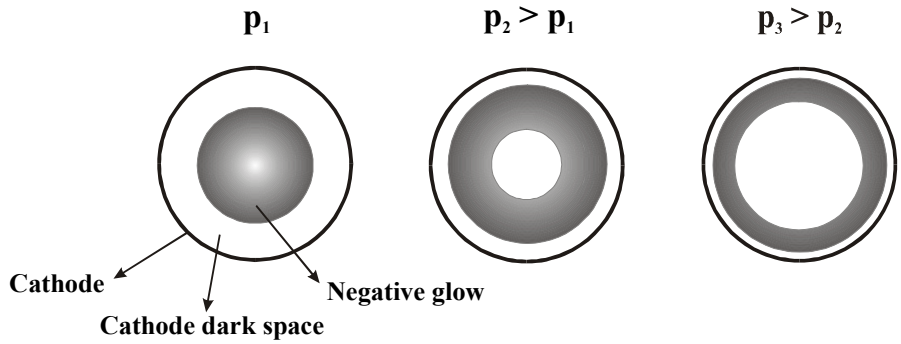


**Figure 3.2:** Evolution of the cathode zones for cylindrical hollow cathode geometry when the pressure increases.

The cathode zones are confined in the opening of the electrode and are followed towards the anode by the Faraday dark space and the positive column (if the electrode distance allow their existence). Increasing the pressure, the cathode layers behave in the same way like in the glow discharge with plane electrodes: shrink and move closer to the cathode. This behaviour of the cathode zones with the pressure is schematically viewed in Fig. 3.2 for a cylindrical hollow cathode. For simplicity, the Aston dark space and the cathode glow, which are very thin layers adjacent to the cathode, are not shown. The microstructures used in our investigations have a hollow cathode geometry and is expected that this will influence the ionization efficiency.

## 3.3. High-pressure glow discharges based on MSE

### 3.3.1. Experimental set-up

The MSE was mounted in a stainless steel vessel of 100 $cm^3$ placed on a xyz movable table (Standa 7T25 /7R129). Two quartz windows of 50 mm diameter laterally mounted allow optical access to the discharge. Different gases or gas mixtures are injected in the discharge chamber through a mass flow controller (Schaefer PSRCE3) and the working pressure is adjusted with a needle valve placed between the reactor and the pump system. A DC power supply (Tennelec TC951) was used to bias the cathode through a load resistor of 100 kΩ. A schematic view of the experimental set-up and the picture of the discharge chamber are presented in Fig. 3.3a and b.

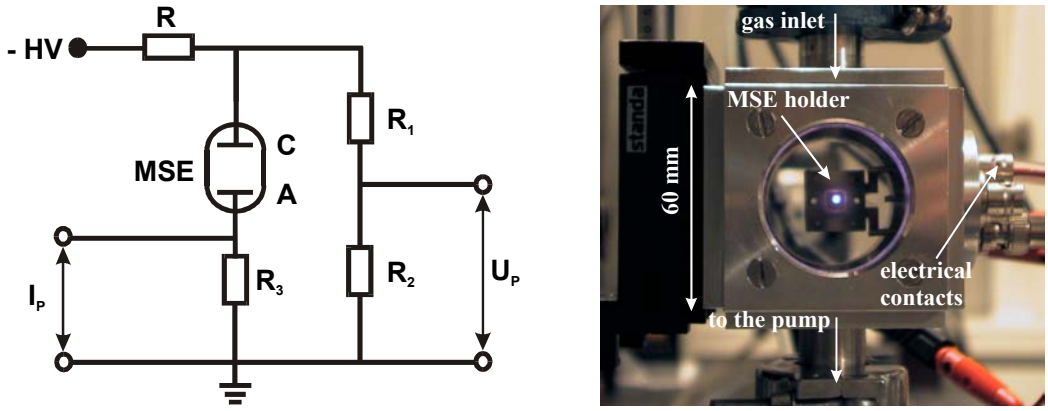


**Figure 3.3:** Schematic view of the experimental set-up (a) and of the discharge chamber (b) used for plasma generation using MSE arrays. R = 100 Ωk and $R_3 << R_2 << R_1$.

The light emitted from the microdischarge was recorded side-on and end-on at the cathode side using a charge coupled device (CCD) camera (Princeton Instruments TE/CCD-1024). The discharge was imaged 1:1 on the detector by a converging lens with 16 cm focal length. When a magnification of the discharge area was needed, a digital camera connected to an optical microscope was utilized to record the optical appearance of the discharge.

### 3.3.2. Breakdown mechanism

For the MSE sustained discharge, the formative time of breakdown measured in noble gases at low over voltages is in the μs range. It clearly indicates that the breakdown is not caused by a spark mechanism. The retardation time for a small gap should be rather large and it was found to be about 50 μs. When a relatively large load resistor limits the increasing of the discharge current, a classical Townsend mechanism (α-γ) of breakdown can be assumed. This type of breakdown should involve the entire discharge gap in a diffuse manner because the space charge effects are not significant. This fact is sustained by the optical appearance of the discharge as shown in Fig. 3.5a. When the discharge is ignited directly at relatively high current density (Fig. 3.5b-d), the space charge effects are already playing an important role in the moment of breakdown and a space charge controlled Townsend mechanism (α-γ-σ) can le considered.

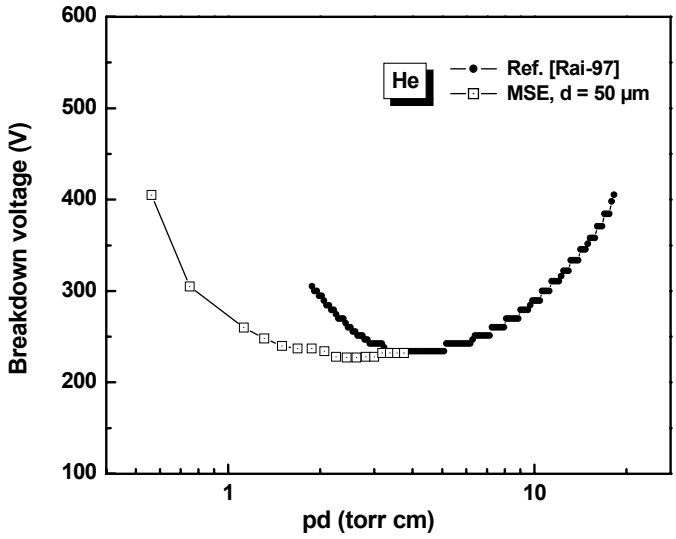


**Figure 3.4:** Breakdown voltage as a function of pd for a single-hole discharge in He.

For the MSE based discharge it was possible to measure the breakdown voltage in noble gases commonly used in our investigations. The breakdown voltage depends on the nature of the gas at the same pd product. A typical Paschen curve is given in Fig. 3.4 for helium. It can be seen that in the region of the minimum, the breakdown voltage corresponds to the one found in [Rai-97]. On the left-hand side of the minimum the

breakdown voltage does not increase so steeply as it does in the Paschen curve provided by literature, which correspond to homogeneous field, low pressure and a relatively large gap. As already discussed in Chapter 2, for small gaps the electric field is locally augmented in the vicinity of edges or microscopic protrusions and the voltage required for breakdown lowers. The pressure was increased up to 1 bar, corresponding to a pd of 3.8 torr·cm for the MSE used. The right hand-side of the Paschen curve was not measured because the pressure was not further increased.

### 3.3.3. Optical appearance of the microdischarge

The current-voltage characteristic of a single microdischarge operating in Ar at a pressure of 200 mbar was measured and simultaneously the spatial distribution of the emitted light was recorded end-on at the cathode side.

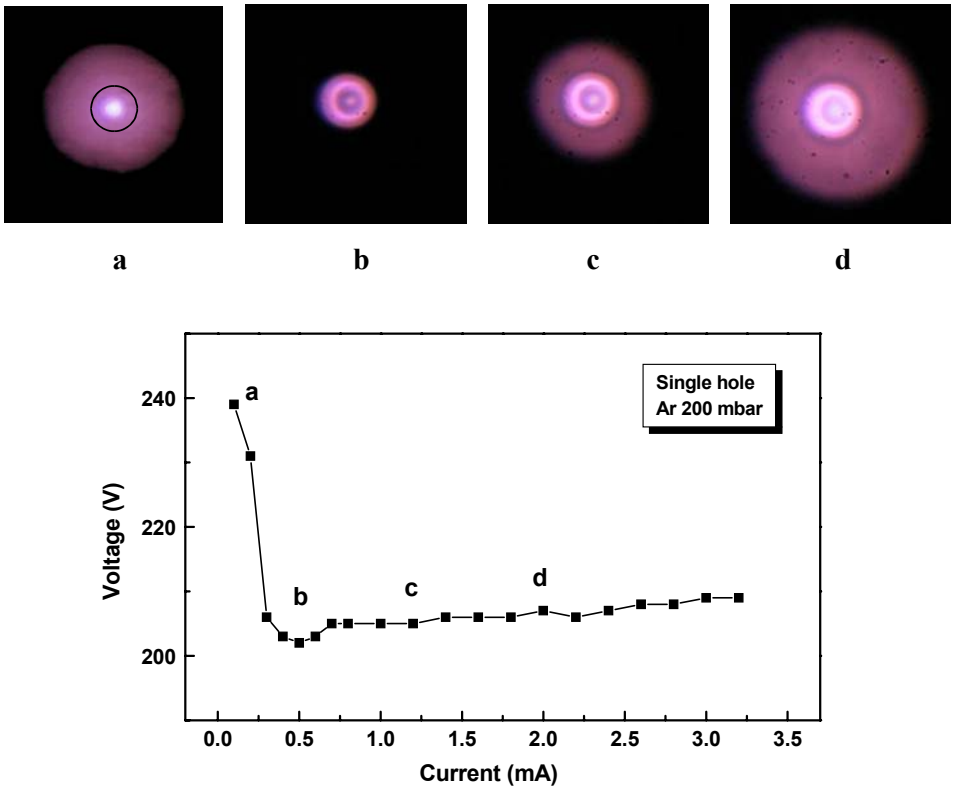


**Figure 3.5:** Optical appearance of a MSE sustained discharge (end-on cathode) and the corresponding current-voltage characteristic. The black circle indicates the hole.

The U-I characteristic of the MSE sustained discharge (Fig. 3.5.) is similar to the well-known characteristic of a low-pressure glow discharge and shows different modes of operation. At low current it presents a Townsend mode followed by a transition to a normal glow discharge. The Townsend discharge is characterized by small current (typically less than 0.3 mA). The charge density in the hole is low and does not disturb the electric field between the electrodes, which is in this case mainly axial oriented. Increasing the current, the axial electric field begins to be distorted by the space charge accumulated inside the cathode and a strong radial electric field develops. The potential distribution in the gap becomes strongly non-uniform and the cathode fall is generated. The enhanced electric field at the cathode facilitates ionization processes and correspondingly a fall in the sustaining voltage and a rise in the current is observed. The discharge concentrates inside the hole. Accordingly, the optical appearance of the discharge changes from diffuse and relatively dark (Fig. 3.5a) to structured and the light emission also becomes more intensive (Fig. 3.5b). A very bright, circular zone forms close to the cathode walls surrounded by dark areas. It suggests the presence of the luminous and dark layers known from low-pressure glow discharges. From now on the current can be increased for more than one order of magnitude at constant gas voltage, a typical signature for a normal glow. Due to the very small dimensions of the inner surface of the cathode, the discharge expands out of the hole above the cathode (Fig. 3.5c,d). Thus the active surface of the cathode is enhanced, the secondary electron emission increases and a rise in current is possible without need of higher sustaining voltage. The fact that the current density at the cathode remains constant when the discharge current is varied is a well-known property of a normal glow discharge. For further rise in current an abnormal glow regime (not present in Fig. 3.5) was observed. It has a resistive U-I characteristic and it is associated with the contraction of the discharge inside the hole. The current density at the cathode grows significantly. The operation of the discharge in the abnormal mode is usually avoided because the very high power density ($kW/cm^2$) often leads to the onset of thermal instabilities and to the damage of the microstructure.

To prove the hypothesis that the luminous and dark layers correspond to the cathode zones known from low-pressure glow discharge theory one has to investigate the behavior of the discharge at different pressures. It is expected that they will become thinner and move towards the walls of the cathode, as the pressure is increased (see Fig.

3.2). The optical appearance of the microdischarge was studied at the cathode side for pressures ranging from 50 mbar to 400 mbar. The discharge was operated in the normal glow mode at 0.5 mA. The side-on respective end-on appearance of the MSE plasma, recorded with an exposure time of 10 ms, is presented in Fig. 3.6a and b for different pressures.

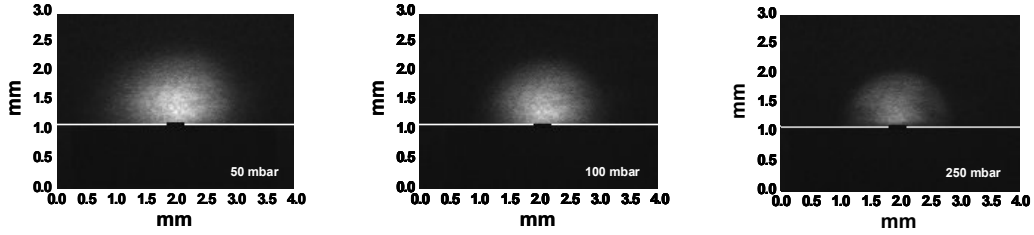


**Figure 3.6a:** Side-on appearance of the MSE sustained discharge at different pressures. The position of the cathode surface and the hole (300 μm diameter) are shown on each picture.

For the pressure range studied the plasma appears to be almost like a spherical calotte fixed on the cathode, which reduces its radius when the pressure increases. By increasing the pressure at constant current the emissive volume above the cathode decreases and the light emitted is less intensive (see Fig. 3.6a). A reason for this behavior might be the higher loss frequency due to collisions. On the other hand, a smaller emissive volume above the surface means that the excited atoms concentrate inside the hole with the pressure. This indicates that the negative glow contracts and moves towards the inner side of the hole. Here it should be mentioned that the cathode zones (cathode dark space, negative glow and Faraday dark space) follow the shape of the cathode and move as a body. When the microdischarge expands out of the hole, the active surface of the cathode is given by the opening in the electrode and by the free metal surface around the hole. Although not visible in the side-on pictures presented here, there it should be also a thin region less bright exactly above the electrode surface. This will be discussed in Chapter 5 related to the study of the excited atoms above the cathode surface.

Fig. 3.6b presents the end-on pictures of the discharge and the corresponding light intensity profiles. Dark and luminous concentric layers are to be seen and as expected, their thickness is pressure dependent. A similar behavior was reported in [Abr-66] in respect to the low-pressure operation of a so-called “superdense” hollow cathode discharge and in [Ern-01] for micro-hollow cathode discharges.

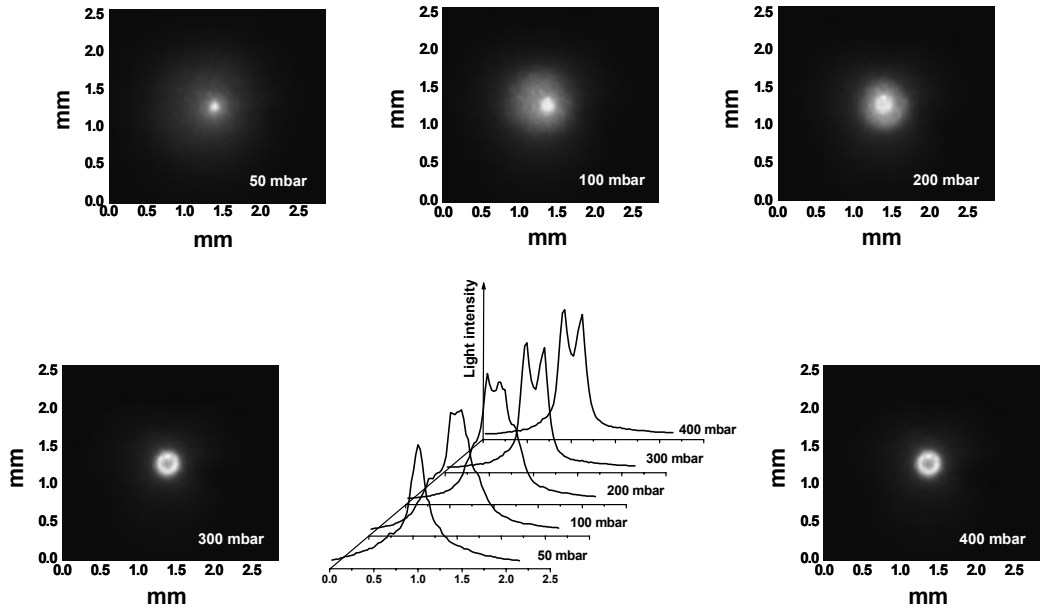


**Figure 3.6b:** End-on appearance of the MSE sustained discharge at different pressures.

At 50 mbar can be seen that there is a common negative glow and by rising the pressure the two negative glows adjacent to the cathode wall separates and the middle of the hole remains dark. The separation increases with the pressure and the Faraday dark space can be clearly observed. For relatively high pressure a positive column may form towards the anode but if the light emitted is not very intense, this cannot be seen when looking at the cathode side. The length of the cathode fall can be estimated at 50 mbar and 100 mbar, but for higher pressure the thickness of the dark and luminous layer in Fig. 3.6 becomes too small to be precisely measured. For 50 mbar the cathode fall thickness was estimated to about 80 μm, which is in good agreement with the theoretical data [Bro-59]. The negative glow should have about the same thickness as the negative glow and its cathodic limit should be well defined and most luminous, as can be seen also in Fig. 3.6b. Due to the fact that the limit of the negative glow opposite to the cathode is not very clear it is difficult to estimate the extend of the luminous area. Taking into account that the diameter of the MSE hole is 280 μm, at 50 mbar the two negative glows should merge and it is indeed the case. For 100 mbar the cathode fall thickness was estimated to about 50 μm, which means that up to now two distinct negative glows should be observed. Indeed in the middle of the hole a less luminous region becomes visible.

The above-presented pictures show qualitatively the evolution of the dark and luminous cathode zones. For quantitative measurements the enlargement of the discharge area is necessary.

### 3.3.4. Current-voltage characteristic

The MSE sustained discharge was studied from the electrical point of view in different gases, for the pressure range 50 - 1000 mbar. The measurements were concerned with single-hole operation and with parallel operation of a large number of microdischarges.

The discharge was first investigated in diverse noble gases (Ar, He, Ne) and their mixtures. In all gases used here the behavior of the discharge was found to be similar, as shown in Fig. 3.7 for a single-hole discharge operated at atmospheric pressure. Usually the microdischarge operates in the normal glow mode, where the sustaining voltage is practically current-independent.

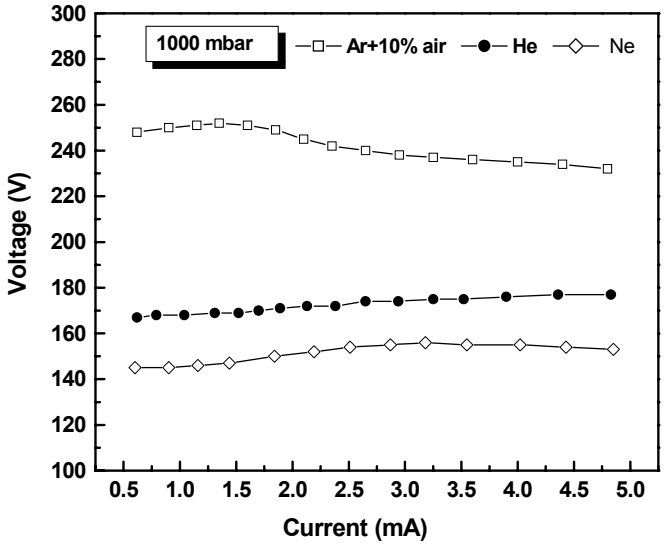


**Figure 3.7:** U-I characteristics in different gases at atmospheric pressure.

The sustaining voltage is determined in each case by the combination gas-cathode material through the first ($\alpha$) and second ($\gamma$) Townsend coefficients. When consider that the ionization is sustained by the same mechanisms in the pressure range investigated, the

sustaining voltage for a given gas depends on the pressure through the reaction rates which are pressure dependent. The slightly negative slope of the U-I characteristic for Ar-air results from gas heating, a much more pronounced effect in Ar than in He or Ne. As the ionization frequency is a function of E/N, where N is the density, a higher temperature implies a lower electric field required for sustaining the ionization.

Typical current voltage characteristics for argon at different pressures are presented in Fig. 3.8. The differences in the gas voltage are relatively small showing that the discharge geometry is appropriate for plasma generation in this pressure range. It seems that the optimum is achieved for 1 bar with these microstructures (100 µm diameter). For MSE with larger holes the minimum of the sustaining voltage was achieved at about 300 – 500 mbar.

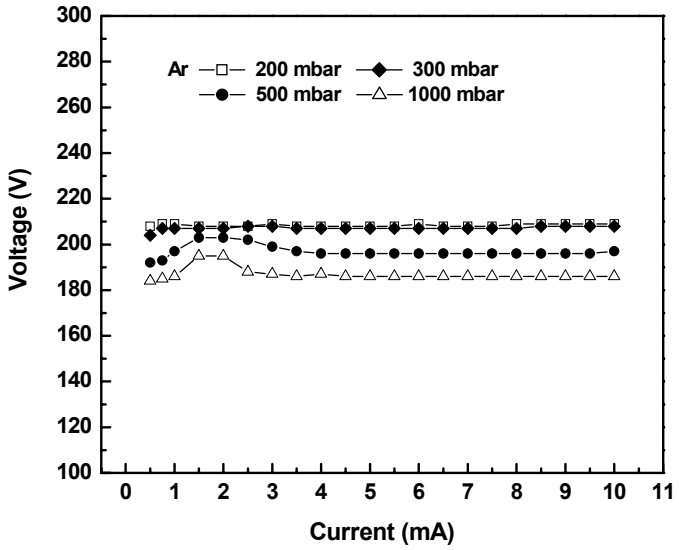


**Figure 3.8:** Current-voltage characteristics in argon at different pressures.

Although the microdischarge was operated in static regime in most of the cases, for different applications a slight gas flow through the hole is advantageous. In respect to the current-voltage characteristic, it changes into a resistive one, as shown in Fig. 3.9. This is a consequence of the fact that the gas flow reduces the thermal effects. By removing the heat locally stored in the MSE hole, processes like thermal enhanced secondary electron emission are hindered. The gas is not necessary cooled, but it is removed from the discharge zone and replaced with cold ambient gas. A positive slope

allows parallel operation of a large number of microdischarges without individual resistive ballast, which is very useful when large area plasma sources are needed.

It has to be underlined that the gas voltage is significantly higher when the discharge is operated in flow. Due to the fact that the charge carriers are removed from the discharge area by the gas flow, a higher electric field and accordingly a larger forward voltage is necessary to keep the ionization grad constant inside the MSE hole. Another aspect is that the U-I characteristic is shifted to higher currents. From the same reason as before, the electric field required for breakdown the gap is higher, the multiplication faster and the discharge start directly at relatively high current. As well, the discharge can be operated at high current density because, like already said, the thermal stress of the MSE is reduced.

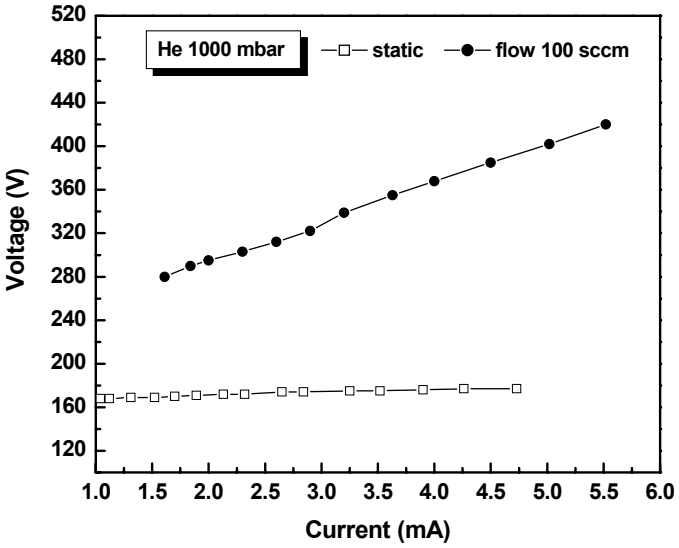


**Figure 3.9:** MSE sustained discharge operated in static and gas flow mode.

The operation of the MSE sustained discharge was studied in mixtures of argon and molecular gases like methane and air, for further applications as waste gas decomposition and surface processing. It is known that the reactive gases commonly used for etching of various materials are containing halogens or oxygen. Therefore the microdischarge was operated in argon with up to 40% air admixture. It is known that the admixture of molecular gases, e.g. air, toluene, methane to a high-pressure discharge operated in noble gases has a stabilizing effect. The current is limited and the thermal

effect as well, because the molecular gases are storing energy in vibrational-rotational motion. In dielectric barrier discharges for example, these mixtures allow to generate a homogenous discharge not a filamentary one [Yok-90] as usually. For about 10% air in argon the breakdown and also the sustaining voltage are 10% higher than in pure argon. The current voltage characteristic is presented in Fig. 3.10, for Ar+12% air using ambient air 50% humidity and synthetic air. It can be seen that the presence of water enables a lower sustaining voltage, a situation encountered also in high power technology where the presence of water or dust particles particle reduces the breakdown voltage.

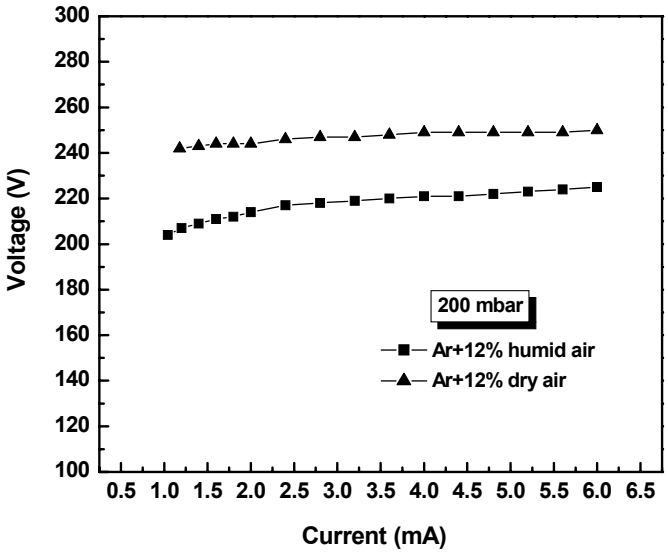


**Figure 3.10:** MSE sustained discharge operated in Ar-air at 200 mbar.

The admixture of small amounts (in the ppm range) of halogenated molecules like $CCl_2F_2$, $CClF_3$, $SF_6$ to noble gases increases the discharge voltage with about 50%. These gases are strongly electronegative and the discharge is controlled by attachment. As an example, a microdischarge which operates at atmospheric pressure in the normal glow mode at a sustaining voltage of 170 V in pure Ar, will need about 270 V to sustain the same discharge current in Ar+50 ppm $CCl_2F_2$ (freon). The breakdown threshold for halogen-containing gases is also very high compared to noble gases, e.g. 100 V/cm·torr for freon and 3.6 V/cm·torr for argon [Rai-97].

It should be stressed that the MSE sustained discharge was usually operated in the normal glow mode characterized by a current independent discharge voltage. Different

types of microstructures with copper electrodes but having various distances between the electrodes and different diameters of the hole have been compared. For a given gas and pressure but different distances between the electrodes e.g. 50 µm and 250 µm the breakdown voltage depends on the length of the discharge gap. Indeed, for a short gap the electric field needed to induce breakdown is achieved at smaller applied voltage. It can be concluded that the parameter important for breakdown is the product pd, where d is the distance anode-cathode. Using MSE with small electrode gap (50 µm) the discharge can be ignited in the normal glow and in the Townsend mode as well. By large distances between the electrodes (250 µm) the discharge starts directly at relatively high current corresponding to the normal glow mode.

It was noticed that the sustaining voltage in the normal glow mode for a given gas and pressure has the same value for MSE with different electrode gaps if the diameter of the hole is constant. For the operation of the microdischarge in the normal glow mode the product $pd_{hc}$, where $d_{hc}$ is the diameter of the cathode opening and p the pressure, has to be considered. Actually, for hollow cathode discharges the cathode thickness and the discharge configuration are important parameters but the decisive one is the diameter of the cathode opening. As already mentioned, the sustaining voltage depends on the cathode opening, which means that the specific geometry of the MSE clearly influence the ionization and excitation processes and accordingly the discharge operation. Based on the MSE previously described, a stable glow discharge can be operated in static and flow mode from 50 mbar to more than 1 bar in noble gases, air and mixtures thereof for discharge current from 0.1 mA up to more than 10 mA.

## 3.4. Parallel operation of MSE sustained discharges

The results displayed up to now refer to single-hole microdischarges. For most practical applications large area plasma has to be generated. This can be achieved by parallel operation of a large number of microdischarges.

Microstructures based on polyimide and ceramic substrates with up to 200 electrically coupled holes were under investigation. The most convenient situation is the parallel operation without individual resistive ballast, but the working point has to be

chosen on a region of the UI characteristic with positive slope. The typical current-voltage characteristic of a MSE array with 16 electrically coupled holes is given in Fig. 3.11.

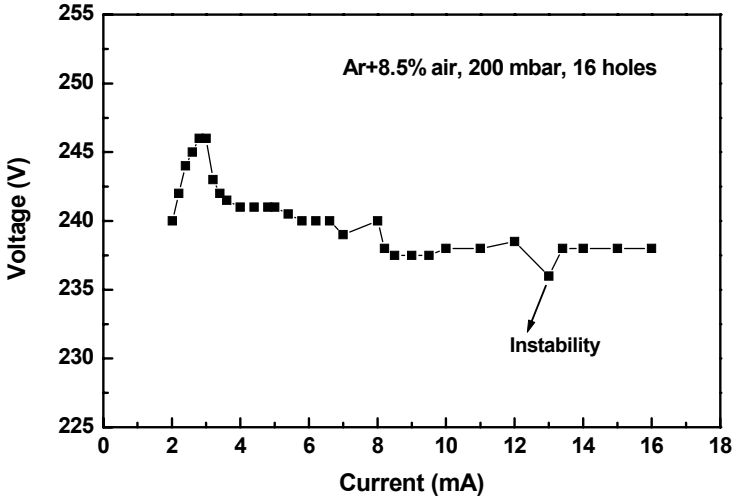


**Figure 3.11:** Current-voltage characteristic of a plasma module with 16 electrically coupled holes.

A positive slope of the U-I curve is achieved at relatively low current per hole (less than 0.2 mA), corresponding to the Townsend discharge. This current range allows the parallel operation without need of resistive decoupling, but microstructures very precise manufactured are required. For higher current density, the transition to normal glow discharge occurs in one of the holes accompanied by a fall in the sustaining voltage (see Fig. 3.11). The other discharges will be further sustained at low current while the one corresponding to the glow mode expands out of the hole on the cathode surface as the current is more increased (Fig. 3.12b). When all the discharges from an array are operated in the Townsend mode the current per hole can be estimated by simply dividing the total current to the number of active holes. After the transition to normal glow occurs in one (or more holes) it can be only said that most of the current is flying through this discharge. This as a consequence of a chain similar to the development of thermal instabilities (i $\uparrow$ T $\uparrow$ $n_e$ $\uparrow$ i $\uparrow$).

At even higher currents, it may happen that the discharge contracts in only one hole, situation indicated in Fig. 3.11 by “instability”, because the reason could be a thermal instability. Without using individual ballast was possible to achieve parallel operation of to 200 microdischarges in argon and argon-air for pressures up to 300 mbar.

A picture of a plasma module with 50x50 $mm^2$ active area (200 holes, 3 mm pitch) is presented in Fig. 3.12a.

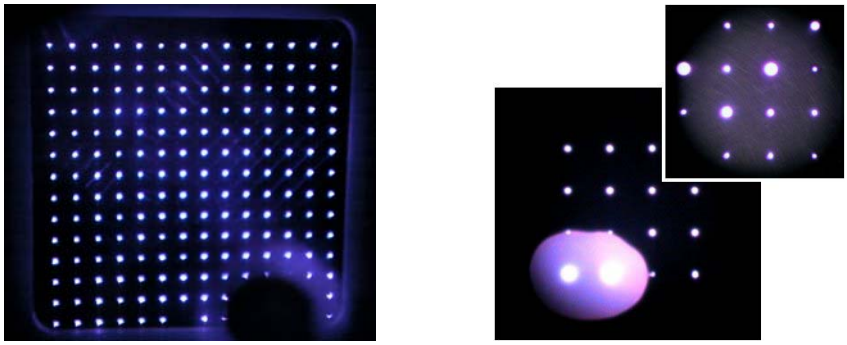

a b

**Figure 3.12:** Parallel operated microdischarges in argon at 200 mbar without resistive decoupling. Stable operation at low current (a) and the effect of local heating caused by the higher b).

In order to increase the pressure range of the parallel operation regime up to one atmosphere, microstructures with resistively decoupled holes have been used. The MSE has a special design, with individual resistors attached to the holes, as schematically shown in Fig. 2.9d. They control the current through each hole and maintain all the microdischarges in the same operation mode. Only when the value of the resistor is strongly different from hole to hole, a situation similar to that presented in Fig. 3.12b right-up corner may occur. Based on these structures was possible to operate plasma modules with 36 holes at atmospheric pressure in different gases at current of about 1 mA per hole corresponding to the normal glow mode.

Regarding the design of the microstructures, it is not necessary to use individual resistors attached to the holes. For simplicity, the decoupling could be obtained by replacing one of the metal electrodes by a high-resistivity material, which provides distributed resistive ballast over the whole microstructure. A disadvantage of the electrical decoupling using individual resistors included in the MSE is the energy dissipated in Joule heat. This energy is lost because it is not transferred to the ionized medium and on the other hand enhances the thermal stress of the MSE. This can be avoided using active circuit elements (e.g. transistors) for controlling the current through each hole independently in spite of passive circuit elements (resistors).

## 3.5. Thermal effects and the contraction of the glow discharge

In high-pressure DC discharges one of the problems is the constriction of the discharge (filamentation) follow by the glow-to-arc transition (GAT) if the current density is further increased. GAT has as main reason the thermal instability that occurs at high current densities. The thermal instability perturbs homogeneous discharges at elevated pressures and sufficiently high current in molecular and atomic gases, independent on the specific discharge geometry. The instability mechanism can be described as follow. The gas temperature T increases locally, the neutral gas density N reduces, the reduced electric field E/N augments, the electron energy increases, the ionization becomes more efficient and accordingly the current density increases, which leads to a further rise of the gas temperature. The mechanism for generation and development of the thermal instability is a closed chain of causal links that can be started at any step [Rai-97] and whose growth rate is determined by the heating of the gas.

The contraction of the discharge may be avoided using a gas with high thermal conductivity, or admixtures of a small amount of molecular gases to noble gases, strong gas flow or cooled electrodes. In our case it is rather impossible to cool the electrodes in the classical way (flowing water) but the use of thick copper mounting for the MSE had a positive effect. Another approach is to replace the DC operation of the MSE sustained discharge with pulsed operation.

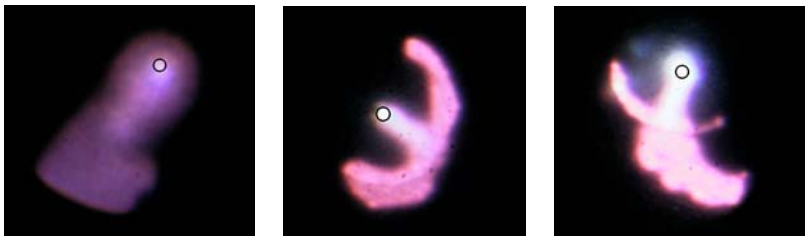

**Figure 3.13:** Contraction of the homogeneous glow discharge, incipient (a) and filamentary discharge (b and c).

In Fig. 3.13a an incipient contraction of a discharge operated in Ar at 500 mbar is shown. The round plasma volume begins to shrink and if the current is further increased a filamentary discharge appears on the cathode surface (Fig. 13b). At still higher currents

(about 10 mA) sparks occur inside the hole as it can be seen in Fig. 13c and the discharge becomes strongly unstable. The power density in the discharge channel changes and the excitation and ionization processes are influenced, as indicated by the different light emission. The white-blue light in the last picture suggests emission of metal vapor of the cathode material.

When the thermal effects begin to play a role, the current is increasing by decreasing gas voltage. This is equivalent with the production of more charge carriers without need of higher electric field. As the temperature of the cathode is increasing, the barrier of potential lowers and a larger number of secondary electrons are released from the surface. This process is called thermal enhanced secondary electron emission. By further increasing the current density, cathode spots are formed, and the discharge contracts to a strongly conductive filament. The degree of ionization and the gas temperature in a filament are much higher than in a homogeneous glow discharge. Taken into account the high gas temperature in the cathode zone and consequently the reduced pressure, the reduced current density $j/p^2$ of a filamentary discharge is on the same order of magnitude as that of a homogeneous glow discharge. When the temperature of the cathode surface becomes locally high enough to enable thermal emission of electrons, the transition to arc regime occurs. The microstructures commonly used do not withstand this operation regime. Anyhow, the purpose of our study is to investigate the glow discharge mode and to hinder as much as possible the evolution of the discharge through an arc.

## 3.6. Conclusions

The MSE sustained discharge is a high-pressure glow discharge, usually operated in the normal glow mode. For this operation range both the optical appearance and the current-voltage characteristic are indicating a stable, non-filamentary glow discharge. The excitation and ionization are enhanced by the hollow cathode geometry of the microstructure. The increase of the ionization efficiency is not necessary caused by pendulum electrons, like in low-pressure hollow cathode discharges but also by metastable atoms and photons, which are confined inside the cathode cavity. As the production of secondary electrons inside the cathode is very efficient, the discharge can be sustained also when the distance between the microelectrodes is smaller than the normal

cathode fall thickness (obstructed discharge). This is a clear advantage because a shorter discharge gap implies a lower breakdown voltage.

The electrical parameters of the MSE sustained discharge and the operation range investigated in this work are summarized in Table 3.1, where p is the pressure, $V_P$ the sustaining voltage in the normal glow mode, I the discharge current and j the current density. As the value of the breakdown voltage depends on the pd product, i.e. the working pressure and the type of the microstructure used, it was decided not to present them in the table below.

| **Gas** | **p (mbar)** | **$V_P$ (V)** | **I (mA/hole)** | **j (A/cm$^2$)** |
|---|---|---|---|---|
| Ar; He; Ne; air; Ar/air; Ar, He /NO; Ar, He/$N_2$; Ar/$CCl_2F_2$ | 50-1000 | 140-270 | 0.05-20 | 0.6-120 |

**Table 3.1:** Electrical parameters for the MSE sustained discharge.

The high-pressure glow discharge based on MSE arrays was studied from electrical and optical point of view and its range of operation was determined, but besides these aspects the intrinsic plasma parameters have to be measured. The knowledge of the plasma parameters for this new plasma source is of major interest regarding the physics of the high-pressure glow discharges and the potential applications of such plasma as well. The next two chapters are concerned with the investigation of these parameters by means of spectral methods.

# CHAPTER 4
# EMISSION SPECTROSCOPY

## Introduction

Emission spectroscopy is the easiest diagnostics method for investigating discharge plasmas. Due to the presence of ionized and excited particles in the discharge, electromagnetic radiation is emitted, the wavelength range depending on the type of emitter and on the amount of energy invested in excitation. The emitted light can be collected and analyzed without perturbing the plasma. This is very helpful in the investigation of high-pressure plasma sources because the choice of diagnostics methods is limited due to the small dimensions of the discharge. For small size discharges it is not possible to use Langmuir probes and the estimation of the plasma parameters could be made mostly through spectral methods, like emission or absorption spectroscopy. The knowledge of the plasma parameters like electron number density, electron and gas temperature is very important for understanding the excitation/ionization mechanisms and the loss processes and for developing a model of the discharge. These intrinsic plasma parameters are also very important in respect to potential applications when a given electron density and/or energy is needed, or when the gas temperature must not exceed a certain value.

## 4.1. Thermodynamic equilibrium

Local Thermodynamic Equilibrium (LTE) implies that all particles present in the plasma, electrons and heavy particles, are in equilibrium at a common temperature. LTE can be expected only if the collisional processes are dominating over the radiative processes, like decay and recombination. For collision-dominated plasma the free electrons have a Maxwellian velocity distribution and therefore one can speak about the

local electron temperature. The number of electron with velocities between v and v+dv is given by:

$$dn_v = n_e 4\pi \left( \frac{m_e}{4\pi k T_e} \right)^{\frac{3}{2}} \exp\left( -\frac{m_e v^2}{2kT_e} \right) v^2 dv \tag{4.1}$$

where $n_e$ is the total number of free electrons and $T_e$ the electron temperature.

For the bound levels the distribution of population densities between the available energy levels follows the Boltzmann distribution:

$$\frac{n_m}{n} = \frac{g_m}{Q(T)} \cdot \exp\left( -\frac{E_m}{kT} \right) \tag{4.2}$$

where n is the total population, $n_m$ is the population of any electronic level m with energy $E_m$ and degeneracy $g_m$ and Q(T) is the partition function given by the relation $Q(T) = \sum_m g_m \cdot \exp\left( -\frac{E_m}{kT} \right)$. The partition function (called also state sum) is temperature dependent, but usually for neutral atoms at relatively low temperatures can be taken equal with the statistical weight of the ground level $g_0$ (g = 2J+1, with J the total angular momentum). For a large number of elements and ionization stages the partition functions have been calculated by Drawin [Dra-65]. From Eq. 4.2 the populations of two electronic levels m and n which are in equilibrium is given by:

$$\frac{n_m}{n_n} = \frac{g_m}{g_n} \cdot \exp\left( -\frac{E_m - E_n}{kT} \right) \tag{4.3}$$

The densities of neutral and ionized particle are related by the Saha-Bolzmann equation. Considering only single ionized atoms and electrons, from the condition of quasi-neutrality of the plasma follows:

$$\frac{n_i n_e}{n} = 2 \frac{Q_i(T)}{Q(T)} \cdot \left( \frac{2\pi m k T_e}{h^2} \right)^{3/2} \exp\left[ -\frac{(E_i - \Delta E_i)}{kT_e} \right] \tag{4.4}$$

where n, $n_e$, $n_i$ are the neutral density, the electron density and the ion density respectively, $Q_i(T)$ and Q(T) are the partition functions for ion and neutral atom. The quantity $\Delta E_i$ represents the lowering of the ionization potential in plasma as a consequence of the Coulomb interactions and can be estimated as:

$$\Delta E_i \approx \frac{e^2}{4\pi\varepsilon_0} \cdot \frac{1}{\lambda_D} \tag{4.5}$$

where $\lambda_D$ is the Debye length. Actually, $\lambda_D$ in Eq. 4.5 is the total Debye length (electron and ions) but being much larger for electrons compared to ions, it will be taken as:

$$\lambda_D(cm) = \sqrt{\frac{\varepsilon_0 kT_e}{n_e e^2}} = 743\sqrt{\frac{T_e(eV)}{n_e(cm^{-3})}} \tag{4.6}$$

The lowering of the ionization potential is important only for plasmas that provide a large density of electrons.

When LTE cannot be assumed, at least Partial Local Thermodynamic Equilibrium (PLTE) can be considered in the sense that the populations of high-excited levels are related to the population of the next ion ground state by the Saha-Boltzmann equation. The required electron density for PLTE is given by [Gri-64]:

$$n_e(cm^{-3}) \geq 7 \cdot 10^{18} \frac{z^7}{n^{17/2}} \left( \frac{kT}{z^2 E_H} \right)^{1/2} \tag{4.7}$$

where $E_H$ is the ionization energy of hydrogen in eV (13.6 eV), z-1 gives the charge state of the particle, n is the principal quantum number of the lowest excited level which is in equilibrium with the free electrons. If Eq. 4.7 is fulfilled for at least one level below the ionization limit in the plasma, this indicates that the free electrons have a Maxwellian velocity distribution. Even if this relation refers to hydrogen or hydrogen-like atoms ($He^+$, $Li^{2+}$), it provides also a reasonable approximation for more-electron systems. For other elements, like Ar here, the appropriate factor $z_{eff}$ has to be introduced:

$$z_{eff} = \sqrt{\frac{E_i}{E_H}} \tag{4.8}$$

where $E_i$ is the ionization energy of the atoms under consideration. According to Eqs. 4.7-4.8, the condition that the excited level with n = 4 in a plasma at $T_e \approx 1$eV to be in LTE with the higher excited levels and with the free electrons, is that the electron density should be higher than $1.6 \cdot 10^{13}$ $cm^{-3}$. This condition applies for an optically thin, homogeneous plasma and usually does not hold for the ground state. In practical situations the lower excited states, and especially the ground state, are overpopulated relative to the equilibrium population. The electron density required to have all levels, including the ground state, in LTE is much higher than that given by relation 4.7 (it should be about $1.5 \cdot 10^{17}$ $cm^{-3}$ comparing to $1.6 \cdot 10^{13}$ $cm^{-3}$). More details about validity criteria for LTE can be found in [Dra-69].

The basic assumption for PLTE is the Maxwellian velocity distribution function of the electrons. If the electron collision processes dominate the heavy particle collisional effects, which is usually true in a plasma that provide a high electron density, the Saha-Boltzmann equations are not invalidated even if the system can not be described by a common temperature.

If it can be considered that the electron impact dominates among collision processes, the determination of the electron temperature as a measure of the electron kinetic energy is of very high importance because the cross sections of different processes involving electrons are dependent on the electron energy. Besides the electron temperature, the kinetic energy of excited atoms and ions should also be measured [Hut-87]. As the electron-electron energy transfer rates are much larger than the electron-ion rates or ion-ion rates [Spi-62] these temperatures may be different even if the individual particle velocity distributions are Maxwellian or close to Maxwellian. A technique that allows the direct measurement of atom and ion temperatures is the thermal Doppler broadening. This method will be described in detail in Chapter 5 in respect with the determination of the neutral gas temperature. Regarding the electron temperature many methods are available but the validity of the PLTE assumption has to be checked. The commonly used approach is to consider PLTE conditions, to determine the electron temperature and density from spectroscopic measured quantities and at the end to verify if the initial assumption is justified or to investigate the degree of departure from equilibrium of the studied plasma. Some of these methods will be briefly described in the following sections.

## 4.2. Experimental set-up for emission spectroscopy

The chamber was coupled to a 1 m focal length scanning monochromator (Ortec BM100) as shown in Fig. 4.1. The discharge was imaged 1:1 on the entrance slit of the monochromator using a 10 mm focal length converging lens. A 1200 lines/mm grating blazed at 450 nm was used to investigate the light emission in the wavelength range 350 to 850 nm. For the measurements presented here the entrance slit was set to 25 μm width.

An Optical Multichannel Analyzer (OMA) with 720 channels assured the detection of the spatially resolved radiation. The dispersion of the system is about 0.83

nm/mm. Actually the dispersion depends linearly on the wavelength as shown in Fig. A.3, Appendix A.

The OMA detector (EG&G 1420 UV) consists of a photo-cathode, a micro channel plate system (MCP), a photo-converter and a diode array. There are 1024 diodes each 2.5 mm high and 13 μm wide arranged at a pitch of 25 μm. Because the MCP used has 18 mm diameter it limits the active area of the array to about 720 channels. The OMA system posses also a control unit (EG&G 1461E) that set the exposure time, the MCP temperature and digitalize the data, which are finally read by a computer.

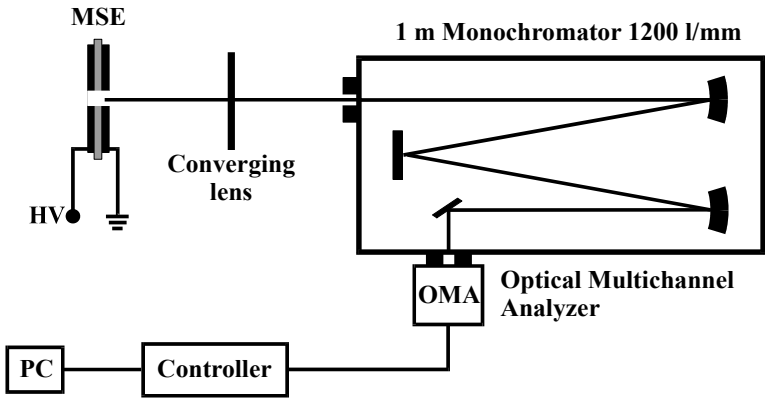


**Figure 4.1:** Experimental arrangement for emission spectroscopy.

The wavelength calibration of the monochromator was performed by means of gas discharge lamps (Pen Ray Lamps) designed for different spectral ranges. In most of the cases, besides the wavelength calibration the relative efficiency of the instrument as a function of the wavelength is required in order to make possible the comparison of lines from different spectral ranges. The system was calibrated for the spectral range 350 - 850 nm using a standard tungsten lamp [Ptb-88] and the relative spectral response of the system is given in Fig. A.1, Appendix A.

When the absolute intensity calibration of a spectral system is required, this could be made by using standards of spectral radiance like deuterium lamp for the UV range (200 - 400 nm) and tungsten lamps for the visible range.

## 4.3. Emission spectra of MSE sustained discharge

The microstructures used for these measurements are Cu/Kapton/Cu with 70 μm thick electrodes and perforations of 100 μm. The emission spectra of a microdischarge in He, Ne and Ar have been qualitatively investigated end-on at the cathode respectively anode side. The working pressure was varied from 200 mbar to 1000 mbar. In the spectral range 350 - 850 nm the light emitted from the microdischarge revealed the spectrum of the gas as expected for a glow discharge. In the case of Ar, atomic transitions (ArI) between highly excited electronic states, as well as lines from single charged ions (ArII) are present as it can be seen in Fig. 4.2. The atomic transitions are clearly dominant. At 200 mbar, using Fig. 4.2 and taking into account the spectral response of the system the estimated ratio ArII/ArI is about 1/5000.

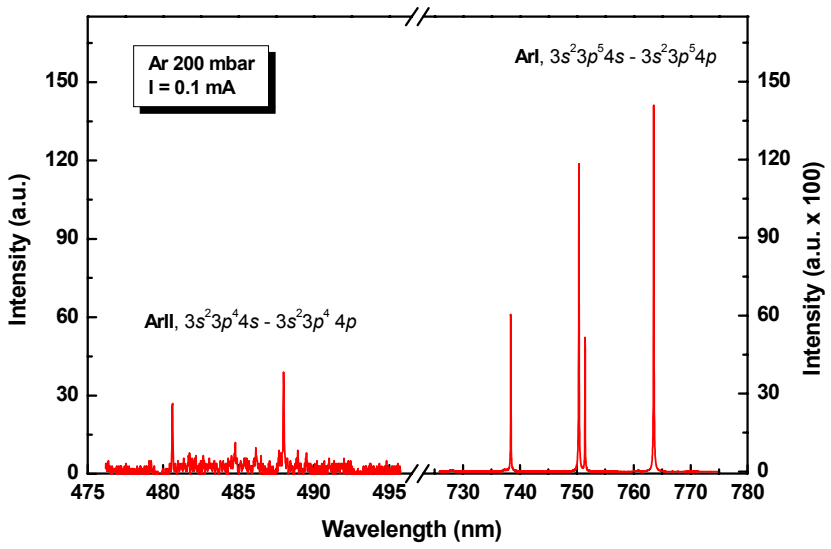


**Figure 4.2:** Emission spectrum in Ar at 200mbar.Wavelength range: 476-496 and 725-775 nm.

In the case of He and Ne only atomic lines have been observed. The lack of ionic transition can be explained by the relatively high ionization potential for He (24.59 eV) and Ne (21.56 eV) comparing to Ar (15.76 eV). In all investigated gases, the energy of the upper level of the detected transitions does not exceed 22 eV. Assuming direct excitation/ionization from the ground state, it can be concluded that the MSE plasma does not contain a large number of electrons with energies higher than about 22 eV. However,

at high-pressure there are also other excitation/ionization mechanisms, which have to be taken into account. The most important processes will be discussed in Chapter 5 for the case of Ar.

Metal vapor lines of the cathode material, e.g. CuI at 465.11 nm were also recorded, but only at high discharge current (some mA) and with low intensity. In hollow cathode discharges due to the higher sputtering rate comparing to classical glow discharges, strong emission from the cathode material was observed [Sch-90].

Atomic and molecular spectra of impurities like oxygen, hydrogen, nitrogen, were noticed even if it was ensured that the discharge chamber is well evacuated and sealed. The following atomic lines are present: the OI triplet at 777.19 nm, 777.42 nm, 777.54 nm with an energy of the upper level of about 11 eV, the $H_\beta$ and $H_\alpha$ Balmer lines at 486.13 nm respectively 656.28 nm with an energy of the upper level of about 12 eV. The first positive system $N_2(B^3\Pi_g) \rightarrow N_2(A^3\Sigma_u^+)$ and second positive system $N_2(C^3\Pi_u) \rightarrow N_2(B^3\Pi_g)$ of nitrogen were also identified with low intensity. Besides the small amounts from these elements present in the working gas, impurities can be desorbed from the walls of the reactor (water) and especially from the MSE during the discharge operation. Kapton is an organic compound, whose constituent elements are N, C, O, and H. The same situation was encountered in previous spectral measurement performed on MSE based on lithium-alumosilicate as a substrate (see Chapter 2). Emission lines from alkali metals (NaI doublet at 588.99 nm, 589.59 nm and LiI 670.77 nm 670.79 nm) with the energy of the upper level of about 2 eV have been observed. The presence of emission lines from chemical constituents of the dielectric substrate, and of metal vapor lines belonging to the electrodes, leads to the conclusion that the microstructure is strongly stressed during the discharge operation (heating, sputtering).

When quantitative measurements are to be done and especially when working in the UV range where the emitted radiation is strongly absorbed by impurities it is advisable to work with gas flow.

Fig. 4.3 presents the behavior of some atomic ArI (426.63 nm, 427.21 nm, 430.01 nm) and ion lines ArII (434.80 nm, 480.60 nm, 487.98 nm) with the pressure. As it can be seen their intensity is decreasing in the same manner, i.e. the relative intensity ratio ArII/ArI is practically constant over the pressure range investigated.

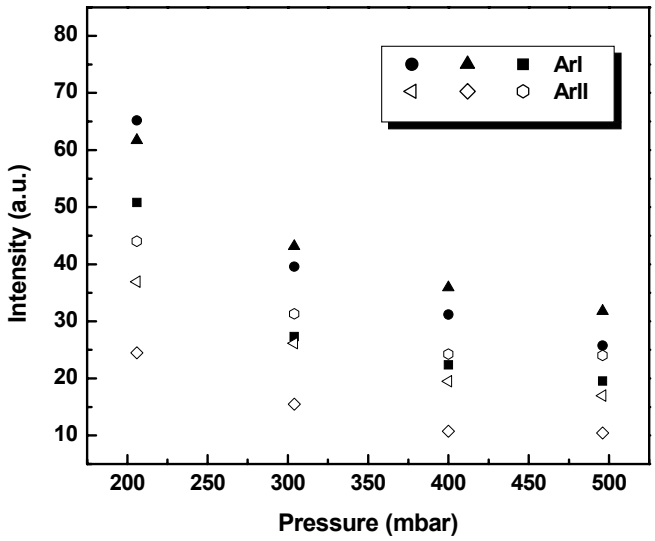


**Figure 4.3:** Pressure dependence of line intensities for atomic and ionic transitions.

Increasing the gas pressure the discharge concentrates inside the hole, the emissive volume decreases and accordingly the intensity of the emitted lines decreases. A constant ArII/ArI intensity ratio with the pressure suggests that the ionization grad remains constant, which means that the electron number density is also increasing with the pressure. This is very promising with respect to atmospheric pressure operation of the microdischarge. At 500 mbar the intensity of the investigated ArII lines (which are less intense) comes close to the detection limit and therefore the pressure was not further increased.

## 4.4. Electron temperature from line intensity ratios

Most easy to be identified and measured are discrete line spectra because they can be distinguished from background and scattered light. For optically thin homogeneous plasma with a length L along the line of sight, the intensity of a line is given by:

$$I_{mn} = \int_{line} I_{mn}(\lambda) d\lambda = L \frac{hc}{4\pi\lambda_{mn}} A_{mn} n_m \qquad (4.9)$$

where $A_{mn}$ is the spontaneous emission coefficient and $n_m$ is the population density of the upper level of the transition. This relation gives the energy emitted per unit of time and solid angle.

### 4.4.1. Different approaches

A method for estimating the electron temperature is to compare relative intensities of spectral lines from the same element and ionization stage [Gri-97]. Here it is assumed that at least the upper levels of both transitions are in PLTE. By measuring the relative intensities $I_1$, $I_2$ of two spectral lines that have a common lower state, the electron temperature can be calculated using Eq. 4.3 as follows:

$$\frac{I_1}{I_2} = \frac{\lambda_2 A_1 g_1}{\lambda_1 A_2 g_2} \cdot \exp\left( -\frac{E_1 - E_2}{kT} \right) \tag{4.10}$$

where E is the energy of the upper levels, I the measured intensity, g the degeneracy of the upper levels, A spontaneous emission probability and $\lambda$ is the wavelength, indices 1 and 2 standing for the two transitions. A condition required for the estimation of the temperature with good accuracy is $E_2$-$E_1$>>kT. The method presented above is not very reliable because the energy separation $E_1$-$E_2$ of the upper levels is on the order of the thermal energy kT.

By comparing the relative intensities of spectral lines from successive ionization stages of the same element the accuracy of the measurements is really improved, but the electron density has to be known from independent measurements. Here the energy difference is increased by the ionization energy and typically is much larger than kT. Using the Boltzmann and Saha equations this can be written:

$$\frac{I_1}{I_2} = 2\frac{\lambda_2 A_1 g_1}{\lambda_1 A_2 g_2} \cdot \frac{(2\pi m_e kT)^{3/2}}{h^3} \cdot \frac{1}{n_e} T^{3/2} \exp\left( -\left( \frac{E_1 - E_2 + E_i - \Delta E_i}{kT} \right) \right) \tag{4.11}$$

A method similar with those presented above, but not so commonly used, is the determination of the electron temperature from relative intensities of spectral lines of different atomic species. For species with very different ionization energy, one species can be significantly ionized while the other species mostly neutral. For different atomic species present in the discharge the Boltzmann and Saha equations are connected by the electron density and temperature. By comparing the relative line intensities of atomic

lines, or of one atomic and one ionic line, belonging to two atomic species with considerable different ionization energy, this ratio is a strong function of the temperature [Hol-68]. The electron temperature is calculated from the following relation:

$$\frac{I_1}{I_2} = \frac{1}{M} \cdot \left( \frac{\lambda_2}{\lambda_1} \right)^3 \cdot \frac{g_1 f_1}{g_2 f_2} \cdot \frac{Q_2^+ \alpha_1}{Q_1^+ \alpha_2} \exp\left( \frac{\Delta E}{kT} \right) \tag{4.12}$$

where f oscillator strength, α is the degree of ionization, $M = n_2/n_1$ is the mixing ratio of the two atomic species, $Q_1^+$, $Q_2^+$ are the partition functions and ΔE is the difference of ionization energies diminished by the difference of excitations energies:

$$\Delta E = E_1^i - E_2^i - \left( E_1 - E_2 \right) \tag{4.13}$$

The oscillator strength f is related to the spontaneous emission probability A by:

$$A_{mn} = \frac{8\pi^2 e^2}{4\pi\varepsilon_0 m_e c \lambda_{mn}^2} \cdot \frac{g_n}{g_m} f_{nm} = \frac{6.670 \cdot 10^{15}}{(\lambda_{mn}(A))^2} \cdot \frac{g_n}{g_m} f_{nm} \tag{4.14}$$

where m and n are the upper and the lower state on the transition, respectively.
This method is not as sensitive as the other regarding the validity of PLTE [Gri-97] and offers real advantages in the study of plasmas operated in Penning mixtures.

In choosing the spectral lines to be studied, one has to make sure that they are not affected by self-absorption, which means that the plasma has to be optically thin for this wavelength.

### 4.4.2. Measurements and discussions

Even if the microdischarge does not provide complete equilibrium conditions it can be assumed that due to the very high collision rate, PLTE can be considered and the Eqs. 4.10-4.12 can be used to estimate the electron temperature T. The electron temperature was determined for a microdischarge operated in Ar at 500 mbar generated on the same MSE type as used in section 4.3.

The method chosen for the determination of the electron temperature was to compare the relative line intensities of different elements present in the plasma, having different stage of ionization (Eq. 4.12). This method does not require an absolute intensity calibration, but the molar fraction M of the elements to be compared and both the partition functions have to be known. It offers also some advantages over the other methods. Comparing spectral lines from elements with different ionization potentials the energy

difference in the right hand side of Eq. 4.12 is increased, leading to a better accuracy [Hol-68].

In the present work this technique was applied to estimate the electron temperature in a MSE sustained discharge operated in Ar with 0.1% $H_2$ admixture (M = 1:99). A small amount of hydrogen (less than 1%) added to the discharge does not influence significantly the discharge operation and therefore could be assumed that the intrinsic plasma parameters like electron density and temperature are not affected. The spectral range investigated was 479 - 492 nm and the spectral lines whose intensities were compared together with their atomic constants [Smi-99] needed for the determination of the electron temperature from Eq. 4.12 are given in Table 4.1. Because the lowering of the ionization potential in the plasma has the same value for both atoms, depending only on the electron density, the unperturbed ionization energies of 15.7596 eV for argon and 13.5984 eV for hydrogen were considered. The partition function for the hydrogen atom was taken as 2, while that for argon ions as 5.5 for our experimental conditions [Dra-65].

| $\lambda_{ij}$ (nm) | Line | $A_{ij}$ ($s^{-1}$) | $f_{ji}$ | $g_i$ | $g_j$ | $E_i$ (eV) |
|---|---|---|---|---|---|---|
| 480.6021 | ArII | $7.983 \cdot 10^7$ | 0.2764 | 6 | 6 | 19.224199 |
| 484.7809 | ArII | $8.546 \cdot 10^7$ | 0.1505 | 2 | 4 | 19.306647 |
| 487.9863 | ArII | $9.526 \cdot 10^7$ | 0.5101 | 6 | 4 | 19.681376 |
| 488.9042 | ArII | $1.881 \cdot 10^7$ | 0.0674 | 2 | 2 | 19.802422 |
| 486.1323 | HI | $4.490 \cdot 10^7$ | 0.2386 | 6 | 4 | 12.749398 |

**Table 4.1:** Atomic transitions used for electron temperature estimation.

It was decided to use ArII lines because if the hydrogen added to the discharge would have a perturbing effect, it may affect the populations of the Ar lower excited states (4s, 4p) by reactive quenching [Cli-78], [Sad-01] but should not change the ion density:

$Ar^* + H_2 \rightarrow ArH^* + H$

Thus the lines under consideration are lying in the same spectral range the correction for the spectral response of the detector is avoided, the only calibration needed being the wavelength calibration. In this spectral range the background can be well extracted because no molecular bands are present and therefore the relative intensity of

the lines can be relatively accurate measured. The use of ionic to atomic lines ratios ensures an energy difference in the exponent large relative to kT (here about 4 eV) and accordingly smaller errors in the estimation of T. The accuracy could be further improved by measuring lines from metal atoms (low ionization potential) and rare gas atoms (high ionization potential). In the present experiment metal lines from the sputtered cathode material have been observed but their intensity was too low (even at high discharge current) to be used for the determination of T.

The electron temperature obtained by this method is in the range 0.6 - 0.8 eV as it can be seen in Fig. 4.4 and does not depend on the discharge current in the measured range. This temperature corresponds to the mean energy in the electron energy distribution function.

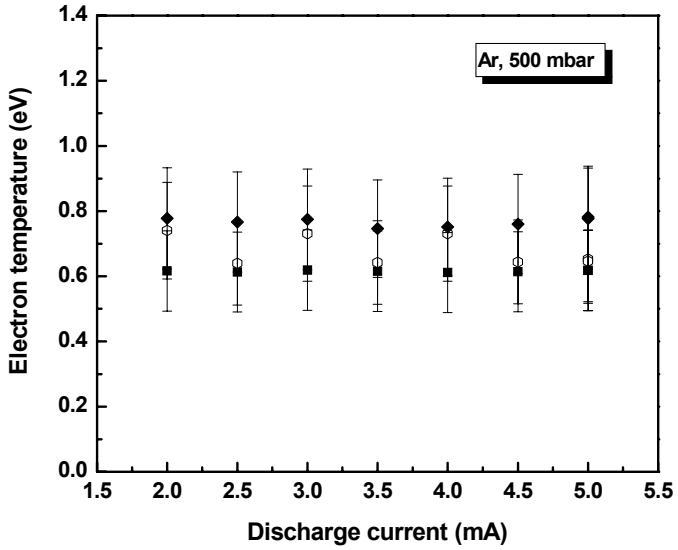


**Figure 4.4:** Electron temperature for an Ar microdischarge at 500 mbar using different spectral lines for comparison.

These are reasonable values taking into account the relatively high pressure in the microdischarge, even if they are lower than expected. The electron temperature measured in low-pressure glow discharges is typically around 2 –5 eV. The electron temperature should decrease with the pressure because the electron mean free path is decreasing and accordingly less energy is gained from the electric field between two collisions. Glow discharges operated at high-pressures are not quite common and only few reports about

the electron temperature are known. For high-pressure glow discharges and for dielectric barrier discharges the electron temperature is about 1 - 2 eV [Kog-97] mostly obtained from plasma simulations [Pet-97]. The electron temperature in the MSE sustained discharge is comparable with that experimentally obtained for micro hollow cathode discharges, where it was found to be about 1 eV [Pet-01]. A possible reason for this rather low temperature is that due to hydrogen admixture the heat conductivity within the plasma may change, affecting therewith the temperature. Also, when spectral investigations are performed end-on at the cathode side, the light collected by the spectrometer may come from the outermost regions above the cathode, which have lower density and temperature than the plasma confined inside the MSE hole. Furthermore, self-absorption may be quite important in these colder zones.

To prove the results, different ArI and ArII lines were compared in the same spectral range 424 - 438 nm, considering the detection efficiency of the spectrometer-OMA as constant. Even if the strongest atomic lines of Ar are in the range 700 - 900 nm, the spectral range investigated was chosen to have both Ar II and Ar I lines. First, the relative intensities of spectral lines from the same degree of ionization (ArI/ArI and ArII/ArII) were compared, using Eq. 4.10 to estimate the electron temperature. The values obtained for the temperature are very small (about 0.2 eV) and even negative values have been obtained. Actually, this method does not count as very reliable because of the very small energy difference between the upper levels of the transitions ($E_2$-$E_1$<2eV). The use of spectral lines from the same element but different ionization stages (here ArII/ArI) can in principle improve the accuracy of the measurements by increasing the energy difference present in the exponent, but the electron density has to be known. The estimation of the electron temperature implies the representation of the relative intensity of the investigated lines multiplied by the appropriate factors as a function of the energy separation between the two upper levels in a so called Boltzmann plot (see Eq. 4.11). Under the PLTE assumption this has to be a straight line, the slope yielding to T. For the present investigations, rather often the measured points are not lying on a straight line or the plot that should have a negative slope has a positive one. Therefore, the values obtained for the electron temperature are not reliable. Even if this method normally would provide an advantage upon the first one, in our case there are also some other reasons leading to the poor accuracy of the results. Large errors are coming from the estimation

the relative intensities. The intensity of the transitions measured is rather low comparing to the background. Regarding the ArII lines, they are very week (ratio ArII/I~1/5000) in the MSE discharge as a consequence of the high pressure and due to their high excitation energy. Regarding the ArI lines, the most intensive Ar atomic transitions are at wavelengths larger that 700 nm like already said, in the spectral range around 430 nm only lines with small oscillator strength being present. Another source of errors is the presence of band emission from molecular nitrogen superimposed on the line spectrum of argon and modifying the real value of the background.

An advantage of the methods presented above is that the absolute intensity calibration of the system spectrometer-detector is not needed. The measurements can be improved by comparing the absolute intensities of spectral lines from the same element, of equal or different stages of ionization. In our case this method was not applied due to the lack of the absolute intensity calibration.

## 4.5. Gas temperature derived from molecular spectra

The observation of molecular spectra makes possible the measurement of the vibrational and rotational distributions of the molecules. Like for the atoms, the rotational and vibrational levels are characterized by quantum numbers. The electronic excitation energies are in the 10 eV range, the vibrational energies are on the order of 0.1 eV while the rotational energies are about 0.01 eV.

For a diatomic molecule the energy of a vibrational level v is given by:

$$E_v = \omega_e(v+1/2) - \omega_e x_e(v+1/2)^2 + \omega_e y_e(v+1/2)^3 + \omega_e z_e(v+1/2)^4 + .... \qquad (4.15)$$

where $\omega_e$, $\omega_e x_e$, $\omega_e y_e$ and $\omega_e z_e$ are vibrational constants for one electronic level, which can be found in literature [Her-50] for different molecules of interest.

The energy of a rotational level of a linear molecule is given by:

$$E_r = B_v J(J+1) - D_v(J(J+1))^2 + H_v(J(J+1))^3 \qquad (4.16)$$

Where J corresponds to the rotational level and $B_v$, $D_v$ and $H_v$ are calculated for different vibrational levels [Rou-93].

### 4.5.1. Vibrational temperature

Like in the case of atomic emission lines (Eq. 4.9), the intensity of a vibrational band depends on the population density of the upper level $n_{v'}$ of the transition and on the transition probability $A_{v'v''}$. For molecular lines, this can be written as:

$$I_{v'v''} = C \cdot h\nu_{v'v''} n_{v'} A_{v'v''} = C \cdot h\nu_{v'v''} n_{v'} \frac{q_{v'v''}}{\lambda^3_{v'v''}} \qquad (4.17)$$

where v' and v'' are representing the vibrational quantum number of the upper and lower level respectively, $q_{v'v''}$ is the Franck-Condon factor (tabled for example in [Lof-77] for nitrogen), $\lambda_{v'v''}$ the wavelength of the transition and C is a constant depending on the emissive volume.

Recording the emission spectrum of the molecule of interest over a wide spectral range one can observe a large number of vibrational lines. For such measurements only spectrographs with middle resolution are required, but the spectral response of the system has to be known. The relative intensities of different vibrational band heads can be compared and the excitation temperature can be extracted assuming a Boltzmann distribution of the vibrational levels characterized by a temperature $T_v$.

For this study, the same type of microstructures as for atomic emission spectroscopy was used (see section 4.3). The discharge was operated in the pressure range 200 - 600 mbar in Ar-$N_2$ and He-$N_2$ mixtures, at discharge current between 0.5 and 1.5 mA. To perturb as less as possible the discharge the mixing ratio of nitrogen to rare gas was usually 1:4000. The light emitted from the discharge was investigated end-on at the cathode side. The emission spectrum was recorded from 300 to 500 nm by a 0.5 m focal length spectrometer (spectral resolution 0.08 nm in the first order) supplied with a CCD camera. All experimentally measured spectra are corrected for the spectral sensitivity of the system after extracting the background. The spectral response of the system spectrometer-CCD camera is given in Fig. A.2, Appendix A.

Typical emission spectra are presented in Fig. 4.6 for the two gases investigated. In He-$N_2$ mixtures, the emission spectrum consists of HeI lines (transitions from $n \leq 5$ to $n = 2$) and of vibrational/rotational bands of nitrogen molecule $N_2$ namely the second positive system $N_2(C^3\Pi_u) \rightarrow N_2(B^3\Pi_g)$ and of nitrogen molecular ion, namely the first

negative system of $N_2^+(B^2\Sigma_u^+) \rightarrow N_2^+(X^2\Sigma_g^+)$. These transitions are shown in the potential energy diagram for nitrogen given in Appendix B.

In He-$N_2$ high-pressure discharges the $N_2(C^3\Pi_u)$ state is excited in the following reactions [Bib-01a]:

- "pooling" reaction of molecules on $N_2(A^3\Sigma_u^+)$ metastable state [Her-99]

$$N_2(A^3\Sigma_u^+) + N_2(A^3\Sigma_u^+) \rightarrow N_2(C^3\Pi_u) + N_2(X^1\Sigma_g^+) \quad k = 1.5 \cdot 10^{-10}\ cm^3s^{-1} \quad (a)$$

- electron impact excitation

$$N_2(X^1\Sigma_g^+) + e_{fast} \rightarrow N_2(C^3\Pi_u) + e \quad \sigma_{e,e}(E) \quad (b)$$

The radiative lifetime (no quenching mechanisms considered) of the $N_2(C^3\Pi_u)$ state is about 37 ns [Pan-98]. The $N_2^+(B^2\Sigma_u^+)$ excited state has a radiative lifetime of 62 ns according to [Pan-98] and is generated via:

- Penning ionization

$$He^* + N_2 \rightarrow N_2^+(B^2\Sigma_u^+) + He + e \quad k = 7.6 \cdot 10^{-11}\ cm^3s^{-1} \quad (c)$$

- charge transfer reactions

$$He_2^+ + N_2 \rightarrow N_2^+(B^2\Sigma_u^+) + 2He \quad k = 8.3 \cdot 10^{-10}\ cm^3s^{-1} \quad (d)$$

where the helium molecular ions are formed in three-body collisions with He ions

$$He^+ + 2He \rightarrow He_2^+ + He \quad k = 1.5 \cdot 10^{-31}\ cm^6s^{-1} \quad (e)$$

- electron impact ionization

$$N_2 + e_{fast} \rightarrow N_2^+(B^2\Sigma_u^+) \quad \sigma_{e,i}(E) \quad (f)$$

The rate constants for the above-mentioned processes are from [Pou-82] and refer to room temperature (300 K).

In the microdischarge the intensity of the $N_2^+$(B-X) band is rather high, compared for example to similar spectra obtained in dielectric barrier discharges (DBD), where the $N_2$(C-B) emission was found to be dominant [Bib-01a]. Actually the quenching of the $N_2^+$(B-X) state due to He atoms is about 40 times higher than for the $N_2$(C-B) state, which means that in the MSE discharge nitrogen is mostly ionized. This suggests a larger density of atoms on metastable states and/or higher electron energies and electron densities in the MSE sustained discharge in respect to DBD.

In Ar-$N_2$ mixtures, only the second positive system of nitrogen $N_2(C^3\Pi_u) \rightarrow N_2(B^3\Pi_g)$ appears with high intensity but no emission from the first negative system $N_2^+(B^2\Sigma_u^+) \rightarrow N_2^+(X^2\Sigma_g^+)$ is present.

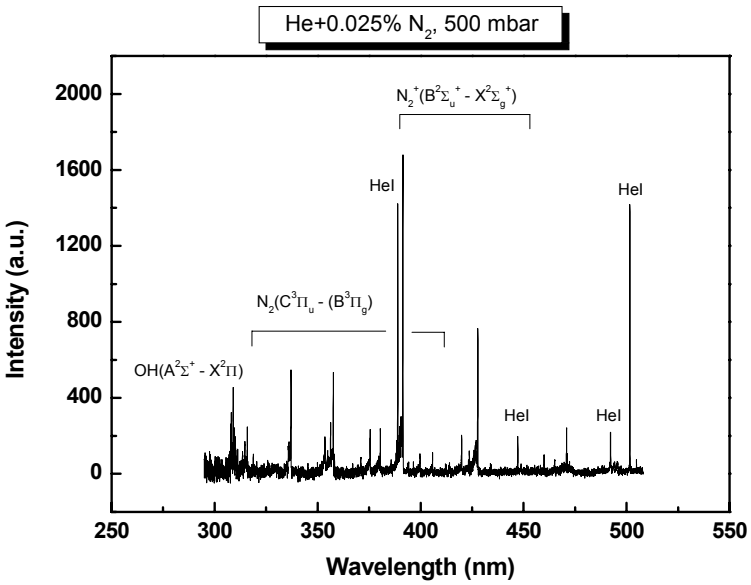


(a)

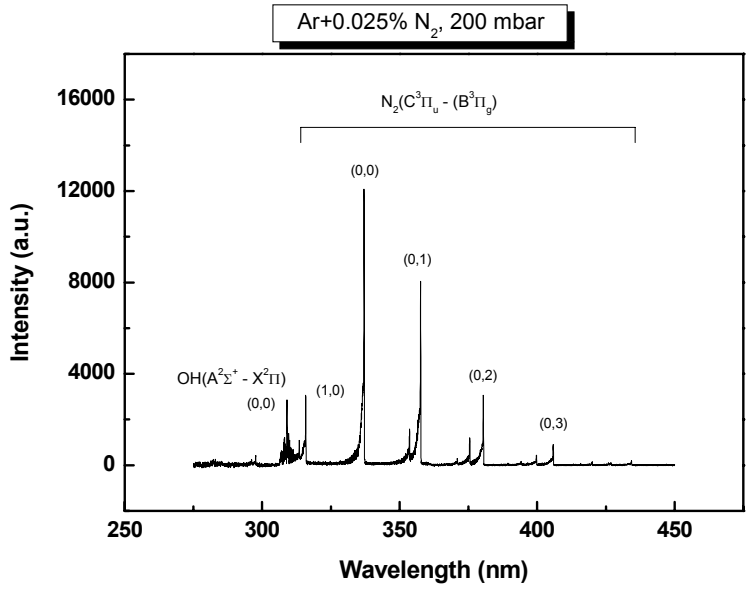


(b)

**Figure 4.5:** Emission spectrum of a microdischarge in He+0.025% $N_2$ at 500 mbar (a) and in Ar+0.025% $N_2$ at 200 mbar (b).

For Ar-$N_2$ discharge gas the $N_2(C^3\Pi_u)$ electronic state of nitrogen is excited very efficiently in reactions with Ar atoms on metastable states [Set-01] which are present in a large number in the microdischarge:

$$A^* + N_2(X^1\Sigma_g^+) \rightarrow N_2(C^3\Pi_u) + Ar \qquad k = 3.6\cdot10^{-11}\ cm^3s^{-1} \quad (g)$$

for the $1s_5$ respective $1s_3$ metastable level ($Ar(^3P_{2,1})$) $\qquad k = 0.8\cdot10^{-11}\ cm^3s^{-1}$

In Ar-$N_2$ plasma the molecular nitrogen ions are formed in the ground state or in the first excited state (metastable) by charge transfer between Ar ions and nitrogen molecules [Smi-81]:

$$Ar^+ + N_2 \rightarrow N_2^+(X^2\Sigma_g^+, A^2\Pi_u) + Ar \qquad k = 1\cdot10^{-11}\ cm^3s^{-1} \quad (h)$$

Because the $N_2^+(B^2\Sigma_u^+)$ state is not excited in a direct process and the probability of stepwise excitation by ions or slow electrons is low, no emission from this electronic state is observed in the spectra.

Besides the above-mentioned transitions, the emission band of OH radicals $OH(A^2\Sigma^+)\rightarrow OH(X^2\Pi)$ around 310 nm was detected in both gases. The OH radicals are formed via excitation/ionization of water molecules, adsorbed on the microstructure or on the walls, by metastable atoms diffusing from the discharge area. The reaction channels are the following:

$$Ar^* + H_2O \rightarrow OH(A^2\Sigma^+)$$

$$He^* + H_2O \rightarrow H_2O^+ + He$$

$$H_2O^+ \rightarrow H + OH(A^2\Sigma^+)$$

For the estimation of the vibrational temperature the relative intensities of different band heads were compared using Eq.4.17 and considering that $I_{v',v''}$ is proportional to $\exp(-E_{v'}/kT_v)$. In Table 4.2 are given the transitions used and their molecular constants taken from [Rou-93] and [Lau-92].

The energy of the upper vibrational levels v' was calculated from Eq. 4.15 for v' = 0 ÷ 4 with the equilibrium molecular constants of the $N_2(C^3\Pi_u)$ electronic state taken as [Rou-93]:

$$\omega_e = 2047.7928\ cm^{-1},\ \omega_e x_e = 28.9421\ cm^{-1},$$

$$\omega_e y_e = 2.24537\ cm^{-1},\ \omega_e z_e = -0.551196\ cm^{-1}.$$

| $N_2(C^3\Pi_u) \rightarrow N_2(B^3\Pi_g)$ | | | |
|---|---|---|---|
| Vibrational sequence | Band v'-v'' | Band origin ($cm^{-1}$) | A ($10^6 \cdot s^{-1}$) |
| $\Delta v = -2$ | 0-2 | 26289.441 | 3.532 |
| | 1-3 | 26636.472 | 4.885 |
| | 2-4 | 26958.860 | 4.045 |
| $\Delta v = -3$ | 0-3 | 24642.031 | 1.086 |
| | 1-4 | 25018.044 | 2.375 |
| | 2-5 | 25369.486 | 3.081 |
| | 3-6 | 25683.388 | 2.972 |

**Table 4.2:** Vibrational sequences used for the estimation of the vibrational temperature.

Displaying the relative intensity ratio multiplied by the appropriate factors as a function of the energy difference of the upper levels in a semi-logarithmic plot, the vibrational temperature can be extracted from the reciprocal of the slope obtained. The result obtained for an Ar-$N_2$ discharge is shown in Fig. 4.6.

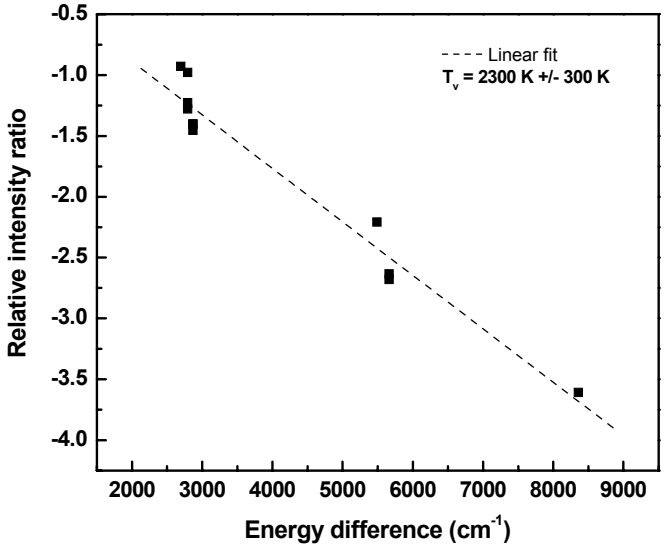


**Figure 4.6:** Vibrational temperature in a MSE sustained discharge in Ar-$N_2$ at 300 mbar.

The vibrational temperature obtained is about 2000 K, as expected being lower than the electron temperature estimated in the previous section.

In the microdischarge, only the lower vibrational levels v < 7 are significantly populated. For the lower vibrational levels, vibration-translation energy transfer is hindered because the period of molecular vibrations is shorter than the interaction time between heavy particles [Bib-87]. The vibration-vibration energy transfer and electronic-vibrational energy transfer in collisions with free electrons are much more efficient. As a result, the vibrational levels tend to follow a quasi-equilibrium distribution at a characteristic temperature $T_v$ [Lau-93]. Such a distribution holds usually for the lowest vibrational levels since for higher levels the vibration-translation energy transfer increases due to the larger period of molecular vibrations and consequently these levels tends to come in equilibrium with the gas. The vibrational temperature $T_v$ equals neither the gas (translation) temperature $T_g$, nor the free electron temperature $T_e$ and usually holds:

$$T_g < T_v < T_e \tag{4.18}$$

Another aspect that has to be underlined is related to the time needed for vibrational relaxation. This time is at least 10 times larger than the rotational relaxation time, which is about 15 ns for the nitrogen molecule. It means that the vibrational relaxation time is in the order of 1 μs. Due to quenching processes, the effective lifetime of the $N_2(C^3\Pi_u)$ state is even smaller than its radiative lifetime, which was found to be 37 ns [Pan-98]. When the vibrational relaxation is not complete the distribution of the vibrational levels is not an equilibrium distribution characterized by a thermodynamic temperature. The distribution is rather determined by the excitation (chemical) processes.

### 4.5.2. Rotational temperature

The vibrational bands consist of rotational lines which corresponds to transitions between upper levels characterized by $v'$ and $J'$ (vibrational and rotational quantum numbers) and lower levels characterized by $v''$ and $J''$. Assuming that the rotational levels are in thermodynamic equilibrium at a rotational temperature $T_r$ the population density of these levels is given by the Boltzmann law:

$$n_{v,J} = n\frac{g_J}{Q_v}\exp(-\frac{E_J}{kT_r}) \tag{4.19}$$

where $Q_v$ is the partition function of the vibrational level and can be calculated using the relation given in [Her-50]. $E_J$ is the energy of the rotational level J (given by Eq. 4.16) and

$g_J$ is its degeneracy ($g_J$ =2J+1). Taking into account the degeneracy due to the nuclear spin, the statistical weight have to be multiplied with a factor Φ [Rom-75].

The intensity of a rotational line is proportional with the population density of the upper level and with the spontaneous emission coefficient, similar to Eq. 4.17. The radiative transition probability can be written as:

$$A_{v'J'v''J''} = \frac{64\pi^2 \nu_{v'v''}^3}{3hc^3(2J'+1)} \cdot S_{mv''J''\Lambda''}^{mv'J'\Lambda'} \tag{4.20}$$

where $S_{mv''J''\Lambda''}^{mv'J'\Lambda'}$ is called the line strength which can be decomposed as the product of three terms: the square of the electronic transition moment, the Franck-Condon factor and the Hönl-London factor. These three terms correspond to the probability of a transition between the two electronic levels, the two vibrational levels and the two rotational levels, respectively.

The intensity distribution between different rotational lines is related to the temperature. From the absolute intensity of the rotational lines or plotting the intensity of different rotational lines in a Boltzmann diagram one can estimate the rotational temperature as follow:

$$\ln\left(\frac{I_{J'J''}^{\exp}}{g_{J'}\nu_{J'J''}^3 S_{J'J''}}\right) \sim -\frac{E_{J'}}{kT} + C \tag{4.21}$$

In order to resolve the rotational lines, a high-resolution spectrograph is required. A double grating spectrograph (0.85 focal length) supplied with a CCD camera was used, allowing a spectral resolution of 0.022 nm. Measurements were performed on a MSE sustained discharge operated in He-$N_2$ mixtures. Although most of the measurement performed in this work deals with argon discharges, for these investigations helium was chosen. The reason is that in Ar-$N_2$ mixtures the very effective energy transfer between the Ar metastables and the $N_2(C^3\Pi_u)$ electronic state perturbs the rotational distribution and leads to a measured rotational temperature higher than the real one. The estimation of the temperature in Ar-$N_2$ mixtures can be done using other electronic transition, e.g. $N_2^+(B^2\Sigma_u^+) \rightarrow N_2^+(X^2\Sigma_g^+)$. In the MSE plasma in Ar-$N_2$ mixtures this transition was not detected even if the partial pressure of $N_2$ was increased up to 2.5%.

The transitions used are the second positive system of nitrogen $N_2(C^3\Pi_u) \rightarrow N_2(B^3\Pi_g)$ and the first negative system of nitrogen ion $N_2^+(B^2\Sigma_u^+) \rightarrow N_2^+(X^2\Sigma_g^+)$. A step-by-step procedure was used to determinate the rotational

temperature. The experimentally measured spectrum is compared with calculated spectra for a set of test temperatures $T_i$ and the best case of agreement is chosen (mean square of the difference between $I_{exp}(\lambda,T)$ and $I_{calc}(\lambda,T_i)$ not larger than the experimental errors). Starting from molecular constants and taking into account the most probable excitation/destruction mechanisms, synthetic spectra can be produced. Here the calculations have been performed for a spectral resolution of 0.022 nm and assuming equilibrium conditions. The emission spectrum of $N_2(C_0\text{-}B_0)$ and the calculated one are presented in Fig. 4.7, the best case of agreement being obtained for a rotational temperature of 370 K.

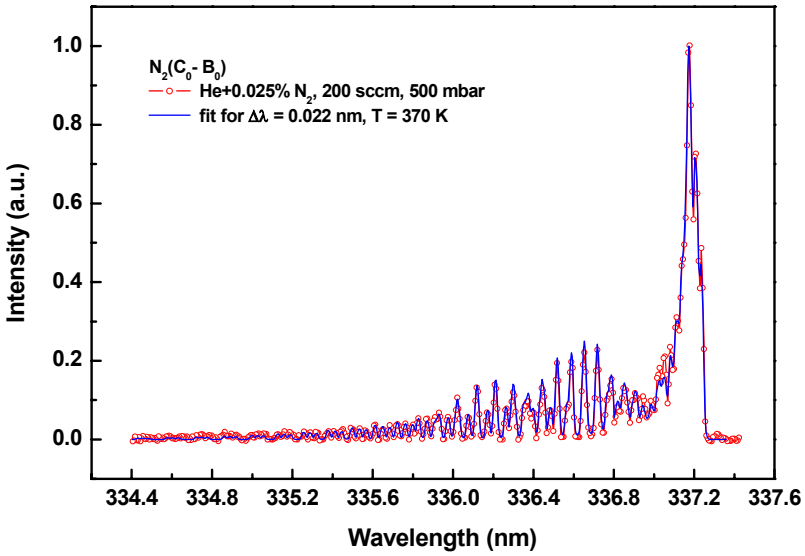


**Figure 4.7:** $N_2(C_0 \rightarrow B_0)$ emission spectrum measured in a He-$N_2$ mixture (circle) and fit (line).

The emission spectrum of $N_2^+(B_0\text{-}X_0)$ and the calculated one are presented in Fig. 4.8. The best fit was obtained for a rotational temperature of 476 K and it can be seen that the agreement between the calculated and the measured spectra is very good. In Fig. 4.8 can be noticed the alternation in the intensity of consecutive rotational lines. This intensity variation appears by homonuclear molecules as a consequence of the nuclear spin of the atoms. In the following measurements only the intensity of the rotational lines with odd quantum numbers was analyzed, the intensity of the transitions from even levels being twice so small.

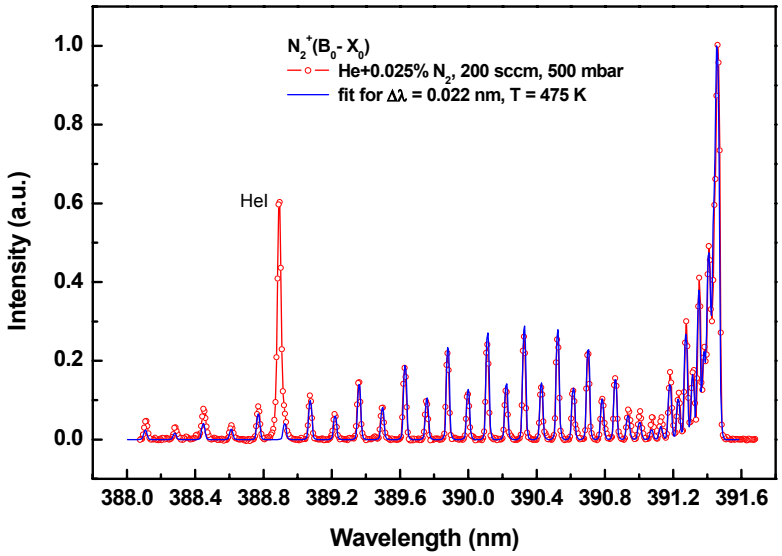


**Figure 4.8:** $N_2^+(B_0 \rightarrow X_0)$ emission spectrum measured in a He-$N_2$ mixture (circle) and fit (line).

Plotting in a semi-logarithmic scale the intensity of different rotational lines as a function of the energy of the upper level (Boltzmann diagram) one can estimate the rotational temperature. Under equilibrium conditions this plot has to be a straight line with the slope yielding $1/T_{rot}$. Due to the small intensity of the rotational lines and the overlapping of different branches this procedure was not applied for the $N_2(C_0\text{-}B_0)$ transition. In the case of $N_2^+(B_0\text{-}X_0)$, the P (J'' = J'+1) and R (J'' = J'-1) branches were analyzed from 389 nm to 391.4 nm. The resulting Boltzmann plot is presented in Fig. 4.9. As it can be seen, the rotational temperature depends on the quantum number of the rotational level in the B-state [Fat-00]. For rotational levels up to n' = 13 the estimated temperature is about 450 K (a so called "cold group") and for rotational levels with quantum number n' > 15 the rotational temperature is about 700 K (a "hot group"). The rotational temperature measured in this way assumes equilibrium distribution of the rotational levels. One can estimate the rotational temperature using the absolute line intensities of the rotational lines. The temperature obtained by this method was found also to be dependent on the quantum number of the rotational level in the upper state and the values are about 360 K for rotational levels with small quantum numbers and 900 K for states with large quantum numbers.

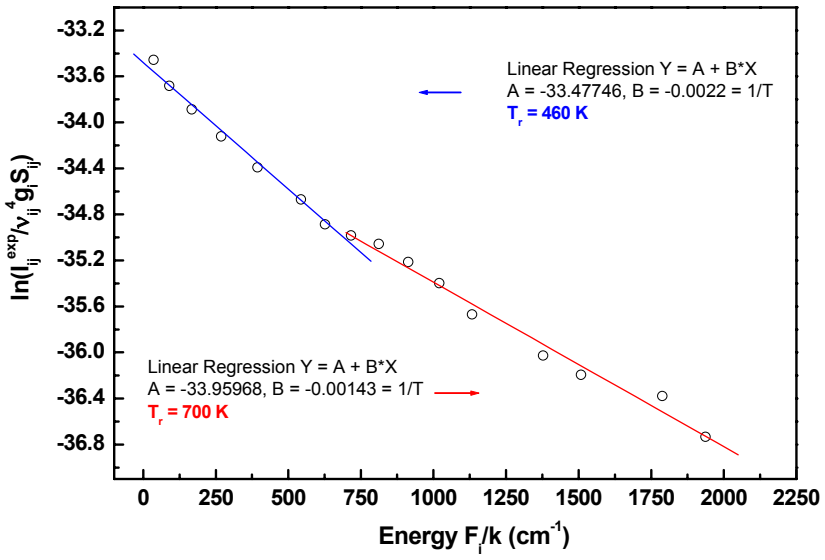


**Figure 4.9:** Measured intensity of rotational lines versus the energy of the upper rotational level.

As the translation-rotation energy transfer is favorable and occurs very rapidly, the rotational levels tend to follow an equilibrium distribution characterized by a temperature $T_r$ close to the kinetic (translation) temperature of the gas $T_g$ [Bib-87]. Diatomic molecules like $N_2$ or $N_2^+$ could be successfully used for gas temperature estimation at high pressures. As the time needed for rotational relaxation is very short (ns) the measured temperature gives the instantaneous gas temperature in the discharge area where the emitters are created.

The rotational temperature measured using the $N_2(C^3\Pi_u) \rightarrow N_2(B^3\Pi_g)$ transition gives the ambient gas temperature, not the temperature in the discharge active area because the upper state $N_2(C^3\Pi_u)$ is excited mostly via pooling reaction of the nitrogen molecule on the $N_2(A^3\Sigma_u^+)$ metastable state (reaction a). Due to diffusion of the long-living $N_2$ metastable molecules this process, which is a slow one, takes place in the bulk gas far from the inner region of the hole. The rotational relaxation can be considered complete since the effective lifetime of the $N_2(C^3\Pi_u)$ state was found to be about 5 ns in our experimental conditions, while the rotational relaxation time is about 1 ns. In this case the rotational distribution in the emission spectrum correspond to the gas temperature.

The temperature in the bulk gas was found to be 360 K ± 10K, which means slightly above room temperature.

The temperature measured by means of the $N_2^+(B^2\Sigma_u^+) \rightarrow N_2^+(X^2\Sigma_g^+)$ transition has to be analyzed more in detail. The dominant excitation channels of the upper state $N_2^+(B^2\Sigma_u^+)$ are Penning ionization involving $He^*$ metastables (reaction c) and charge transfer involving $He_2^+$ molecular ions (reaction d). The effective lifetime of He atoms on metastable states in the MSE discharge is in the μs range. Therefore, they may leave the discharge area, diffuse towards colder zones and ionize the $N_2$ neutrals. As discussed before, it is expected that the rotational distribution of the $N_2$ ions produced in this way to correspond more to the ambient gas temperature, than to the temperature in the discharge area inside the MSE hole. The $N_2$ ions produced by charge transfer are created inside the "hot" discharge area where the $He_2^+$ are present, and therefore their rotational distribution will reflect the local temperature which can be as high as 700-900 K.

Another aspect that has to be considered is the effective lifetime of the $N_2^+(B^2\Sigma_u^+)$ state. This depends on the rates of the emission process $N_2^+(B^2\Sigma_u^+) \rightarrow N_2^+(X^2\Sigma_g^+)$ and the quenching processes with ground state nitrogen molecules, helium atoms and electrons. The electron quenching can be neglected, as well as the effect of $N_2$ due to its small partial pressure. Under our experimental condition the effective lifetime of the $N_2^+(B^2\Sigma_u^+)$ state was estimated to about 1 ns. When quenching processes are taken into account the rotational relaxation time decreases from 62 ns to about 1 ns. Due to the fact that the effective lifetime and the rotational relaxation time are comparable, it is possible that the rotational relaxation of the $N_2^+(B^2\Sigma_u^+)$ state is not complete, and therefore the rotational temperature measured would be an excitation temperature. The two temperatures obtained in Fig. 4.9 can be explained as well in this way.

The excitation/ionization of nitrogen molecules by electron impact (reactions b and f) was not discussed because these processes require highly energetic electrons (electron energy above 10 respectively 18 eV), which are present only in small concentration in the discharge.

## 4.6. Discussion and conclusions

The light emitted from the microdischarge is dominated by the spectrum of the gas, a typical behavior for a glow discharge. The relative intensity ratio of ionic to atomic lines was found to be pressure independent. This suggests a constant ionization grad over the pressure range investigated, which implies that the electron number density should augment when the pressure increases.

The electron temperature measured in the MSE sustained discharge is comparable with the electron temperatures experimentally and theoretically estimated for other high-pressure plasma sources, but is lower than expected. Generally, the errors in calculating the electron temperature from relative intensities ratios can arise from the measurement of the integral over the line profile (the line intensity), from uncertainty in the transition probabilities and from a non-Maxwellian velocity distribution of the free electrons. It is well known that in classical hollow cathode discharges the electron energy distribution function is not Maxwellian. Experimental studies [Bor-77] have shown that the electron distribution function presents an excess of slow electrons (energy below 3 eV) comparing to a glow discharge but also a larger number of highly energetic electrons (energy above 16 eV). Detailed investigations [Gil-77] on the electron energy distribution in the negative glow have revealed the presence of a second peak in the electron distribution function at energies above 10 eV. Even if this investigations were performed at relatively low pressure, such a behavior can be expected also in the microdischarge. Another aspect, which has to be discussed, is that calculating the electron temperature in this way it was assumed that the excited levels are populated by electron impact. This is not necessary true in high-pressure plasmas where cumulative processes, photo-excitation and three body collisions are playing an important role. Due to this processes the population density of different levels may not follow the equilibrium (Boltzmann) distribution. Even if highly excited levels are chosen, which usually tend to be in equilibrium with the free electrons, the temperature obtained under these conditions does not correspond to the real electron temperature. Nevertheless by choosing ionic lines the accuracy of the temperature estimation can be improved.

In respect to the estimation of the gas temperature using molecular spectra, it can be concluded, that due to different excitation mechanisms the excited particles in the

plasma may have different temperatures [Bib-01b], not necessarily equal to the temperature of the bulk gas. Radicals or molecular ions, which are produced in the discharge directly in an excited state, deposit a part of the formation energy in the form of rotational energy. In this case the rotational temperature measured using this species does not reflect the gas temperature, if the relaxation of the rotational levels is not complete. But usually at high pressures, due to the very fast relaxation times, the rotational distributions are very useful tools for gas temperature measurements.

Speaking about plasma emission has to be underlined that light emitted from the discharge can be used as well for lightning, surface treatment or sterilization, not only for spectroscopical purposes.

# CHAPTER 5
# DIODE LASER ATOMIC ABSORPTION SPECTROSCOPY

## Introduction

Absorption spectroscopy is a well establish method in the study of discharge plasmas due to the fact that as every specie has its own emission spectrum, it posses also an absorption spectrum. Main characteristics as absolute number density of excited atoms in the discharge, gas temperature and electron number density can be measured by this method. By studying the decay of the excited species in the afterglow plasma, the apparent lifetime of the excited states can be calculated and the relative importance of different production/loss processes in the plasma can be determined. Atoms in the ground state or on excited levels, as well as molecules can be investigated by means of absorption spectroscopy using suitable radiation sources with narrow or broadband, depending on the type of absorber.

In the case of high-pressure gas discharges this method is not commonly used, like in low-pressure discharges, because most of these plasma sources operating at elevated pressures have relatively small sizes, which implies a short absorption path. Otherwise, this method offers some advantages in comparison with emission spectroscopy or probe technique. The instrumental broadening of the spectral lines may be a problem in emission spectroscopy, for high-resolution measurements expensive equipment being required. The instrumental broadening is avoided performing absorption spectroscopy with narrow band lasers, like diode lasers. Absorption technique is a non-intrusive method, a low power laser as radiation source does not perturb the plasma like a probe will do. In the following diode laser atomic absorption spectroscopy performed on the MSE sustained discharge will be presented. Despite the fact that the absorption length is very small, it was possible to measure the population density of excited atoms and to calculate the plasma parameters (gas temperature and electron number density) from the analysis of the absorption line profiles. These investigations demonstrate that even in high-pressure regime absorption spectroscopy can be applied.

## 5.1. Diode lasers for optical spectroscopy

Due to the ongoing rapid progress and remarkable development of laser diodes during the last years, several new fields of physics as well as applications areas have been opened. Diode lasers are mass-produced for compact disk-players, laser printers, optical data storage systems and telecommunication equipment. Those operating in the range from 635 nm to 690 nm are replacing the traditional HeNe laser in many commercial products due to their lower cost, compact size and superior long-term reliability. Some of these laser diodes have excellent spectroscopic properties, which make them attractive radiation sources for spectral studies and spectrochemical analysis.

The diode lasers are very useful tools for spectroscopic applications due to their special properties: they are highly monochromatic and tunable light sources. In the following, the main characteristics of AlGaAs laser diodes, which emit in visible and IR wavelength range will be briefly described. More details about diode lasers regarding basic physics, properties and application fields can be found in the review articles of Camparo [Cam-85], Wieman [Wi-91] and Franzke [Fra-93]. However, semiconductor diode lasers have been steadily improved in reliability, power and wavelength coverage, while continuously decreasing in price.

### 5.1.1. Construction and operation of a diode laser

A semiconductor diode laser consists of p-type and n-type semiconductor layers that are separated by a thin active layer in which laser action takes place. The typical construction of a diode laser is shown in Fig. 5.1.

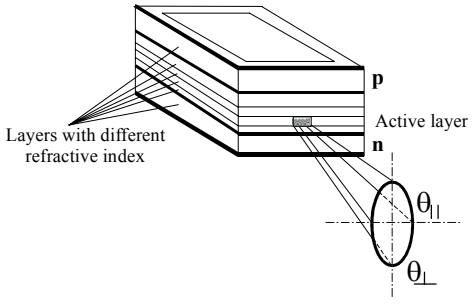


**Figure 5.1:** Typical construction of a diode laser.

In all laser diodes, the mechanism of light emission involves the recombination of electrons with holes within the region of the active layer when passing an electric current ("the injection current") through the p-n junction. The photons produced have an energy equal with the difference between the energy levels of electrons and holes, which is essentially determined by the bandgap of the active layer. The mole fraction of Al in the p and n-type cladding layers is greater than in the active layer and since the refractive index is a decreasing function of the Al concentration [Cas-78], the active layer acts as a dielectric waveguide for the laser light.

Index-guided AlGaAs lasers typically produce single-mode (spatial and longitudinal) output powers of tens of mW with just the cleaved facets of the semiconductor serving as laser's mirrors [Wie-90].

### 5.1.2. Spectral emission of diode lasers

The spectral emission of diode lasers consists of a main component characterized by a Lorentzian profile and some additional components with much lower intensity. Usually the main component is about 100 times stronger than the side modes and has a full width at half maximum between 10 and 100 MHz. The line width is at least 10 times less than the atomic line widths that are observed at room temperature under low-pressure conditions. This feature makes a diode laser very useful for the investigation of atomic transition in discharge plasmas. The full width at half maximum of the emitted line is given by:

$$\Delta\nu_{FWHM}=(h\nu/8\pi P_0)L^{-2}\ln(R)[\ln(R)-\alpha L]v_g^2 n_{sp}(1+\alpha^2) \qquad (5.1)$$

where h is the Planck constant, $\nu$ the central frequency, L the laser cavity length, $P_0$ is the output power of the diode, $n_{sp}$ is the spontaneous emission factor due to the fact that population inversion is not complete and shows the losses in the laser cavity, $v_g$ is the group velocity and $\alpha$ is the ratio between the real part and the imaginary part of the refractive index.

The relaxation side modes are situated a few hundreds of GHz far from the main component and their presence is mainly due to the fact that the refractive index depends

on the population inversion. When a photon is emitted, population inversion is produced also at damping resonance relaxation frequencies [Cam-85].

### 5.1.3. Wavelength tunability by current or temperature

The laser wavelength is determined primarily by the bandgap of the semiconductor material and then by the diode temperature and by the operation current. The optical output power of a diode laser as a function of the injection current and temperature is presented in Fig. 5.2a. This shows the onset of laser action at the threshold current and the increase of the threshold with the temperature. The current density required to achieve laser operation (threshold current density) is typically in the region of several thousand A/cm$^2$ but, as these devices are very small, the actual current required is often below 100 mA.

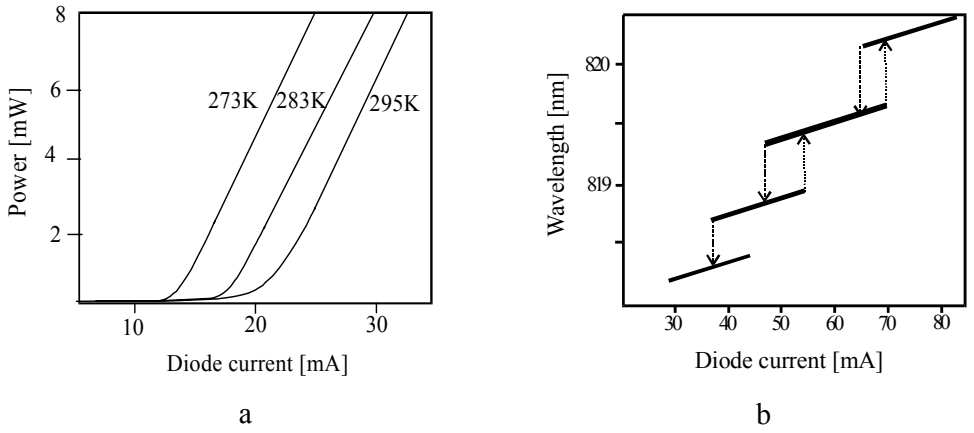


**Figure 5.2:** Typical output power (a) and output wavelength (b) of a diode laser versus injection current.

A diode laser allows single mode operation and continuous tuning over the absorption line profiles, the tunability with current or temperature being the most important property of a diode laser that is used by the investigation of atomic transitions. The mode structure of a laser diode it is characterized by regions of continuous tunability (modes) followed by mode hopes. Usually the mode hopes are connected with wavelength gaps in the tuning range [Fra-93]. For most applications it is easy to implement current tunability at a given diode temperature. The wavelength coverage on an oscillation mode

is a few tens of pm, depending on the intrinsic properties of the diode laser. Without using specific optical feedback, the tunability of a commercial laser diode is covering a few nm. When needed, additional techniques of optical feedback can increase the working range also over the mode hopes [Zyb-97].

### 5.1.4. Polarization

Because the transversal dimension of the active region of a diode laser is much smaller than the lateral dimension, the laser's active region can be considered as a slab dielectric waveguide in which the lateral structure of the waveguide is taken as infinite and uniform [Yar-76]. In such a structure there are two spatial field patterns that can be distinguished, the TE and TM modes. The polarization results from a distinction between the threshold conditions for these modes. In a single-mode diode laser the emission is polarized in the direction parallel to the junction plane. The polarization results because TE modes, with their electric field oscillating parallel to the junction plane have a lower threshold for lasing. In practice the laser diode emission is not completely linearly polarized and this is due to the defects in the crystal. The polarization of the laser beam is very important in experiments involving frequency doubling and frequency mixing techniques.

### 5.1.5 Typical mounting of a laser diode

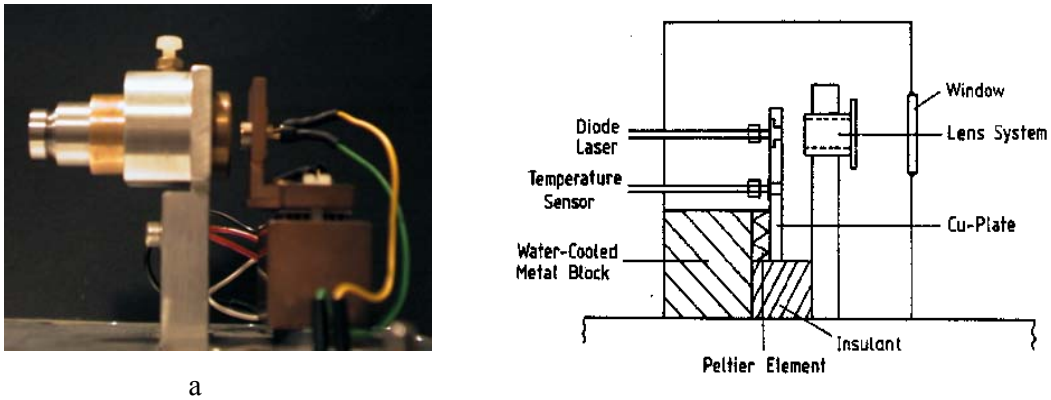


a b

**Figure 5.3:** The diode laser arrangement (a) used in our measurements and schematic view [Fra-93] of a diode laser housing (b).

The experimental arrangement used, together with a schematic view of a typical laser diode housing are presented in Fig.5.3a and b. Since the cross-sectional dimensions of the laser's active region are not much larger that the lasing wavelength, the laser beam is highly divergent and has to be collimated or focused, depending on application. Most laser diodes require a collimating lens with large numerical aperture.

It has to be underlined that the diode laser is mounted on a water-cooled copper block and its temperature is controlled by a Peltier element. To avoid condensation of water on cooled laser diodes, the housing has to be filled with dry nitrogen or dry air.

## 5.2 Modulation techniques used in atomic absorption spectroscopy

Modulation techniques are frequently used in absorption spectroscopy when an increased sensitivity of the measurements ($10^{-7}$ a.u.) is desired because they increase the signal to noise ratio and correspondingly the detection limit. These techniques imply the modulation of the laser wavelength, the modulation of the plasma, or both. Different modulation techniques commonly used in atomic absorption spectroscopy are briefly presented below.

The Wavelength Modulation (WM) technique [Sil-92], [Bom-92] comprises of modulating the laser frequency (or the wavelength) at one frequency *f* prior to interaction with the absorbing atoms and to perform phase sensitive detection. The 2f-detection, with a lock-in amplifier whose reference signal is at twice the modulation frequency, is most commonly used.

Plasma modulation (PM) technique coupled with phase sensitive detection is a very well known method in analytical atomic spectroscopy where absorption values less than $10^{-2}$-$10^{-4}$ a.u. has to be measured. This technique improves significantly the sensitivity of the absorption measurements. The plasma is switched *on* and *off* with a frequency *f* and the excited species in the plasma behave in the same way. The detection is performed with a phase sensitive amplifier, usually a lock-in amplifier at the modulation frequency. The modulation of the plasma not only increases the sensitivity of the measurements, but also suppresses wavelength dependent changes of the laser intensity, such as interference effects in the optical path. But there is also a disadvantage of this method. The emission of the plasma, which appears also at the modulation

frequency, can produce a certain background in the absorption signal. In order to reduce the effects of the plasma emission, interference filters or gratings can be used.

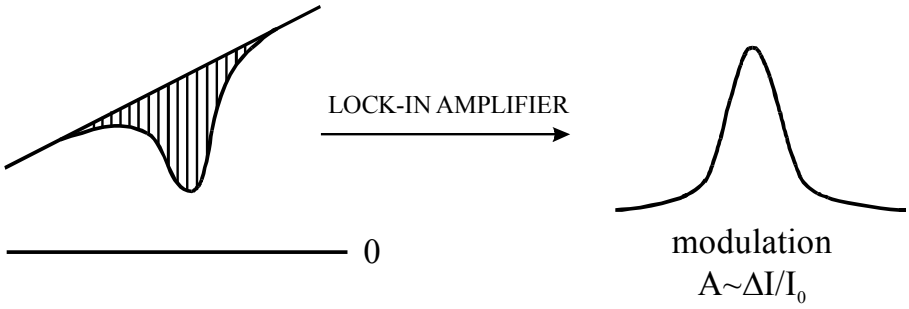


**Figure 5.4:** Schematic view of the principle of Plasma Modulation technique

Double Modulation technique is a combination of WM and PM techniques and consists in the modulation of the laser wavelength and of the absorbing species in the plasma with detection on the sum or difference of these two frequencies.

When performing diode laser atomic absorption spectroscopy on the MSE discharge, especially at high pressures where the absorption length decreases, the direct absorption signal was to low to be measured directly and was necessarily to use a modulation technique to increase the detection limit. The Wavelength Modulation technique would not be advantageous in our case because of the noise induced by the interference due to the small dimensions of the hole. The appropriate method to be used in our measurements is the Plasma Modulation technique.

## 5.3. Experimental arrangement for absorption spectroscopy

The populations of the excited argon atoms on resonance and metastable levels, which are produced in the MSE plasma were studied using diode laser atomic absorption spectroscopy (DLAAS). The MSE sustained discharge was investigated through the hole (from anode to cathode) as well as above the cathode surface. These two different measurements provide information about the integral number density of the excited states in the plasma channel and about the spatial distribution of these excited atoms above the cathode.

### 5.3.1. Discharge configuration and DLAAS set-up

A single MSE sustained discharge was DC operated in the normal glow mode at 0.5 mA in pure argon for pressures between 50 and 400 mbar and constant gas flow of 100 sccm through the chamber. The microstructure used for this study had a total length of 300 μm, the diameter of the hole was 300 μm, the electrodes are 130 μm thick copper while the insulator is 50 μm thick Kapton.

The investigations were focused on the first four excited argon levels ($1s_i$, i=2÷5, Paschen notation). For these measurements, 3 single-mode diode lasers (DL) were used as radiation sources. Their operational parameters are presented in Table 5.1.

| Central wavelength | Transition | DL operation parameters |
|---|---|---|
| 801.699 nm | $1s_5$ - $2p_8$ | Sharp/ 12.57°C, 67 mA |
| 800.838 nm | $1s_4$ - $2p_6$ | Sharp/ -1.75°C, 70 mA |
| 772.633 nm | $1s_3$ - $2p_2$ | Sharp/ 12.51°C, 65 mA |
| 826.680 nm | $1s_2$ - $2p_2$ | Hitachi/ 2.5°C, 95 mA |

**Table 5.1:** The diode lasers used as radiation sources for DLAAS and the operation parameters corresponding to the central wavelength of each studied transition.

A diode laser driver (Profile Optische ITC 502) was used to supply the diode laser current and also to control and stabilize its temperature. A classical absorption experiment schematically viewed in Fig.5.5 was used to investigate the microdicharge through the hole of the MSE.

The diode laser beam is passing through the discharge channel (300 μm diameter, 300 μm length) and is detected by a fast photodiode (Si PIN S6036) placed far enough from the plasma (0.5 m) to make shore that the light emitted from the discharge does not reaches the detector. Before passing the discharge the radiation was attenuated by neutral filters (NF) in order to avoid the saturation of the optical transition. By varying the diode laser current the wavelength was continuously scanned across the absorption line with very low frequency (7-8 mHz) and was measured with a wavemeter (Burleigh WA-10, spectral resolution 1 pm). Simultaneously, a small part of the laser radiation was separated

by a beam splitter (BS) and directed onto a confocal Fabry-Perot interferometer (free spectral range FSR=2 GHz) that gives the frequency calibration for the line profiles. The transmitted signal from the photodiode (PH) and the interference fringes were simultaneously recorded on a 2-channel oscilloscope (Tektronix TDS 360, 200MHz, 1GS/s).

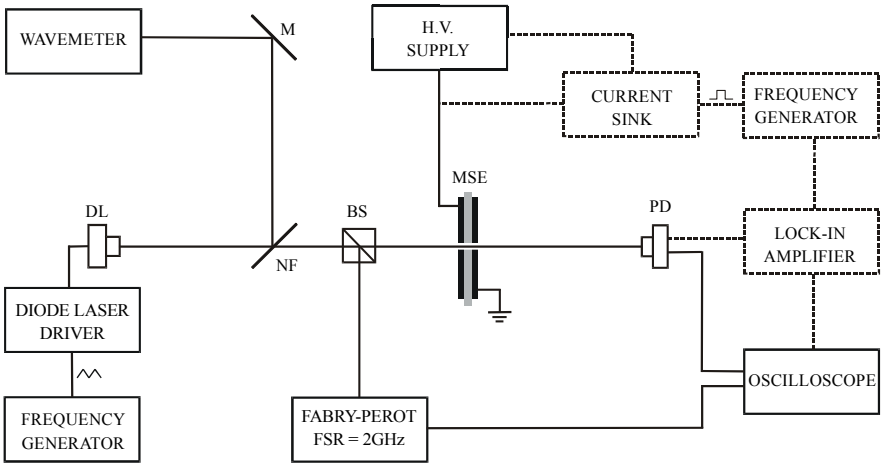


**Figure 5.5:** Experimental arrangement for diode laser absorption measurements through the MSE discharge channel.

Due to the small dimensions of the MSE, when passing the laser beam through the hole diffraction patterns are observed at the detector, inducing noise in the transmitted signal. Taking into account that the intensity of the central maximum is 84% from the total intensity, only the zero order of diffraction has been selected from the total transmitted beam. Fig. 5.6 presents for exemplification the diffraction pattern obtained when the laser beam is passing through the hole of the microstructure.

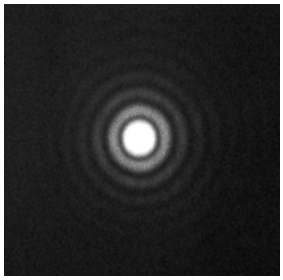

**Figure 5.6:** Diffraction pattern obtained when passing the laser beam through the MSE hole.

As it was shown in Chapter 2, the active volume of the microdischarge is not confined between the cathode and the anode but especially at relatively low pressures (50-200 mbar), the discharge expands out of the hole at the cathode. Side-on investigations at the cathode allowed us to measure the distribution of the excited atoms. For space resolved measurements above the cathode surface, a set-up similar with that one used in [Kun-01] was build-up, which is presented in Fig.5.7.

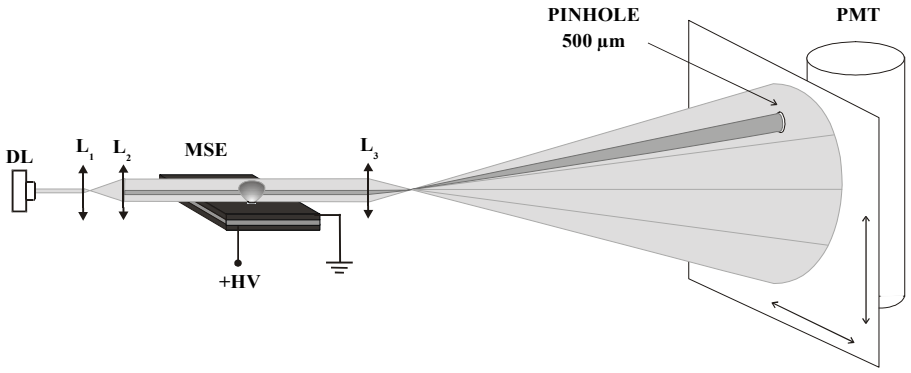


**Figure 5.7:** Experimental set-up for spatially resolved absorption measurements above the cathode surface.

The microstructure was placed horizontally with the cathode at the upper side and the collimated laser beam (with an area of 50 $mm^2$) was directed parallel to the cathode surface through the plasma volume which extends out of the hole. A lens with 10 cm focal length placed after the discharge magnifies the laser beam. A pinhole with a diameter of 500 µm placed on a XY movable system at 1 m distance from the focus of this lens collects the radiation. By changing the position of the pinhole in the expanded laser beam, the whole discharge volume was investigated. A photomultiplier (Hamamatsu R 406) with an active area of 250 $mm^2$ (PMT) was used for the detection of the transmitted signals. This arrangement enables to measure absorption signals above the cathode surface with a spatial resolution of 50 µm.

### 5.3.2 Plasma modulation

The plasma modulation technique was used when the direct absorption signal was low (absorption smaller than 2-5%), especially at higher pressures where the plasma

volume decreases. The discharge was modulated with low frequency (about 200 Hz) through a homemade current sink and the absorption signals were recorded by a lock-in amplifier (Stanford Research Systems SR830) as shown in Fig. 5.5. Where it was possible, the absorption signals were recorded both directly on the oscilloscope and with the lock-in amplifier for correlation. By varying the modulation frequency it was noticed that a constructive detection with the lock-in could be performed for frequencies higher than about 150 Hz but lower than about 800 Hz, as it can be seen in Fig. 5.8.

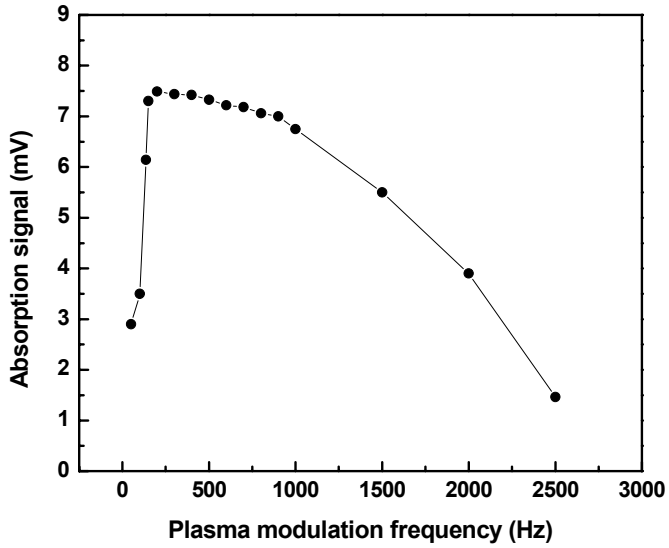


**Figure 5.8:** Dependence of the absorption signal for 801.966 Ar transition on the plasma modulation frequency.

For low frequency modulation the time period when the plasma is on is small comparing with the time constant of the lock-in amplifier and accordingly the measured signal is small. For higher frequencies the interval between two pulses is too short, the excited species are not decaying completely and the absorption signal is decreasing as a consequence of the detection method.

## 5.4. Study of the first excited levels of Ar

The first four excited states of Ar are two metastable and two resonance levels. The metastable levels are $1s_5$ and $1s_3$ (Paschen notation) at 11.55 eV and 11.72 eV above

the $1p_0$ ground state, respectively. The lifetime of the metastable levels is 55.9 s for the $1s_5$ level and 44.9 s for $1s_3$ [Fil-00]. The resonance levels are lying close to the metastable levels i.e. the $1s_4$ level at 11.62 eV and the $1s_2$ level at 11.83 eV above the ground state. The lifetime of the resonance levels is 9.5 ns and 0.24 ns for $1s_4$ and $1s_2$, respectively [Smi-99]. The metastable levels have forbidden dipole transition to the ground state, which determines their long lifetime. The resonance levels can decay to the ground state by emission of radiation at 106.666 nm ($1s_4 - 1p_0$) and 104.822 nm ($1s_2 - 1p_0$). In practice, these resonance states are also long-lived levels due to imprisonment of the resonance radiation and collisional transfer processes with the near-lying metastable states. In high-pressure discharges, as a consequence of the strong collisional coupling the lifetime of the resonance levels becomes comparable with that of the metastable levels.

In the partial diagram energy level of Ar in Fig. 5.9 are shown the investigated levels together with the corresponding transitions studied in absorption.

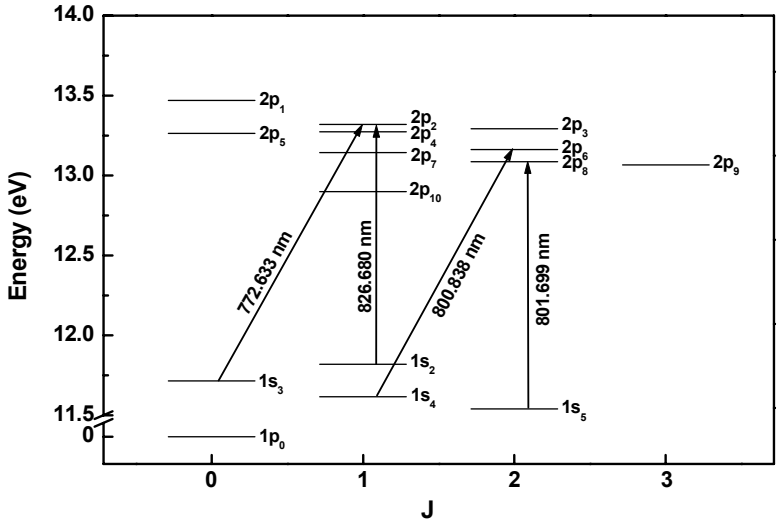


**Figure 5.9:** Partial diagram energy level of Ar and the transitions studied in these measurements.

Excited Ar atoms on metastable and resonance levels are produced in the microdischarge between the electrodes as well above the cathode due to the following processes [Gor-56]:

- electron impact excitation from ground state,

$$Ar + e_{fast} \rightarrow Ar^{*} + e, \qquad \sigma_{e,e}(E) \qquad (a)$$

- radiative recombination between ions and slow electrons,

$$Ar^{+} + e_{slow} \rightarrow Ar^{*} + h\nu, \qquad k = 10^{-11}\ cm^3 s^{-1} \qquad (b)$$

- radiative cascading from higher excited levels,

$$Ar^{**} \rightarrow Ar^{*} + h\nu \qquad (c)$$

- fast ion and fast neutral collisions,

$$Ar + Ar^{+}(Ar) \rightarrow Ar^{*} + Ar^{+}(Ar), \qquad \sigma_{i/a,e}(E) \qquad (d)$$

- dissociative recombination between molecular ions and slow electrons,

$$Ar_2^{+} + e_{slow} \rightarrow Ar^{*} + Ar \qquad k = 10^{-6}\ cm^3 s^{-1} \qquad (e)$$

- photoexcitation.

$$Ar + h\nu \rightarrow Ar^{*} \qquad (f)$$

The production rate close to the cathode is mainly given by ion and atom impact excitation because the ions and atoms have very high energy. In negative glow, electron impact excitation and the dissociative recombination should be the predominant production mechanisms.

The loss processes of the excited Ar atoms taken into account are:

- electron impact ionization from the metastable levels,

$$Ar^{*} + e_{fast} \rightarrow Ar^{+} + 2e \qquad \sigma_{e,i}(E) \qquad (g)$$

- electron impact excitation from metastable levels to higher energy levels,

$$Ar^{*} + e_{fast} \rightarrow Ar^{**} + e \qquad (h)$$

- two-body collisions with atoms in the ground state,

$$Ar^{*} + Ar \rightarrow Ar + Ar \qquad k = 2.3 \cdot 10^{-15}\ cm^3 s^{-1} \qquad (i)$$

- three-body collisions with ground state atoms leading to dimmer molecules,

$$Ar^{*} + 2Ar \rightarrow Ar_2^{*} + Ar \qquad k = 1.4 \cdot 10^{-32}\ cm^6 s^{-1} \qquad (j)$$

- energy transfer to the nearby resonance states by collisions with thermalized electrons (electron quenching),

$$Ar^{*}_{m} + e_{slow} \rightarrow Ar^{*}_{r} + e \qquad k = 2 \cdot 10^{-7}\ cm^3 s^{-1} \qquad (k)$$

- ionizing collisions between two excited atoms,

$$Ar^{*} + Ar^{*} \rightarrow Ar^{+} + Ar + e \qquad k = 6.4 \cdot 10^{-10}\ cm^3 s^{-1} \qquad (l)$$

- Penning ionization of sputtered cathode atoms,

$$Ar^{*} + M \rightarrow M^{+} + Ar + e \qquad (m)$$

- quenching doe to impurities,

$$Ar^{*} + Q \rightarrow Ar + products \qquad (n)$$

- diffusion followed by quenching at the wall,

$$D_{Ar} = 54 \text{ cm}^2\text{s}^{-1} \qquad \text{(o)}$$

Near the cathode, the high production rate is balanced by diffusion, which tends to reduce the metastable density. In the negative glow, the loss is almost completely caused by electron quenching to the resonant states and stepwise ionization. The rate constants are taken from [Bog-95], [Rho-84] and refer to room temperature.

The density $N_i$ ($i = 2 \div 5$) of the $1s_i$, level can be calculated using the relation [Mit-71]:

$$\int k_\nu d\nu = \lambda_{0i}^{\,2} \frac{g_j}{gi} \frac{A_{ji}}{8\pi} N_i \left(1 - \frac{g_j}{gi} \frac{N_j}{N_i}\right) \qquad (5.2)$$

For the i-j transition $\lambda_{0i}$ is the central wavelength, $g_i$ and $g_j$ are the statistical weights of the lower respectively upper level and $A_{ji}$ the spontaneous emission probability. The absorption coefficient $k_\nu$ is derived from the Beer-Lambert law for optically thick transitions:

$$\int_0^L k_\nu dx = k_\nu L = \ln\left(\frac{I_0}{I_\nu}\right) \qquad (5.3)$$

where $I_0$ is the transmitted radiation in the absence of absorbers, $I_\nu$ the transmitted intensity at the frequency $\nu$ in the presence of absorbers and L is the absorption length assuming a homogeneous medium. The term $\ln\left(\frac{I_0}{I_\nu}\right)$ is known as the optical depth.

In noble gas discharge plasmas the density of the upper level $N_j$ is at least three orders of magnitude less than that of the $N_i$ level in the case of 1s-2p transitions. The density $N_i$ of the lower level can be approximated by:

$$N_i = \frac{\int k_\nu d\nu}{\lambda_{0i}^{\,2} \frac{g_j}{gi} \frac{A_{ji}}{8\pi}} \qquad (5.4)$$

Equation 5.4 is very useful in calculating the number density of the excited atoms on a level because it implies only the integral over the line profile and no knowledge of the mechanisms that produce the broadening of the profile is required.

The absorption profiles were measured first with the diode laser beam passing through the plasma channel using the set-up shown in Fig. 5.5. The optical depth for all

transitions used to investigate the $1s_i$, (i = 2÷5) levels is presented in Fig. 5.10 for a pressure of 100 mbar. It has to be underlined that in the pressure range 50 - 400 mbar all measured line profiles are Voigt profiles as a consequence of Doppler and pressure broadening, with the total width of the profiles depending on the collisional broadening parameters of each transition. This subject will be discussed in detail in section 5.5.

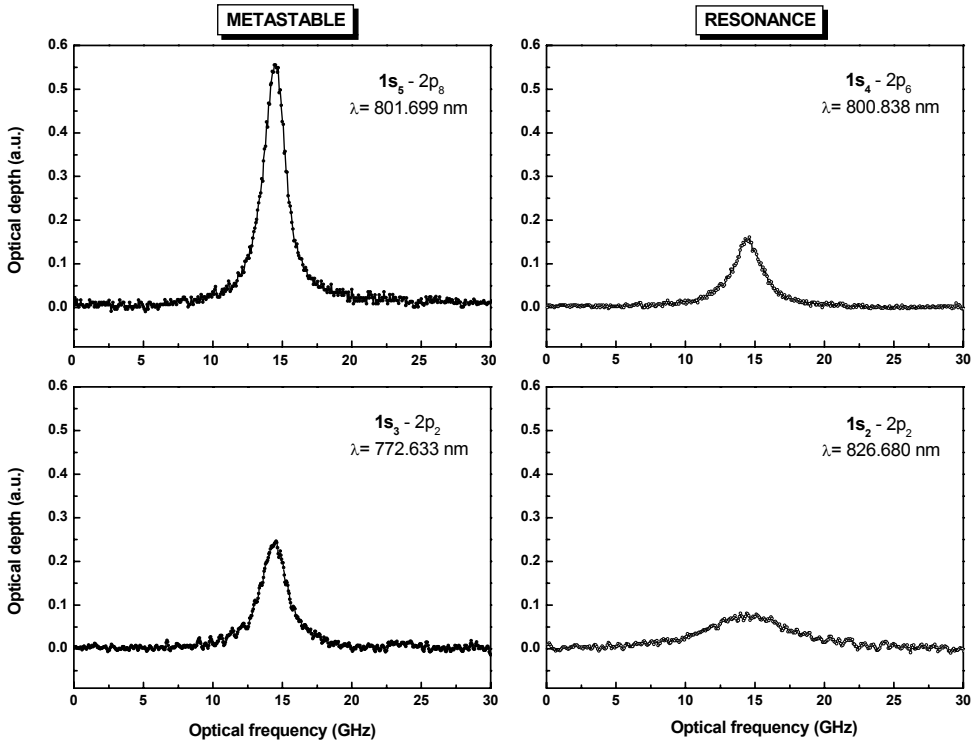


**Figure 5.10:** Optical depth for all studied transitions. On each plot is indicated the optical transition and the corresponding vacuum wavelength.

In order to calculate the integral number density of the excited states in the plasma channel, the absorption length has to be known. Small changes in the absorption length can produce significant changes in the population density of the investigated levels. Difficulties in evaluating the absorption length arise from the following reasons: i) the small dimensions of the discharge, ii) no possibility to constrict the discharge between the electrodes and to measure the population density only inside the hole, iii) the dimensions of the plasma above the cathode are changing with the pressure. The absorption length can be estimated from spatially resolved measurements above the cathode.

### 5.4.1. Distribution of excited Ar atoms above the cathode

The optical appearance of the microdischarge recorded side-on by a CCD camera gives qualitative information about the extension of the plasma out of the hole. Because two of the transitions of interest for these measurements are at 801.699 nm and 800.838 nm, a narrow band filter centered at 800 nm and having a FWHM of 10 nm was used to select this wavelength range from the total emitted light. For the pressure range studied the emissive volume above the cathode is gradually decreasing with the pressure (similar to Fig. 3.6a) and is expected that the involved excited atoms are concentrating inside the hole.

In order to obtain quantitative information, the distribution of the excited atoms above the cathode surface was measured for one metastable ($1s_5$) and one resonance ($1s_4$) level using the experimental set-up presented in Fig. 5.7. The diode laser was tuned on the central wavelength of the studied transition (801.699 nm respectively 800.838 nm) and the absorption signals in different positions above the cathode were measured modulating the plasma and using the lock-in amplifier for the detection. For each position, the values of the signals measured with the lock-in amplifier were normalized to the corresponding absorption length. The dependence of the lateral plasma extension as a function of the distance from the cathode is qualitatively known from the optical investigation of the microdischarge by means of a CCD camera. The relative densities of the excited atoms on the metastable $1s_5$ and resonance $1s_4$ levels are presented in Fig. 5.12a and Fig. 5.12b for different pressures.

The pressure was increased up to the value where no signal was detected. For the transition from the $1s_4$ level this limit was at 200 mbar, while for the transition from the $1s_5$ level at 250 mbar. Even for pressures higher than 250 mbar there are excited atoms produced above the cathode but their number density is low because the discharge tends to concentrate inside the hole. Within the spatial resolution of the set-up (50 μm), the spatial distribution of the excited atoms was evaluated with accuracy in the position of ± 25 μm.

The absolute number density of excited atoms immediately above the cathode is $8.3 \cdot 10^{12}$ $cm^{-3}$ at 50 mbar for the $1s_5$ metastable level and $4.2 \cdot 10^{12}$ $cm^{-3}$ for the $1s_4$ resonance level and is decreasing drastically with the pressure.

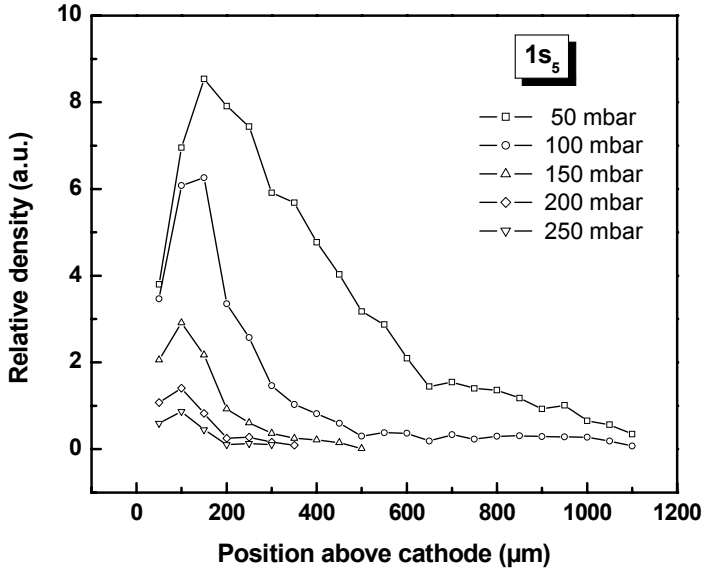


**Figure 5.12a:** Distribution of excited atoms on the metastable ($1s_5$) level above cathode.

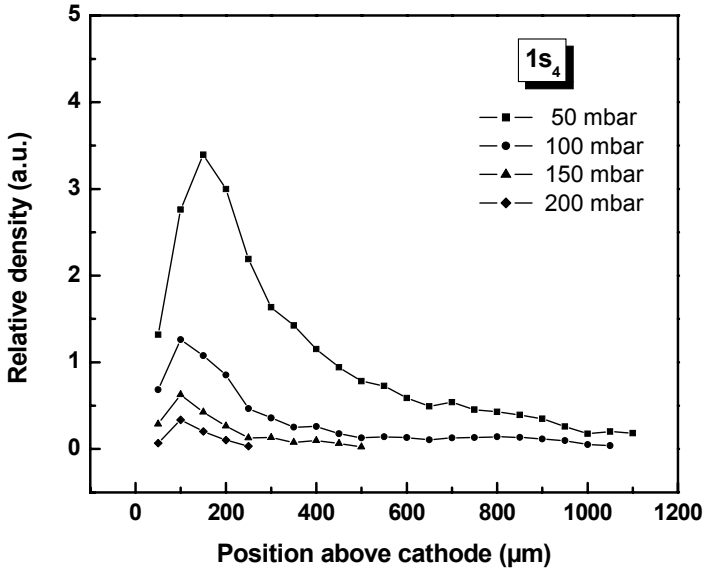


**Figure 5.12b:** Distribution of excited atoms on the resonance ($1s_4$) level above cathode.

Above the cathode, the shape of the distribution of excited atoms on both resonance and metastable levels as function of the position from the electrode is identical. The density of excited atoms has a maximum at a distance of about 150 µm from the cathode for a pressure of 50 mbar. Increasing the pressure this maximum is moving closer

to the cathode. Taking into account that the cathode fall thickness at 50 mbar should be about 80 μm as it was show in [Rai-97] these results prove that the excited atoms are efficiently produced in the negative glow. The displacement of the maximum towards the cathode can be correlated with the decrease of the cathode fall thickness with the pressure [Eng-65]. After reaching its maximum the density of excited species is decreasing with the distance from the cathode surface. For both $1s_4$ and $1s_5$ levels excited atoms are still present at 1 mm above the electrode at 50 mbar. When the pressure is increased to 200 mbar the maximal distance where an absorption signal can be detected is about 250 μm. In low-pressure discharges, the excited atoms on resonance levels are present mostly in the excitation area and are decaying fast with the distance. A similar behavior of the excited atoms above the cathode for both levels sustains the theory of strong collisional coupling of the energy levels present in high-pressure discharges.

### 5.4.2. Absolute population density of excited atoms on $1s_i$ (i=2÷5) levels

In order to calculate the absolute number density of excited atoms one has to divide the integral of the optical depth to the absorption length. When the diode laser beam is passing through the MSE hole absorption occurs inside the hole and above the cathode as well.

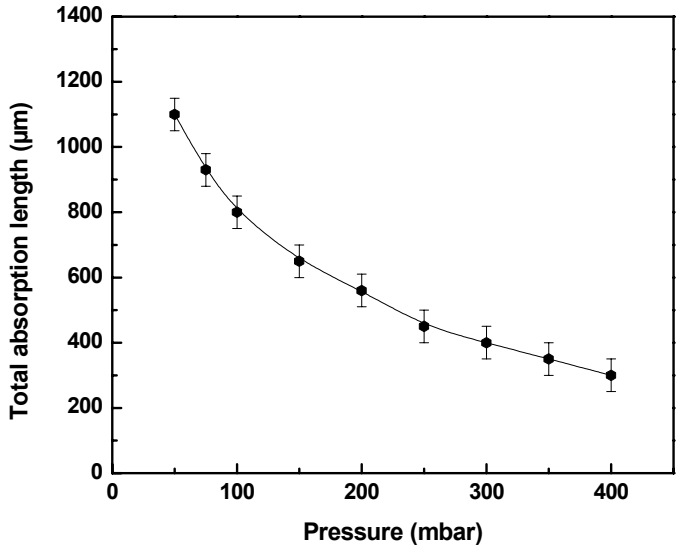


**Figure 5.13:** Total absorption length as a function of pressure.

The total absorption length can be taken as the sum between the length of the hole and the absorption length outside the hole. The absorption length outside the hole was evaluated from the space-resolved measurements previously presented as the distance above the cathode where the relative density of excited atoms decreases to approximately 10% from its maximum value. The dependence of the total absorption path as a function of the pressure is given in Fig. 5.13.

The absolute number density of the excited atoms in the microdischarge was calculated using Eq. 5.4 from the integral absorption profiles normalized to the total absorption length. The quantity $\lambda_{0i}^2 (g_j/g_i)(A_{ji}/8\pi)$ in Eq. 5.4 is a constant given in Table 5.2 for the studied transitions.

| $\lambda_0$ [nm] | $E_i$ [eV] | $E_j$ [eV] | $g_i$ | $g_j$ | $A_{ji}$ [$s^{-1}$] | $\lambda_{0i}^2 \frac{g_j}{gi} \frac{A_{ji}}{8\pi}$ [$m^2/s$] |
|---|---|---|---|---|---|---|
| 801.699 | 11.549 | 13.095 | 5 | 5 | $9.553 \cdot 10^6$ | $2.4 \cdot 10^{-7}$ |
| 800.838 | 11.624 | 13.172 | 3 | 5 | $4.657 \cdot 10^6$ | $1.98 \cdot 10^{-7}$ |
| 772.633 | 11.723 | 13.328 | 1 | 3 | $1.271 \cdot 10^7$ | $9.05 \cdot 10^{-7}$ |
| 826.680 | 11.828 | 13.328 | 3 | 3 | $1.680 \cdot 10^7$ | $4.57 \cdot 10^{-7}$ |

**Table 5.2:** The transitions studied for the investigation of the $1s_i$ levels and their characteristics.

Fig. 5.14 presents the results for the first four excited levels of argon. For the density of the metastable $1s_3$ level only two values were obtained because the diode laser used for probing this transition was destroyed during the measurements. From the density plot it can be seen that the values are varying from $2.3 \cdot 10^{12}$ $cm^{-3}$ to $9.5 \cdot 10^{12}$ $cm^{-3}$ at 50 mbar for the highest $1s_2$ and the lowest $1s_5$ level respectively and from $2.5 \cdot 10^{12}$ $cm^{-3}$ to $1.8 \cdot 10^{13}$ $cm^{-3}$ at 400 mbar. These values are giving a minimum density of excited atoms. The errors in evaluating the density of the excited atoms are about 20% and are mainly due to the evaluation of the absorption length, due to the wavelength calibration of the line profiles and due to the uncertainty of the Einstein coefficients $A_{ji}$. The density of excited atoms is decreasing up to 150 mbar and then is slightly increasing with the pressure due to the rise in the current density. The shape of this dependence suggests that at low pressures a large number of excited atoms are produced above the cathode surface

while increasing the pressure the production of excites states inside the hole gains importance.

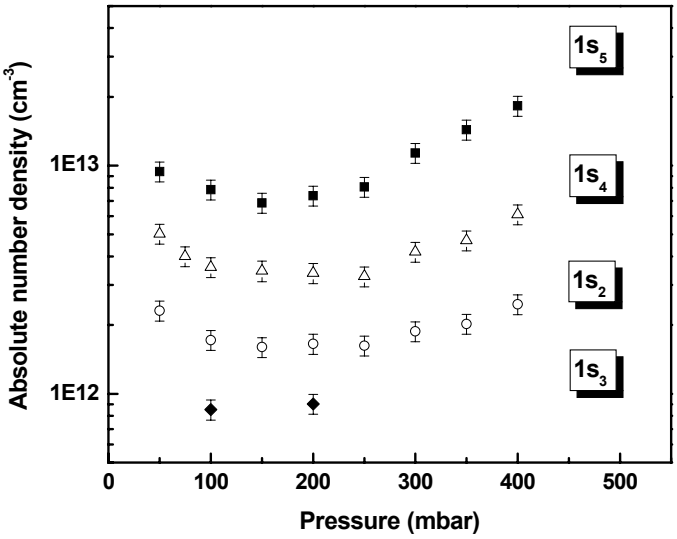


**Figure 5.14:** Absolute number density of the $1s_i$ (i=2÷5) excited levels of Ar in the MSE sustained discharge for the pressure range 50-400 mbar.

For a pressure of 50 mbar, comparing the integral density of excited atoms measured through hole with the density obtained at 50 μm above the cathode, the values are not significantly different (e.g. $9.4 \cdot 10^{12}$ $cm^{-3}$ respectively $8.3 \cdot 10^{12}$ $cm^{-3}$ for the $1s_5$ level). The ratio between the excited atoms measured through the hole and outside is about 1.15 at 50 mbar and is increasing to about 2.3 at 100 mbar. This result sustains the hypothesis that with the increase of the pressure the negative glow contracts and moves towards the inner side of the hole.

It has to be underlined that inside the hole of the MSE both the production and destruction of excited states are very efficient. Due to the high current density a large number of excited atoms are produced, especially in the negative glow adjacent to the cathode. The geometrical dimensions of the hole being small, diffusion plays an important role in the destruction of the excited species even if the pressure is rather high. The excited atoms are easily reaching the walls of the hole where they are strongly quenched. The contribution of the diffusion to the depopulation of the excited levels decreases with

the increasing of the pressure. Other processes that are responsible for the depopulation of the excited levels are the two- and three-body collisions, whose importance rises with the pressure. The density of charged particles in the region outside the hole is lower than inside the hole and is expected that only a small fraction of excited atoms are produced by electron impact. The plasma volume above the cathode surface can be considered a spatial afterglow, where the excited atoms are mostly created in recombination processes. The destruction mechanism above the cathode is also partially different: the depopulation of the excited levels occurs mostly due to volume processes like two and three body collisions, quenching due to impurities in the gas or coming out from the cathode.

### 5.4.3. The effect of impurities on the population density

In order to estimate the effect of the gas purity on the population density, the discharge was operated in static conditions, without gas flow through the chamber where the MSE is mounted. It was observed that the absorption signal and correspondingly the density of excited atoms, decreases drastically in time.

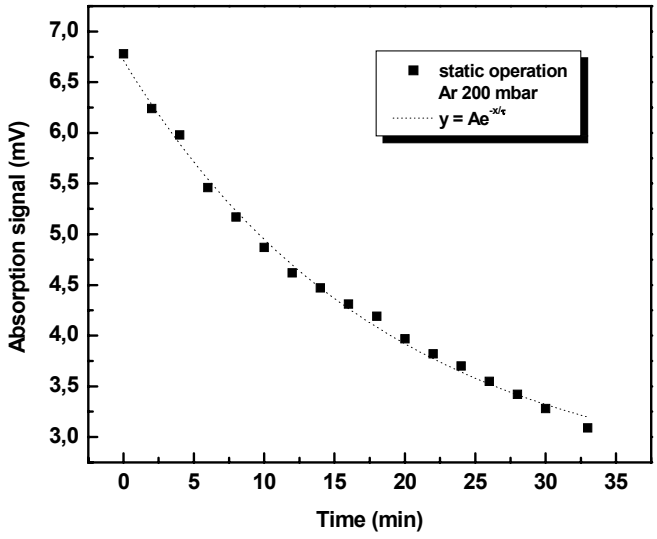


**Figure 5.15:** The quenching of the Ar metastable due to impurities.

The temporal evolution of the absorption signal after switching off the gas flow is presented in Fig. 5.15. The severe decrease in the density of excited atoms is due to the

collisional quenching of the metastable states of Ar by nitrogen, oxygen and other impurities released from the microstructure during the operation of the discharge. Energy transfer between Ar metastables and excited nitrogen molecules on the $N_2(C^3\Pi_u)$ level is almost resonant (see the potential energy diagram for nitrogen in Appendix B). Other loss channel involves $H_2O$ molecules resulting in the formation of $OH(A^2\Sigma^+)$ radicals.

## 5.5. Plasma parameters calculated from line profile analysis

The measurement of the electron number density and gas temperature in the microdischarge is based on the analysis of the absorption line profiles. A major advantage of the absorption technique using narrow spectral lasers is that the instrumental broadening is eliminated. The analysis of the line profiles of the Ar transitions at 801.699 nm ($1s_5$) and 800.838 nm ($1s_4$) revealed besides Doppler broadening also pressure broadening and shift caused by the interaction of the absorbing atoms with neutral (resonance /van der Waals broadening) and charged particles (Stark broadening). It is rather unusual to use the line profiles of non-hydrogenic atoms for evaluating the electron number density because these spectral lines undergo a quadratic Stark effect with much smaller impact in the line width than the linear Stark effect. We will demonstrate that using DLAAS argon excited atoms transitions can be used to derive the electron number density if this is higher than $5 \cdot 10^{14}$ $cm^{-3}$.

### 5.5.1. Theoretical considerations

In discharge plasmas, depending on the operation conditions, different mechanisms can contribute to the broadening of the atomic transitions. In high-pressure plasmas the absorption line profiles are mainly broadened and shifted due to the effect of the gas pressure, charged particles and thermal movement. The natural broadening, caused by the Heisenberg uncertainty principle applied to the energy of the initial and the final state of the transition, is typically orders of magnitude smaller than Doppler and pressure broadening and can be neglected.

Doppler broadening arises from the random thermal movement of the absorbing particles along the observation path. If the absorbing atoms have a Maxwell velocity

distribution characterized by a temperature $T$, the intensity profile of a Doppler broadened spectral line follows a Gauss distribution. The full width at half maximum (FWHM) $\Delta\lambda_G$ of this distribution is related to the temperature $T$ through the relation [Dem-96]:

$$\Delta\lambda_G = \lambda_0 \sqrt{\frac{8kT\ln 2}{m_a c^2}} = 7.16 \cdot 10^{-7} \lambda_0 \sqrt{\frac{T}{M}} \tag{5.5}$$

where $m_a$ is the atomic mass, white M is the mass number of the absorbing particle, k is the Boltzmann constant and $\lambda_0$ the central wavelength of the transition.

Pressure broadening is a consequence of the interaction of the excited atoms under consideration and neutral atoms (collision broadening) and of the micro-fields produced by the presence of charged particles (Stark broadening).

The interaction of the absorbing atoms with neighboring neutral atoms generates a broadening of the line profile and also a shift of its central wavelength. Interactions between atoms of the same kind give rise to resonance broadening ($R^{-3}$ dependent interaction potential, where R is the distance perturber-excited atom) if one of the states in the absorbed line has allowed dipole transition to the ground state. Interactions with atoms that do not share a resonance transition with the absorbing particle give rise to van der Waals broadening (long-range interaction potential $R^{-6}$ dependent) and produce also a shift of the line centre, usually to higher wavelengths. The relations that give the FWHM and shift for the collision broadening are:

$$\Delta\lambda_{Lwidth}^{\ coll} = 2\gamma N \tag{5.6}$$

$$\Delta\lambda_{Lshift}^{\ coll} = \beta N \tag{5.7}$$

where $2\gamma$ and $\beta$ are collision broadening parameters specific for each transition.

Stark broadening is caused by the Coulomb interaction of the absorbing atom with the charged particles present in the plasma. The non-hydrogenic atoms are subject to quadratic Stark effect, which induce a broadening of the line and also a shift, usually towards longer wavelength. In this case the full width at half maximum $\Delta\lambda_{Lwidth}^{\ Stark}$ and the shift $\Delta\lambda_{Lshift}^{\ Stark}$ are complex functions of $N_e$ and $T_e$. The expressions for the Stark broadening are [Hud-65]:

$$\Delta\lambda_{Lwidth}^{\ Stark} = 2 \cdot (1 + 1.75 \cdot 10^{-4} N_e^{\ 1/4} \alpha (1 - 0.068 N_e^{\ 1/6} T_e^{\ -1/2})) 10^{-16} w N_e \tag{5.8}$$

$$\Delta\lambda_{Lshift}^{Stark} = (d/w + 2\cdot 10^{-4} N_e^{1/4}\alpha(1-0.068 N_e^{1/6} T_e^{-1/2}))\cdot 10^{-16} w N_e \qquad (5.9)$$

where $w$ is the electron impact width, $d/w$ is the relative shift and $\alpha$ is the ion broadening parameter, all given in [Gri-62].

Collision and Stark broadened line profiles have a Lorentzian intensity distribution. The total Lorentz contribution $\Delta\lambda_L^{total}$ to the line profile is given by:

$$\Delta\lambda_L^{total} = \Delta\lambda_L^{coll} + \Delta\lambda_L^{Stark} \qquad (5.10)$$

where $\Delta\lambda_L$ is the width of the line profile. A similar relation holds for the shift of the line. The convolution of the Gauss and Lorentz distributions is the Voigt profile. The equation relating the Voigt, Gauss and Lorentz FWHM is:

$$\Delta\lambda^2_G = \Delta\lambda^2_V - \Delta\lambda_V \cdot \Delta\lambda_L \qquad (5.11)$$

The main idea here was to de-convolute the experimentally obtained Voigt profiles and to separate the Gauss contribution (which dominates the profile near the line centre) and the Lorentz contribution (which governs the wings of the line). The procedure was the following: first we estimated the total width and shift $\Delta\lambda_V$ from the experimentally measured optical depth $\ln(I_0 / I_\nu)$ of the studied transitions. For the evaluation of the total Lorentz contribution, the values of the optical depth were measured far out of the centre of the absorption line where the Lorentz distribution *P(λ)* can be approximated:

$$P(\lambda) = \frac{A}{2\pi}\frac{\Delta\lambda_L^{tatal}}{(\lambda-\lambda_0)^2} \qquad (5.12)$$

where A is the area of the absorption profile and ($\lambda$-$\lambda_0$) is the deviation from the line centre. The Gauss width was calculated using Eq.5.11. Further the collision contribution calculated with the broadening parameters given in [Mou-87] and [Tac-82] was extracted from the total Lorentz width and the remaining part was assigned to Stark broadening.

### 5.5.2. Plasma parameters and discussions

In Fig. 5.16 are presented the line profiles of the 801.699 nm Ar transition at four different pressures, from 100 to 400 mbar. It can be seen that the line width and the shift of the central wavelength are strongly increasing with the pressure.

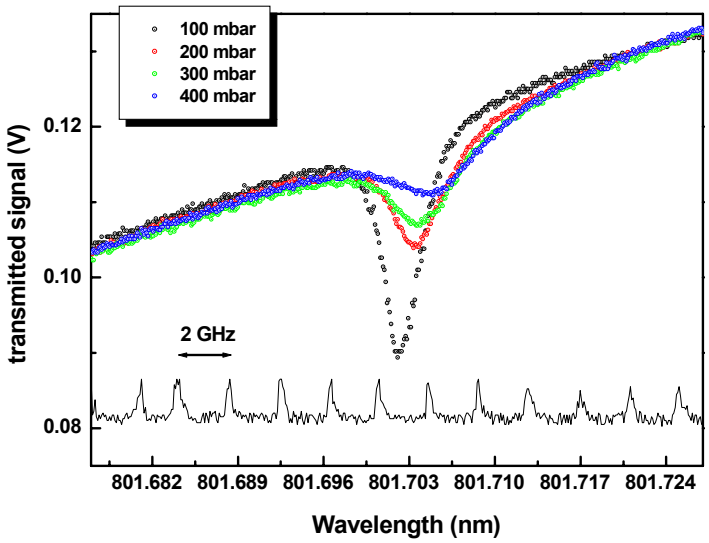


**Figure 5.16:** Effect of the pressure in absorption line shape for the 801.699 nm line.

A. Gas temperature

According to the model previously presented, the absorption line profiles of the ($1s_5$ - $2p_8$) Ar transition at 801.699 nm were deconvoluted and the Gauss contribution to the line profile was extracted. Using Eq. 5.5, the temperature was calculated and is presented in Fig. 5.17 for the pressure range 50 - 400 mbar. In the same figure is plotted the temperature obtained from the analysis the line profiles of the $1s_4$ - $2p_6$ transition at 800.838 nm. There is a good agreement between the values obtained using these two transitions, which gives confidence in the accuracy of the results. The temperature determined in this way is not an excitation temperature, it is a measure of the thermal (translation) movement atoms and therefore gives the gas temperature. Note that the gas temperature corresponds to the plasma region with the highest population density. This method gives the gas temperature of the discharge confined inside the hole of the MSE. Recording the absorption signals immediately above the cathode surface, the FWHM of the line profiles is much smaller, corresponding only to collision broadening. This means that outside the MSE hole the temperature of the ambient gas is about room temperature.

The gas temperature has a linear dependence on the discharge pressure $p$. By increasing the pressure the electron mean free path reduces (at 400 mbar being about 0.2 μm), the energy gained by electrons between collisions is small and the probability of

transferring this energy to heat the gas is increasing. As the power input in the discharge is constant and the plasma volume is decreasing with the pressure, it results in a higher current density and consequently to a more pronounced heating of the gas. Even if the gas temperature increases locally up to about 1000 K at 400 mbar, the microdischarge produces non-equilibrium plasma.

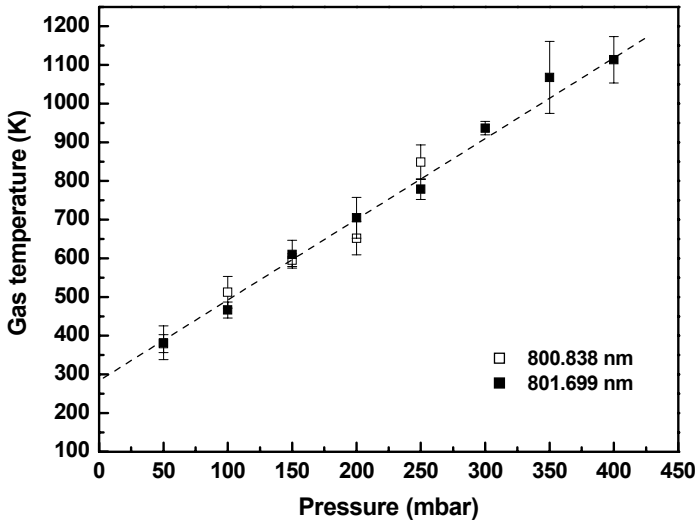


**Figure 5.17:** Gas temperature in the microdischarge.

B. Evaluation of the electron number density

The total Lorentz contribution was measured experimentally far in the wings of the absorption line profiles for the transitions at 801.699 nm and 800.838 nm.

| Transition | $2\gamma$ /N ($10^{-20}$ $cm^{-1}$ $cm^3$) | $\beta$ /N ($10^{-20}$ $cm^{-1}$ $cm^3$) | Authors |
|---|---|---|---|
| 801.699 nm | 2.8 ± 0.3 (3900 K)<br>2.9 ± 0.3 (1130 K) | 8.5 ± 0.5 (3900 K)<br>15.1 (1130 K)<br>7.95±0.39 (300 K) | Vallee et al.<br>Copley and Camm<br>Aeschliman et al. |
| 800.838 nm | 3.54±0.39 (300K)<br>4.05±0.2 (1130K) | 3.7±0.19 (300K) | Aeschliman et al.<br>Copley and Camm |

**Table 5.3:** Broadening and shift coefficients for the 801.699 nm and 800.838 nm Ar lines from [Tac-82]. In brackets is indicated the gas temperature of the plasma source where they have been measured.

The total Lorentz contribution is presented in Fig. 5.18a for the transition from the metastable level. On the same figure is plotted also the collision broadening contribution, calculated in accordance with Eq. 5.6, Eq. 5.7 and the data given in Table 5.3. For the 801.699 nm line the values of the broadening coefficients from Table 5.3 were adjusted to the discharge temperature using the $T^{0.3}$ dependence (Lindholm–Foley theory), while the broadening parameters of the 800.838 nm line were assumed temperature independent (resonance broadening theory). The neutral gas density was determined by using the ideal gas law $p=NkT_g$ and considering the discharge pressure and the temperature previously estimated. For both transitions investigated there is a big difference between the total Lorentz width and the collision broadening width.

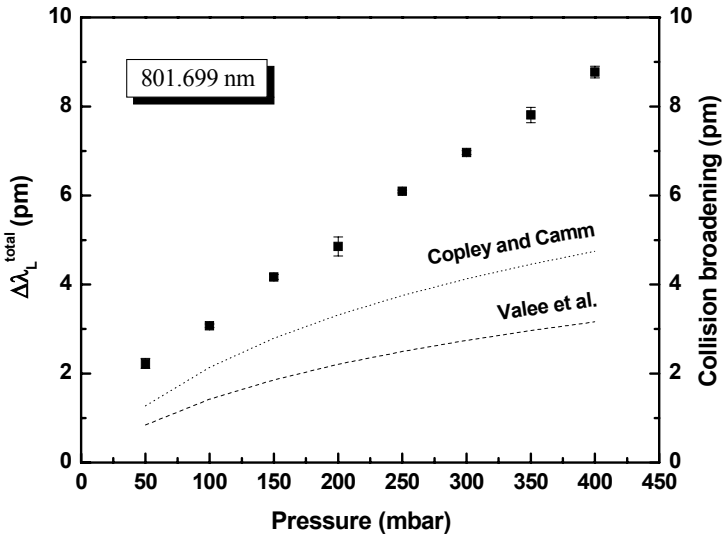


**Figure 5.18a:** Experimentally measured width (■) due to pressure broadening for the transition at 801.699 nn and the theoretical collision broadening (line) for this transition.

The instrumental broadening can be considered negligible in our case because the diode lasers have a FWHM even smaller than the natural broadening of an atomic transition [Cam-85]. Therefore, the difference in the broadening of the line profile is a consequence of the quadratic Stark effect and can be described by the Eq. 5.8.

As predicted by the theory, for the transition from the metastable $1s_5$ level there is a measurable shift of the central wavelength that increases with the pressure (see the

signals at 50 mbar and 400 mbar in Fig. 5.16). The total experimentally measured shift and the theoretical collision shift are plotted for comparison in Fig. 5.18b.

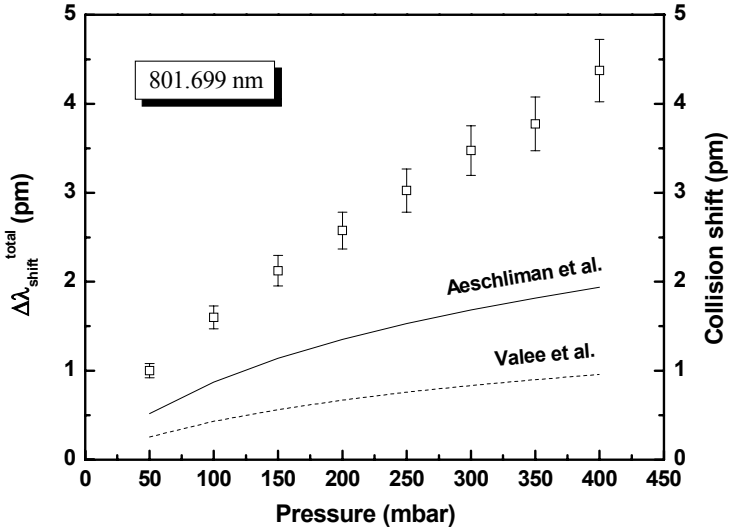


**Figure 5.18b:** Experimentally measured shift (□) due to pressure broadening for the transition at 801.699 nn and the theoretical collision shift (line) for this transition.

In the case of the transition from the resonance $1s_4$ level, the line shift at 50 mbar is too small to be measurable with our setup (less than 1 pm) and is pressure independent.

| Transition | | 5000 K | 10000 K | 20000 K |
|---|---|---|---|---|
| 801.699 nm | *w* | 0.037 | 0.049 | 0.065 |
| | *d/w* | 1.63 | 1.34 | 0.99 |
| | $\alpha$ | 0.038 | 0.031 | 0.025 |
| 800.838 nm | *w* | 0.036 | 0.047 | 0.062 |
| | *d/w* | 1.65 | 1.38 | 1.03 |
| | $\alpha$ | 0.040 | 0.032 | 0.026 |

**Table 5.4:** Calculated Stark broadening parameters [Gri-62] for the Ar transitions 801.699 nm and 800.838 nm for the possible electron temperature range in the microdischarge.

This is in accordance with the theory of resonance broadening which predicts no collision shift for lines with allowed dipole transition to the ground state. The errors in the evaluation of the experimental shift are rather large due to the fact that it was not possible to measure the central wavelength very precisely (wavemeter accuracy 1 pm).

Subtracting the collision contribution from the total Lorentz width and shift, the electron density was estimated from Eqs. 5.8 and 5.9, using the Stark broadening parameters listed in Table 5.4. The electron temperature was taken 1 eV ± 0.3 eV, a value that agree also with [Pet-01]. The correspondence between electron density and Stark width and shift is given in Fig. 5.19a and 5.19b respectively, for different electron temperatures. The values at 15000 K in Fig. 5.19a are extrapolated.

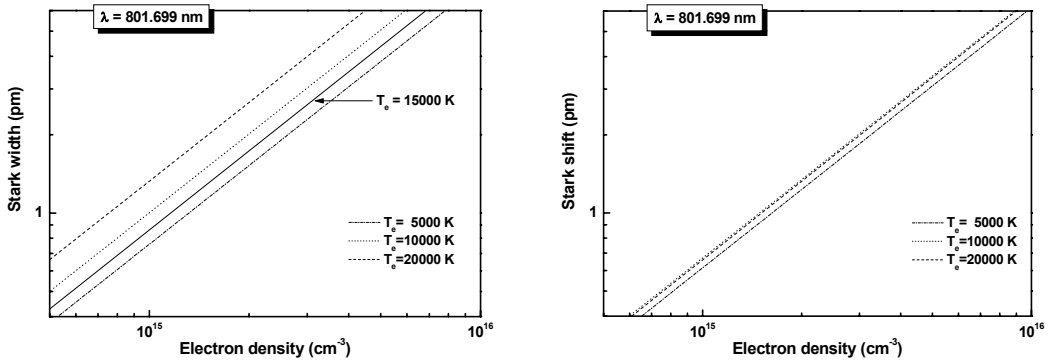


a b

**Figure 5.19:** Theoretical Stark width (a) and shift (b) calculated for 801.699nm Ar transition at different electron temperatures.

The approximate expressions (5.8) and (5.9) are sufficiently accurate if the following conditions are fulfilled:

$$10^{-4} \cdot \alpha N_e^{1/4} < 0.5 \quad \text{and} \quad 9.0 \cdot 10^{-2} N_e^{1/6} T_e^{-1/2} < 0.8 \qquad (5.13)$$

In our case these inequalities are satisfied, but the electron number density cannot be calculated very accurate because different values of the collision width and shift could be found in literature (see Fig. 5.18 and Table 5.4). The range for the electron number density is presented in Fig. 5.20. The electron number density in the microdischarge is pressure dependent and was found to be on the order of $10^{15}$ cm$^{-3}$.

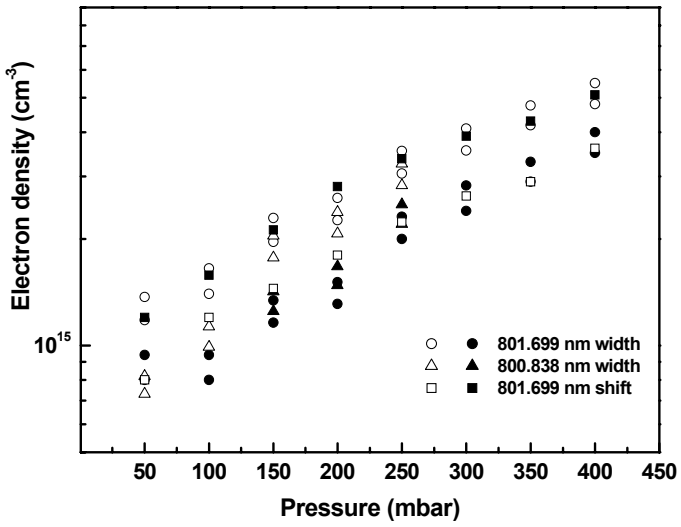


**Figure 5.20:** Electron number density in the MSE sustained discharge as a function of pressure at constant current.

It can be seen that the electron number density is increasing by a factor of 5 in the pressure range 50 – 400 mbar and is expected that it will increase more close to atmospheric pressure. The present measurements are giving the electron number density in the discharge area, i.e. inside the MSE hole.

From the line profiles measured immediately above the cathode surface (100 μm) was concluded that there is no measurable broadening due to Stark effect, which means that outside the hole are very few electrons. The secondary electrons released from the external surface of the cathode have to be accelerated by the field lines towards the anode in order to sustain the discharge current. Accordingly, these electrons will be directed into the hole, if they are not lost due to collisions with heavy particles.

Taking into account the density of neutral atoms and the electron density it can be concluded that the degree of ionization in the MSE sustained discharge is about $10^{-3}$. Using emission spectroscopy, similar results for the electron number density were obtained from the line broadening of the $H_\beta$ Balmer line due to linear Stark effect.

## 5.6. DLAAS at atmospheric pressure

Atmospheric pressure plasma was generated in argon using a microstructure based of $Al_2O_3$ as insulator and having Pt electrodes. The discharge current was 2 mA and the sustaining voltage was 170 V. The absorption measurements performed at 1 bar have shown that excited atoms on the metastable levels still can be detected. The $1s_5$ metastable level was chosen because is the lowest excited level of Ar (see Fig. 5.9) and in consequence the most populated. The 811.754 nm line ($1s_5$-$2p_9$) was used to investigate the population density on the $1s_5$ metastable level due to the fact that is the transition with the highest oscillator strength. One major disadvantage when performing DLAAS at 1 bar is that at such high pressure the absorption length decreases dramatically and even measuring with a lock-in amplifier the signal to noise ratio is about 10 - 20. At 1 bar the absorption length should be given essentially by the length of the cathode, which is in this case 20 μm. Another disadvantage was the diameter of the hole, which is in this MSE design 100 μm. The microstructures used in the previous measurements have 300 μm hole diameter and accordingly the volume of the absorbing medium inside the hole is about ten times larger, leading to higher absorption signals and better signal to noise ratio. Regarding the line profile, the FWHM of the Voigt profile increases due to both Doppler and pressure broadening mechanisms. For 1 bar and an assumed gas temperature of 2000 K extrapolated from Fig. 5.17, the estimated value of the FWHM is about 25 pm. Therefore it is difficult to scan the diode laser wavelength across the whole line profile. Under these conditions only a rough estimation of the absolute number density of excited atoms on $1s_5$ level was possible, the value being about $2 \cdot 10^{13}$ $cm^{-3}$. This value is not much larger than that obtained at 400 mbar and an explanation could be that at atmospheric pressure the depopulation processes like three body collisions, ionizing collisions with slow electrons, quenching, are very effective. Even if it was not possible to tune the diode laser across the absorption profile, a total shift of the central wavelength of about 10 pm was measured. Using the broadening coefficients for the 811.754 line given in [Tac-82], at 1 bar and 2000 K the collision shift should be about 3 pm. Assuming a Stark shift of about 7 pm, the electron number density at atmospheric pressure is on the order of $10^{16}$ $cm^{-3}$. This value is in agreement with the one that would be obtained by extrapolating the plot of the electron number density as a function of pressure given in Fig. 5.20.

## 5.7. Conclusions

The study of the MSE sustained high-pressure glow discharge by diode laser absorption spectroscopy has revealed very useful information about the excited species and about plasma parameters. The results are summarized in Table 5.5. Due to the high number density of excited atoms on metastable and resonance levels in the microdischarge, the DLAAS technique can be successfully applied to investigate the MSE plasma, in spite of the very short absorption length (hundreds of μm). The discharge was investigated along the plasma channel and spatially resolved above the cathode surface, for better understanding the processes taking place at the cathode. Due to their long lifetime the atoms on the first excited states, especially on metastable levels are a deposit of energy in the discharge. They play an important role in sustaining the ionization in high-pressure discharges [Mas-98], where besides the electron impact ionization the stepwise ionization becomes significant. The excited neutrals can release very efficient secondary electrons at the cathode, or may interact strongly with other surfaces and therefore be suitable for plasma assisted cleaning and/or activation [Rot-01].

| Gas | p (mbar) | $n_{m,r}$ ($cm^{-3}$) | $n_e$ ($cm^{-3}$) | $T_e$ (eV) | $T_g$ (K) |
|---|---|---|---|---|---|
| Ar | 50 → 400 | $10^{12} \rightarrow 2 \cdot 10^{13}$ | $8 \cdot 10^{14} \rightarrow 5 \cdot 10^{15}$ | ~ 0.8 | 380 → 1100 |

**Table 5.5:** Plasma parameters, where $n_{m,r}$ is the density of excited atoms on metastable/resonance states, $n_e$ the electron density, $T_e$ the electron temperature and $T_g$ the gas temperature in the discharge.

To our knowledge, absorption spectroscopy of the excited atoms in high-pressure DC glow discharges was reported up to now only in respect with the population density of the $1s_5$ level of Xe measured for pressures lower than 100 mbar in a hollow cathode discharge with 2 mm electrode gap. The results concerning the number density of excited atoms presented in this work are comparable with the absolute metastable Xe $[3/2]_2$ density [Bus-01]. Due to the small dimensions of the discharge, the accurate determination of the density of the excited atoms was really a challenging task.

When the absolute number density of atoms on a given excited level is known the electron temperature can be estimated in a procedure similar to that discussed related to

emission spectroscopy. The assumption made is that the direct electron impact is the dominant excitation mechanism. The temperature obtained using the absolute number densities of the $1s_i$, (i=2÷5) levels of Ar is about 0.8 eV and is slightly decreasing with the pressure. These results are in good agreement with those presented in Chapter 4.

The gas temperature and the electron number density were evaluated from the absorption line profiles taking into account the significant broadening mechanisms. The gas temperature in atmospheric pressure small-size discharges operated in air or nitrogen may reach values of 2000 K, as reported in [Lei-00] and [Pet-01]. Taking into account that the input power for air and nitrogen is significantly higher than in argon, the gas temperature obtained in our measurements is realistic. Although the plasma confined inside the hole may reach gas temperatures up to 1000 K, the ambient gas temperature immediately above the microstructure exceed only slightly the room temperature. These results confirm the measurements presented in Chapter 4 where the gas temperature was estimated from rotational distributions of nitrogen excited states. The electron number density measured in the present work is comparable with that reported in [Pet-01] where the method used was emission spectroscopy of the Balmer $H_\beta$ line.

The present study may help in analyzing the role of the lowest excited states in processing plasma and in the generation of UV radiation. Due to the high density of excited species, the MSE sustained discharge provides appropriate conditions for generating excimer radiation taking into account that the atoms on metastable states are the precursor of excimer molecules. Studies concerning the generation of UV and VUV radiation in high-pressure discharges with dimensions in the submillimetric range [Kur-99], [Mos-01] are known. Microdischarges operated at high pressure in rare gases and rare gas halides [ElH-00] could be an alternative to the currently available excimer lamps based on dielectric barrier discharges [Kog-97] if the excessive heating of the gas is prevented.

Extending the operation range towards atmospheric pressure is expected that the gas temperature will increase, while the electron temperature should decrease but these two temperatures will still be highly different. It can be concluded that the MSE sustained discharge provides non-equilibrium plasma conditions in high-pressure gases and offers the premises for efficient surface treatment or waste gas decomposition. The next chapter reports on the potential applications of the MSE based plasma.

# CHAPTER 6
# APPLICATIONS

## Introduction

As demonstrated in the previous chapters, the MSE sustained discharges operated at high-pressure have characteristics that recommend them for non-thermal plasma processing, e.g. surface treatment and plasma chemistry. Besides the ease of use that not require expensive vacuum equipment, the high-pressure discharges offer also a high density of active species. In many applications the free radicals generated in the plasma are more important than the electrons and ions themselves.

Different attempts were made for proving the reactivity of the MSE sustained discharge with regard to processes that take place at the surface and in the gas phase. The microdischarge was used for inducing reduction of pollutants and surface modification. The evolution of the species concentrations was visualized by Mass Spectrometry (MS).

The modification of the surface properties was investigated through Water Contact Angle (WCA) measurements, the chemical composition of the treated area was determined by means of X-rays Photon Spectroscopy (XPS) and the topography of the surface was imaged using Scanning White Light Interferometry.

## 6.1. Surface treatment

The principle of plasma assisted surface modification is to use the active species produced in the discharge to change the surface characteristics of solid materials.

As already mentioned in Chapter 3, large area high-pressure plasma can be generated by parallel operation of microdischarges. A plasma module with 50x50 $mm^2$ active area consisting of 200 parallel-operated holes was used to induce surface modification on polymer films. The diameter on the holes is 300 μm and they are arranged at 3 mm pitch. To investigate how far in the lateral direction a modification of

the surface can be still obtained a MSE consisting of 36 holes and an active surface of 15 x15 $mm^2$ was used. Due to the large number of microdischarges parallel operated, the current per hole was relatively low for hindering the onset of thermal instabilities. For the same reason most of the measurements were performed at 50 mbar in a mixture of Ar and 10% air. Air was added to the Ar gas because the commonly used mixtures for inducing surface modification on organic materials are containing oxygen and it has also a stabilizing effect on the discharge. The discharge current, gas flow and pressure, as well as the distance MSE-substrate have been varied during this experiment.

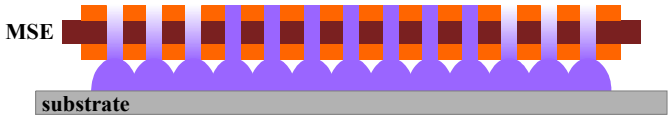


**Figure 6.1:** Schematic view of surface experimental arrangement for surface modification.

Different organic substrates like polyethylene (PE) and polypropylene (PP) have been used, being placed either at the anode or cathode side. The experimental set-up usually employed for the study of the parallel regime was changed to allow the mounting of the substrates to be treated. The polymer films were placed between two metallic rings to ensure a plane surface i.e. to keep the same distance between MSE and substrate over the whole area exposed to the discharge. The sketch of the experimental arrangement is given in Fig. 6.1.

The degree of modification was qualitatively investigated through Water Contact Angle (WCA) measurements using distilled water at room temperature. This is a common method used for qualitatively measuring surface energies. The WCA for an untreated polymer film is about 110° in the case of polyethylene (PE) and about 100° for polypropylene (PP). The images of a water drop on a wettable and non-wettable surface are presented in Fig. 6.2 upper and down and it can be noticed that the evolution in time is different for the two surfaces. This is a clear evidence of the changes induced to the substrate by plasma. The effect of evaporation is negligible up to 1 minute, as viewed in Fig. 6.2a.

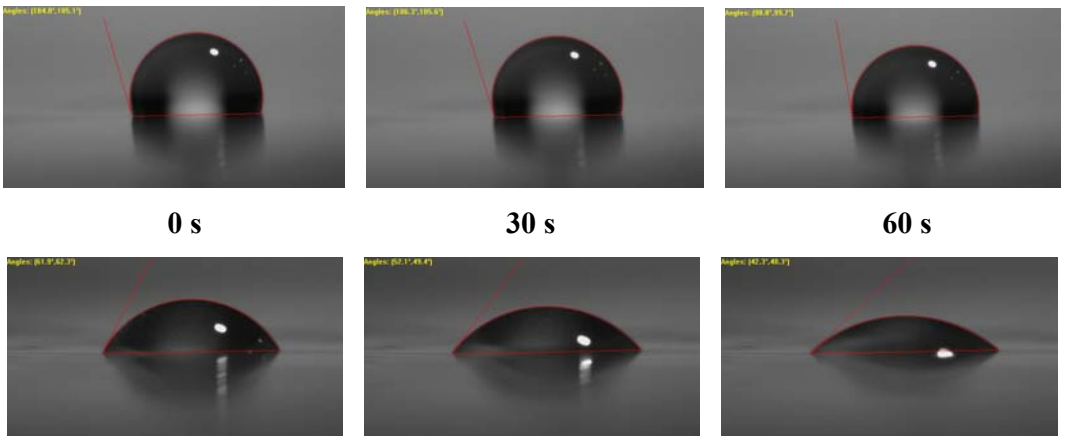


**Figure 6.2:** Time evolution of a drop of water on the untreated PP sample (non-wettable surface) and on the surface exposed to the discharge (wettable surface).

The dependencies of the water contact angle (WCA) on various parameters are shown in Fig. 6.3a to d. It should be mentioned that a smaller WCA corresponds to a higher surface energy. For many industrial applications a rather high surface energy is required, equivalent to WCA of about 50% or less. In our measurements the absolute value of the surface energy was not measured because this is usually done using standard liquids with well-controlled viscosity. Only the variation of the WCA relative to that on an untreated film was observed, as a measure of the surface wettability.

For the same discharge current, pressure, gas flow and exposure time the dependence of the WCA with the distance has a different shape for the samples placed at the cathode and anode side as shown in Fig. 6.3a. It suggests that the involved processes are of different nature.

For the samples placed at the cathode side there is an optimum distance, which depend on the nature of the sample (Fig. 6.3b). For this distance the incoming particles are able to transfer their energy very efficient to the surface (quasi-resonant). At the anode side the degree of modification decreases exponentially with the distance. In the lateral direction the discharge may act up to about 10 mm for a working pressure of 50 mbar and a gas flow of 50 sccm.

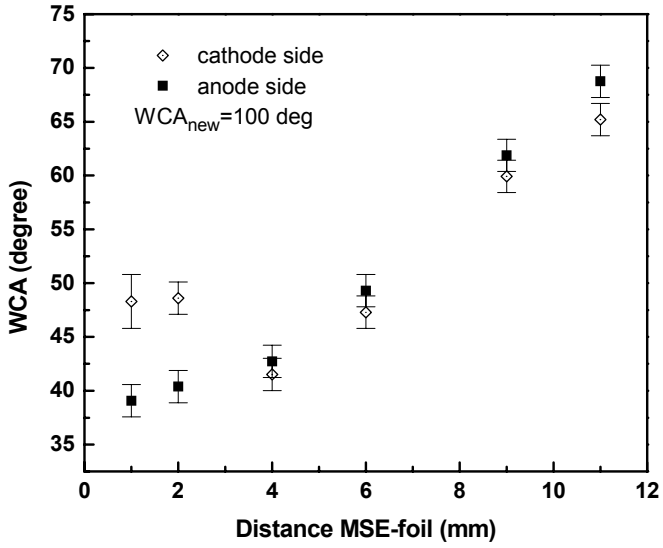


**Figure 6.3a:** Dependency of the WCA on the distance from the MSE for samples placed at anode respective cathode.

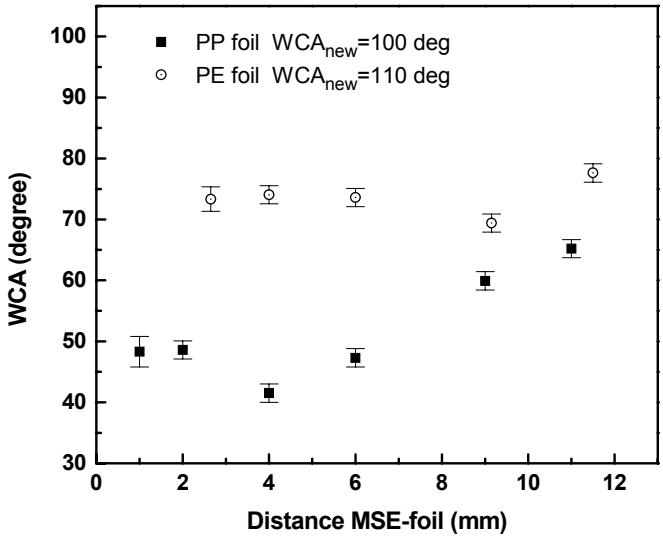


**Figure 6.3b:** Dependency of the WCA on the distance from the MSE for PP and PE samples.

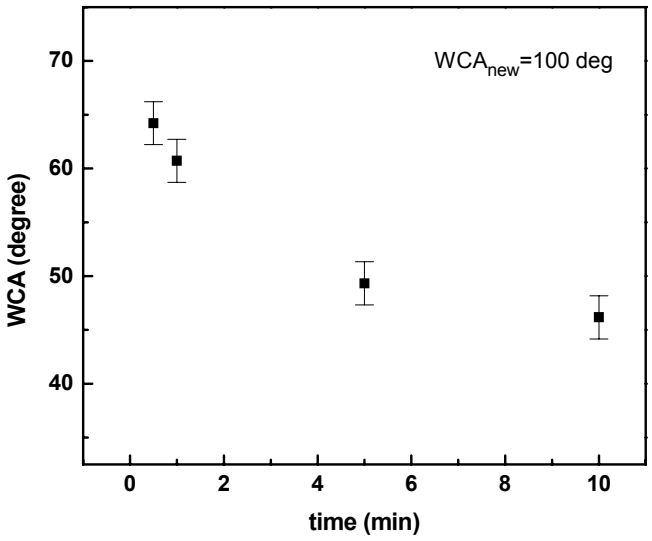


**Figure 6.3c:** Dependency of the WCA on the exposure time for a PP sample placed at 4 mm above the cathode surface.

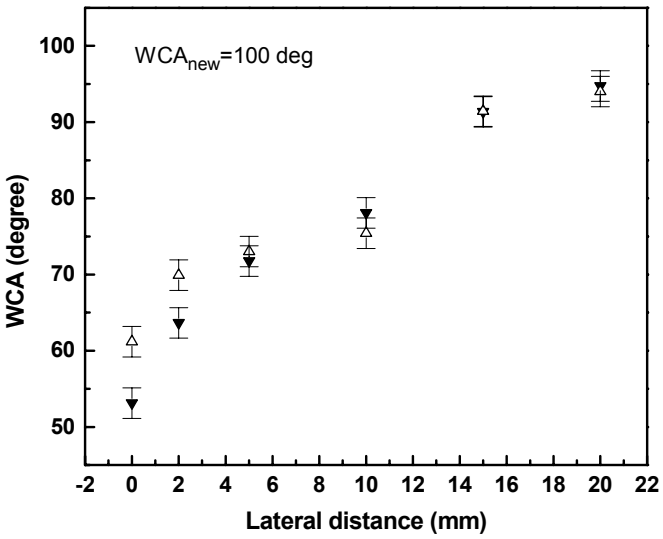


**Figure 6.3d:** Dependency of the WCA on the lateral distance from the MSE.

The degree of modification increases for longer exposure time but as it can be seen in Fig.6.3c, after a certain value a kind of saturation effect occurs and the properties of the surface does not change significantly.

To check the reproducibility of the treatment different PP film were exposed to the discharge under similar conditions. For distances higher than about 4 mm the values of the WCA for different films are comparable. In Fig. 6.3d it can be seen that that only at smaller distances there are differences in the surface energy. This is not related to the modification process but only to the fact that at smaller distances the treatment is not uniform and the measurement of the WCA depends on the position relative to the holes.

By increasing the discharge current and gas flow the wettability increases too. When using MSE with smaller pitch the power density is increased and accordingly the modification enhanced. Furthermore, the treatment should be more uniform at smaller distances. In order to increase the working pressure up to atmospheric, microstructres with smaller hole diameter should be used.

In order to understand the mechanism that results in the modification of the surface energy, the treated samples were investigated from the point of view of chemical composition and surface topology. Due to the fact that the polymer films are non-conductive samples, it is not possible to use scanning electron microscopy, unless they are coated with a thin metal layer. However, optical methods can be applied.

The polymer films were investigated by means of a three-dimensional surface structure analyzer (Zygo, New View 5000). This system uses scanning white light for imaging and measuring the microstructure and the topography of surfaces. One of its advantages is that provides information about surface structure without touching the sample. Basically such a device consists of a microscope, an interferometric objective and a high-resolution camera. The measurements are three-dimensional. Normal to the surface they are performed interferometrycally while in the surface plane the pixel size is calculated from the field of view of the objective.

The optical aspect of the surface confirms the hypothesis that at anode respectively cathode the processes responsible for the increase of the surface energy are different. For the samples exposed to the cathodic side of the discharge the surface changed significantly. It became rather smooth (Fig. 6.4b) comparing to the untreated sample imaged in Fig. 6.4a and which presents a relatively rough surface.

**a**

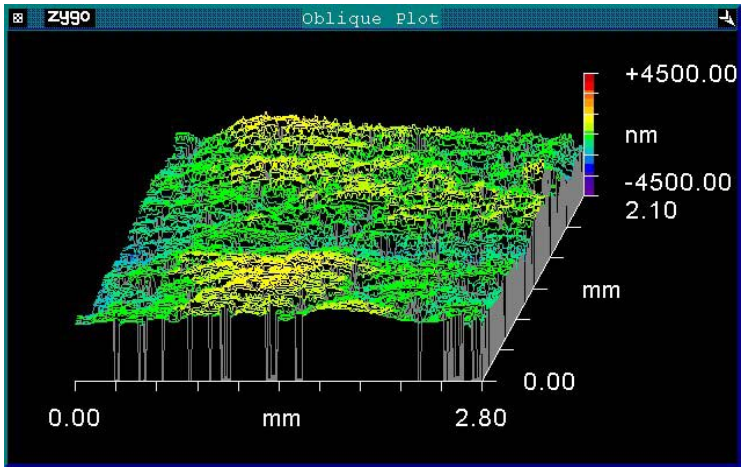


**b**

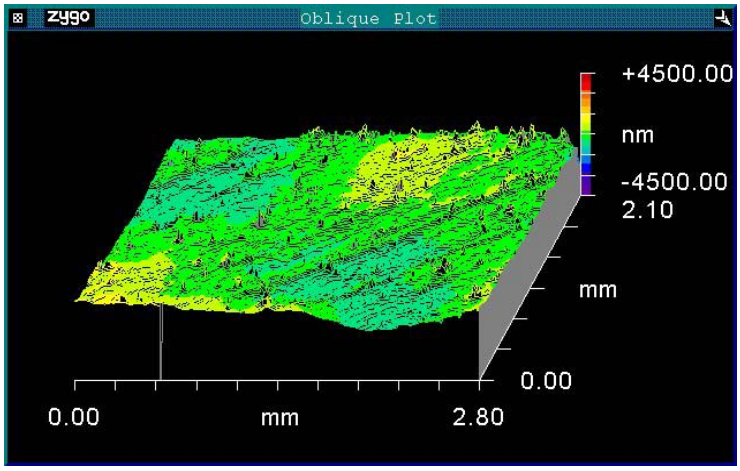


**c**

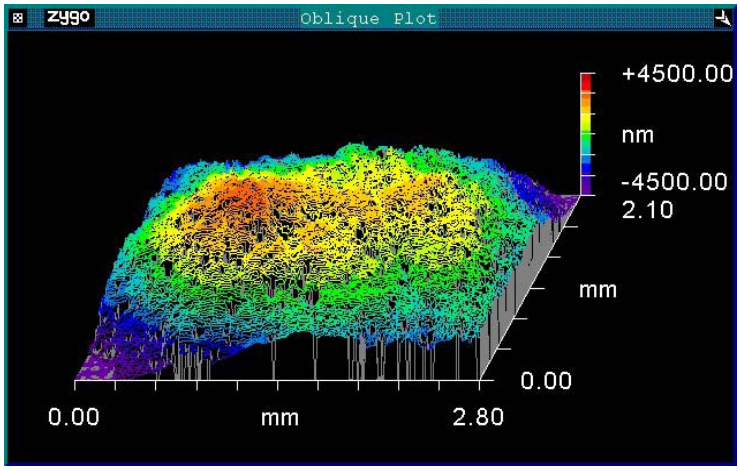


**Figure 6.4:** Interferometric images showing the surface structure of a new sample (a) and of samples treated at the cathode (b) respective anode side (c).

At the cathode side the surface structure changes as a consequence of a sputtering process induced by Ar ions and metastable atoms. The high density of excited Ar atoms on metastable states ($10^{13}$ $cm^{-3}$) makes this process very effective. The spectral investigations performed in this pressure range but without gas flow through the MSE hole shown that at about 1.2 mm above from the surface there are still excited atoms. When passing the gas through the hole the metastable produced inside the hole are transported by the gas flow at higher distances. Although at 4 mm the density of excited atoms is lower than immediately above the cathode surface, their velocity has another orientation which is important taking into account the fact that sputtering is a threshold process in respect to the momentum of the incoming particle. If the distance is further increased the number of the excited atoms decreases and gradually becomes insufficient to break chemical bonds. For a distance of 9 mm the surface reminds more on an untreated film, fact confirmed also by the WCA value that is only slightly lower than for a new sample.

For the samples that were placed at the anode side, the roughness of the surface does not show a significant modification (Fig. 6.4c). It is expected that the modification is of chemical natured, caused by the negative oxygen ions and free radicals. This idea is sustained also by the dependency of the WCA on the distance from the anode surface. The density of active species is high close to the hole and decreases exponentially with the distance.

Plasma surface treatment may change the properties of the superficial monolayers of a material in a physical or a chemical process. The chemical composition of the treated area was determined by means of X-ray Photon Spectroscopy (XPS). The depth below the surface analyzed by XPS is typically 3-5 nm, that means that the method gives information about the chemical constituents of the surface, not implanted in the material. Anyhow the energy gained by the particles in the microdischarge is not high enough to produce implantation. It was found that a large amount of oxygen atoms is bonded on the polymer surface. There are the so-called functional groups like carbonyl, hydroxyl or carboxyl, which attached to a surface are able to increase its wettability [Rot-01].

## 6.2. Plasma chemistry

To study the reactivity of the MSE plasma regarding the decomposition of exhaust gases (diesel engines) experiments have been performed in mixtures of NO with He and Ar at pressures up to one atmosphere. The experimental set-up used for these investigations is presented in Fig. 6.5.

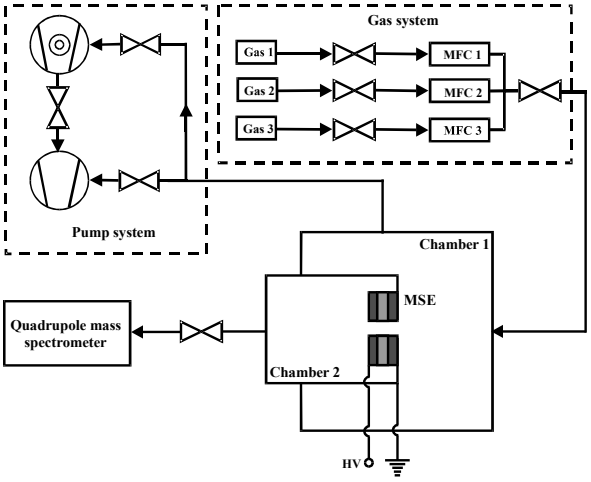


**Figure 6.5:** Experimental set-up for plasma chemistry measurements.

Different gases or gas mixtures are injected into the first chamber of the reactor through a mass flow control (MFC) system. A high-precision valve placed between the second chamber and the pump system controls the working pressure. The gas to be studied is flowing through the microdischarge. The concentrations of some molecules of interest ($N_2$, $O_2$, NO and $NO_2$) are monitored by a quadrupole mass spectrometer coupled to the reactor through a 1 m long capillary. The detection was performed in the Multiple Ion Detection mode (MID), which allow following the time evolution of the selected species.

The measurements have been performed in He and Ar with 500 ppm NO admixture. The working pressure was varied from 0.5 bar to atmospheric pressure, at a gas flow of 5 sccm and 20 sccm directed from anode to cathode. In He/NO mixture the discharge was switched on at 0.1 W and during the measurement the power was linearly increased up to 0.4 W. A typical mass spectrum is presented in Fig. 6.6.

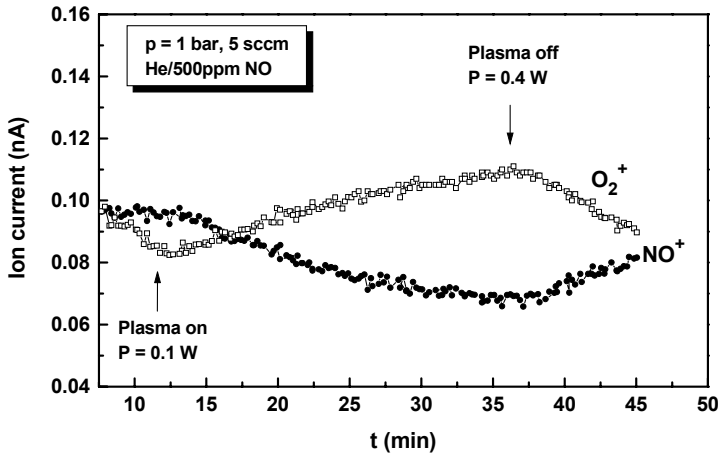


**Figure 6.6:** NO decomposition in a planar MSE discharge at 1 bar in He with 500 ppm NO.

As long as the discharge operates there is a removal of NO. Simultaneously the concentration of molecular and atomic oxygen and that of atomic and molecular nitrogen increases showing that the main products are $N_2$ and $O_2$. A decrease in the concentration of $NO_2$ and the formation of higher nitrogen oxides ($NO_3$, $N_2O_3$, $N_2O_5$) were not detected. When the plasma is turned off the decomposition process stops and the NO concentration rises up to its initial level.

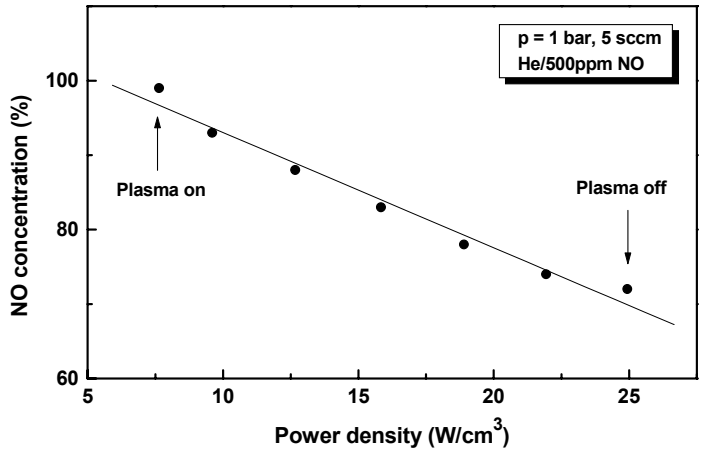


**Figure 6.7:** Decrease in the NO concentration as a function of the power density in the microdischarge.

The removal efficiency is proportional to the power coupled into the discharge, as it can be seen in Fig. 6.7. To estimate the power consumption one has to know the active discharge volume. Optical measurements have shown that at pressures higher than about 400 mbar the discharge is concentrated inside the hole. For the currently used MSE the plasma volume is estimated to be about $1.5 \cdot 10^{-5}$ $cm^3$. This leads to a power density of about 25 $kW/cm^3$ and 45 $kW/cm^3$ at 0.4 W/hole and 0.7W/hole, respectively. At 0.4 W discharge power the removal efficiency of NO in He plasma is about 15% at 0.5 bar and 30% at 1 bar. The amount of molecular oxygen increases up to 60% and that of atomic oxygen up to 30%, while the enhancement in the nitrogen concentration is about 10%. The removal efficiency depends also on the retention time of the pollutant in the active volume, thus by increasing the gas flow the decomposition efficiency decreases. Under the same discharge condition but for 20 sccm gas flow the decomposition rate is less that 15%.

In Ar/NO mixtures using at low gas flow (5-10 sccm) an enhancement in the NO concentration was noticed, as viewed in Fig. 6.8.

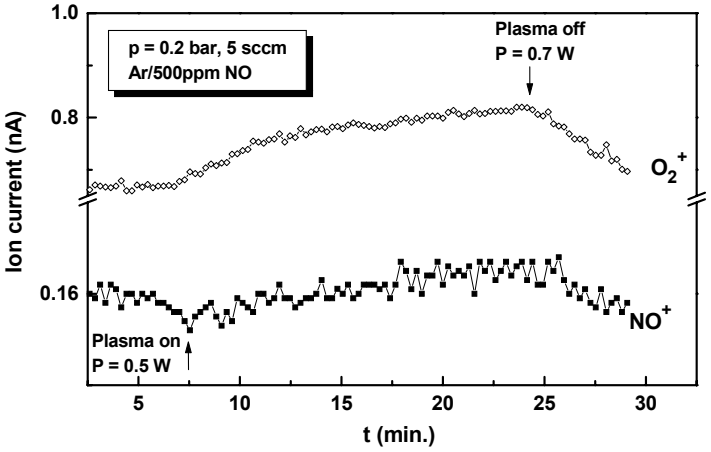


**Figure 6.8:** NO generation in a MSE plasma in Ar with 500 ppm NO at small gas flow.

For a discharge power of 0.5 W the NO concentration increases up to 3% and for 0.7 W twice this value. This means that about 30 ppm NO are created in the discharge for a power density of about 40 $kW/cm^3$.

The generation of small, well-defined quantities of NO is very important for medical studies [Bal-01]. The product concentration depends on the power applied to the microstructure and is therefore adjustable.

The high-pressure glow discharge generated using MSE arrays can be implemented as well in analytical spectrometry. Preliminary experiments in this direction have been already performed. A single-hole microstructure (100 μm diameter) based on $Pt/Al_2O_3$ was used to generate a DC glow discharge at atmospheric pressure. To investigate the decomposition of halogenated molecules, the MSE sustained discharge was operated in mixtures of noble gases with small amounts (in the ppm range) of reactive gases ($CCl_2F_2$, $CClF_3$, $SF_6$). These gas mixtures are commonly used for etching in the semiconductor industry and usually they are not completely decomposed. The waste gas has to be additionally reduced to a nontoxic state. The decomposition efficiency of different reactive gases containing halogens was studied in Ar as buffer gas by means of optical emission spectroscopy. For analyte concentrations lower than about 30 ppm, the emitted line intensity of the halogen atoms depends linearly on the amount of the introduced molecules. The detection limit, important when performing analytical measurements, could be extended up to the ppb range.

## 6.3. Conclusions

Free radical chemistry at moderate and high pressure is extremely fast and thus allows high production and destruction rates as well as high-speed treatment of surfaces [Kog-97].

The increase of the surface energy of organic substrates commonly used in the packaging industry is very important because it is desirable to use non-toxic water-based paintings. In the present study was demonstrated that the MSE sustained discharge is capable of inducing surface modification. The surface energy could be increased and accordingly the wettability of a material (here a polymer film) could be improved by exposure to the microdischarge. The modification was found to be permanent whenever the substrate is placed at the anode or the cathode side, but different processes are responsible for the change of the surface energy. When the polymer film is placed at the cathode side the surface is strongly sputtered by ions and fast neutrals or ablated by UV

photons, while at the anode side the processes are mainly of chemical nature involving negative ions and free radicals.

Due to their high power density, atmospheric pressure non-equilibrium plasmas generated by means of MSE could be used as atomization sources for analytical spectrometry. Such devices present an interesting alternative to other microplasmas integrated in miniaturized analytical systems for on-line measurements and 'high - throughput' screening methods.

Different plasma enhanced syntheses could be carried out in proving that the MSE sustained discharges are suitable as a catalyst for chemical processes. Furthermore, due to their sub-millimetric dimensions the MSE arrays are ideally applicable as catalyst in micro-reactors. The efficiency can be further increased by reducing the diameter of the hole and accordingly increasing the power density in the active volume or by switching on more microstructures successively. By operating a large number of microdischarges in parallel one can implement the MSE as a versatile gas filter at atmospheric pressure.

# CHAPTER 7
# AGING OF THE MICROSTRUCTURES

## Introduction

Up to now it was demonstrated that the MSE arrays could be used to generate high-pressure homogeneous plasma. The range of operation, discharge characteristics as well as the intrinsic plasma parameters make the MSE sustained discharge a good choice for applications that requires high-pressure conditions. The applicability of the MSE sustained discharge to surface modification and waste gas treatment was demonstrated. Another aspects very important for industrial applications, besides the efficiency of a given process, are the long-term reliability and the low cost. As the microstructures are essential for this new plasma source, their aging induced by the discharge operation has to be investigated. The different processes resulting in the deterioration of the MSE have to be determined and solutions to improve the lifetime of the structures have to be found, keeping a relatively low production cost. To this aim, the MSE have been investigated through optical microscopy (OM), surface profilometry (SP) and scanning electron microscopy (SEM) coupled with energy dispersive X-rays analysis (EDX). The results of this study will be presented in the following.

## 7.1. Optical microscopy and surface profilometry

Usually, before using the MSE they are qualitatively investigated through an optical microscope having a maximal magnification of 400. Although in most of the cases the multilayer is very precise structured, it may happen that in some places the metal surface has defects or the insulator is perforated. This can be attributed to errors in executing the mask used for chemical etching or to defects in the raw material. An example is presented in Fig. 7.1a for Cu-Kapton-Cu. For parallel operation of a large

number of microdischarges it is very important that the whole MSE has a good quality because this reflects directly in the evolution of individual discharges.

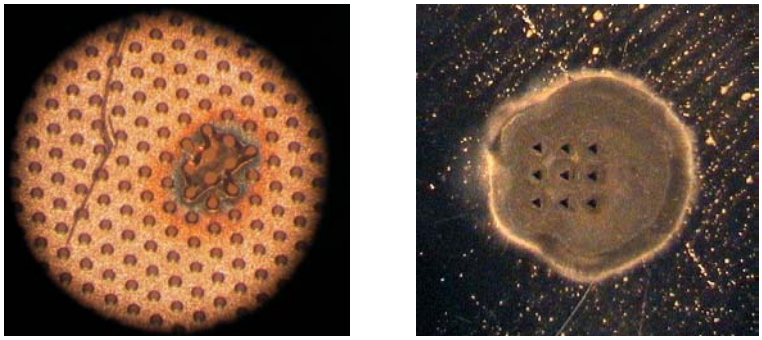

a b

**Figure 7.1:** Defects of the MSE caused by the manufacturing procedure (a) and sputtered Al cathode after atmospheric pressure operation (b).

Investigations were performed also on used microstructures to see the effects of the discharge. It was observed that the electrodes, especially the cathode, are strongly sputtered. This effect is shown in Fig. 7.1b, for thin Al electrodes (1 μm) under atmospheric pressure discharge conditions. Around each hole the metal is removed up to the moment when a homogeneous discharge cannot be further sustained and contracts to a filament. In this case the MSE becomes unemployable.

A consequence of the high power density in the discharge area is the heating of both the gas and the microstructure. This effect can be visualized through the different colors of the metal surface caused by different oxides created at different temperatures.

Besides the sputtering of the electrodes, the high energy density in the microdischarge discharge should have an effect also on the insulator placed between the two metal electrodes. An advantage of the optical microscopy is that it can be used to analyze dielectric substrates, where scanning electron microscopy cannot be applied due to the up charging of the surface. Non-conductive materials can be examined through SEM if a thin metal film (in nm range) is deposited on their surface, but this procedure cannot be always applied. For most of the investigations performed in this work, MSE based on Kapton as insulator have been used due to the flexibility in choosing the discharge configuration and the low price. To estimate the modifications induced to the

insulator, the metal electrodes have been removed by chemical etching. The polyimide film used as insulator is strongly affected by the discharge. Fig. 7.2 shows the evolution of the hole in insulator (Kapton) from a new to an extremely damaged hole.

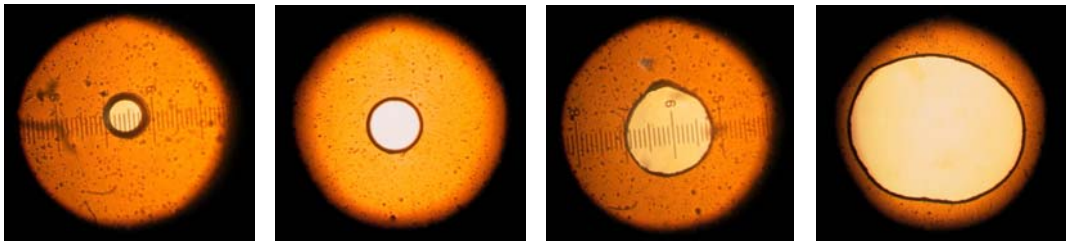

**Figure 7.2:** Effect of the microdischarge on the polyimide insulator viewed after removing the Cu electrodes.

Depending on the working gas, discharge current and operation time, the hole in insulator can increase up to 70 times the original diameter. For relatively low discharge current (up to 1 mA) and moderate pressure (about 200 mbar), these effects are not so dramatic. Under these conditions the hole in the insulator is increasing only with up to 30-40%, which does not perturb the discharge operation.

The microstructures were further investigated using an alpha-stepper, one of the reasons being to find out where the sputtered metal is deposited. An alpha-stepper is a prolifometer, a versatile system that allows measuring very precisely the roughness of surfaces [Ten-01].

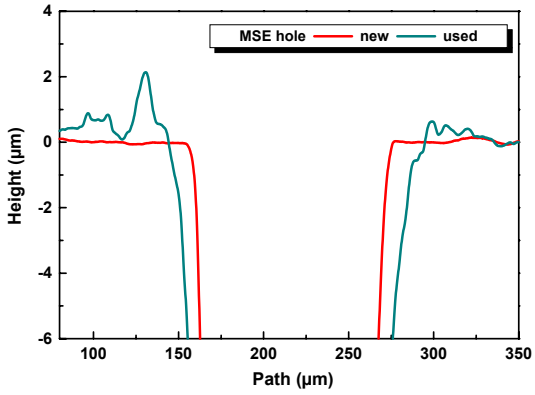


**Figure 7.3:** Profile of a MSE hole measured with an alpha-stepper.

The electrode surface as obtained from the manufacturing process is very smooth and the edges of the hole well defined. For a used MSE it can be clearly seen that material from the cathode was removed and deposited on the surface, around the hole. A larger amount of material is deposited on the left-hand side of the picture. A possible explanation could be that the MSE was mounted with this side downwards and the distribution of the sputtered material is a consequence of gravitation. The sputtered metal can deposits as well on the walls of the hole and connect the two electrodes by a thin conductive layer resulting in a short circuit. Actually, this is a frequent situation when Cu electrodes with a high sputtering rate are used.

The profilometer used is not adequate for measuring long and narrow channels like the MSE. Therefore only the upper side of the hole in metal was possible to be measured. The shape of the hole (here cathode side) changes and its diameter increases noticeable.

## 7.2. Scanning electron microscopy

For a better visualization of the modifications induced to the microstructres by the discharge operation, they were investigated by means of scanning electron microscopy (SEM). A new hole is imaged in Fig.7.4a. A used MSE is imaged under the same magnification (600) in Fig. 7.4b and c at the anode and cathode side. The MSE was operated in Ar at 500 mbar and discharge current up to 5 mA for about 10 hours.

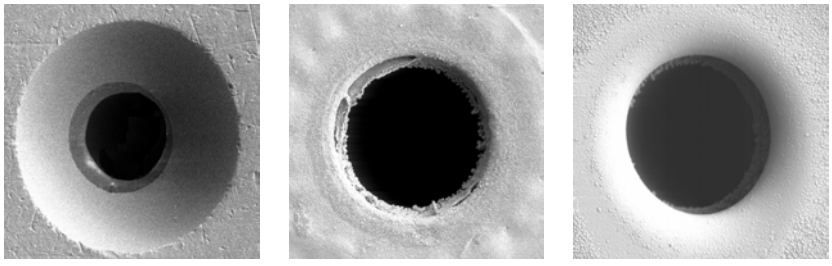

**a** **b** **c**

**Figure 7.4:** SEM pictures of a new MSE hole (a) and of a microstructure operated in argon (b) anode side and (c) cathode side.

The microstructure presented is based on Kapton as insulator. Due to the manufacturing procedure (photolithography) these MSE are of extremely good quality. From hole to hole the reproducibility is very good, as discussed in Chapter 2 and shown in Fig. 2.7a. The holes are perfectly circular and present very precise edges as evidenced in Fig. 7.4a. By a used MSE the hole diameter at the cathode side increases with up to 10% and the edges are rounded, while the anode edges remains almost unchanged.

Like in low-pressure DC glow discharges, the ions accelerated in the cathode fall could be very effective in inducing sputtering. Spectral measurements have revealed also the presence of a large number density of exited atoms in metastable states. They are produced in the negative glow adjacent to the cathode and may interact strongly with its surface. The sputtering coefficient increases strongly with the atomic weight and the energy of the bombarding particle. Experimentally, it was noticed that the cathode erosion is much more pronounced in Ar plasma than in Ne or He discharges. The Ar ions are not only heavier than the Ne or He ions, but they can gain a higher energy from the electric field in the cathode fall. Considering the values for a normal glow discharge at low pressure, the normal cathode fall $V_n$ for the three gases mentioned is comparable but the cathode fall length for Ar is much smaller. As an example, for a discharge with Fe electrodes the cathode fall thickness was determined as 0.33, 0.72 and 1.3 torr cm for Ar, Ne and He, respectively [Bro-59]. The normal current density $j/p^2$ at the cathode is much higher for Ar than for Ne or He. For Fe or Ni electrodes the values are 160, 6 and 2.2 $\mu A/torr^2\ cm^2$ for Ar, Ne and He, respectively [Rai-97].

Although the density of metal atoms and ions is much lower than that of the gas particle, the sputtering process by metal ions should be taken into account as very effective because the metal ions are heavier than the rare gas ions.

Like already mentioned, not only the cathode is strongly sputtered but also the dielectric substrate. This effect is clearly visible only for the polyimide substrate. The glass and ceramic substrates have a low sputtering rate and withstand high temperature. In this case the effect was evidenced only by means of emission spectroscopy when emission lines belonging to the insulator constituents were detected. However, SEM can illustrate very well the way in which the free surface of the polyimide film is altered.

In order to analyze the inner surface of the hole, which comes in direct contact with the discharge, the microstructure was carefully cut through the middle of one hole.

The side-on SEM image of a hole is given in Fig. 7.6a and b for new and used MSE. respectively.

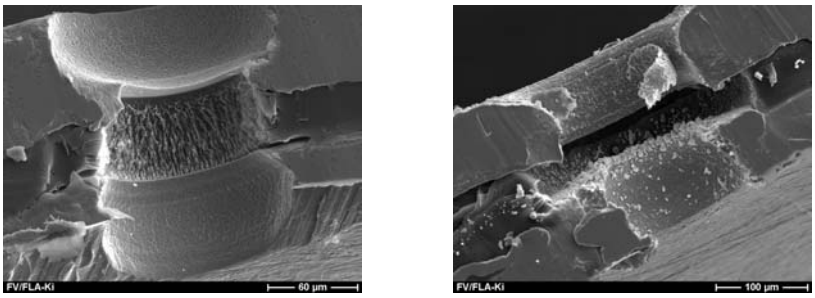


**a** **b**

**Figure 7.6:** Transversal cross-section through a new MSE hole (a) and used (b).

Here is visible again that the cathode (on top) is strongly sputtered while the anode is practically unchanged. Between the electrodes the insulator (Kapton) is practically removed. The modification of the polyimide film could be of pyrolytic type [See-98]. This material does not withstand temperatures higher than about 400 °C and above this value should begin to shrink [Dup-01]. This modification could be a photolytic process as well, because it is known that Kapton can be modified by exposure to UV light [Dup-01]. The emission of UV radiation was proved for the MSE sustained discharge as reported in [Pen-01]. As well, due to the presence of highly energetic electrons and of a large number density of metastable atoms in the microdischarge it is very probable that excimer radiation is generated. There are experimental studies, which have shown that polyimide films are strongly modified when are exposed to dielectric barrier discharges [See-00].

Microstructures with incorporated resistive ballast have been also investigated. As described in Chapter 2, around the hole, the copper layer was removed up to the insulator and the resulting channel was filled up with a resistor paste (see Fig. 7.7). Energy Dispersive X-rays analysis (EDX) method was used to investigate from the chemical point of view the MSE surface that was in contact with the discharge. EDX technique gives information about the presence of different chemical elements on the investigated sample. On the surface of a new microstructure mostly Cu was detected, and traces of other elements (Cl, S), most probably resulting from the manufacturing procedure and the storage conditions. However for a used MSE, the chemical composition of the surface

depends on the position relative to the center of the hole. The areas where EDX analysis was performed are marked in Fig. 7.8.

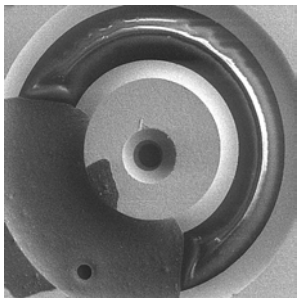

**Figure 7.7:** MSE with incorporated resistive ballast.

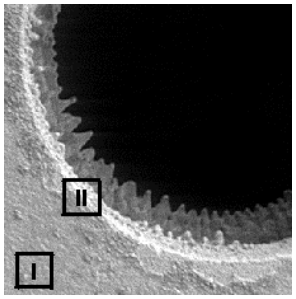


**Figure 7.8:** Detailed view of a hole. The regions of interest for EDX are marked.

Relatively far from the hole the same elements as for a new MSE were detected, which means that in region I the characteristic line of Cu is dominant. Adjacent to the hole (region II) and inside it elements as O and C are definitely dominant but also Cu and traces from Cl were detected. These elements are constituents of the polyimide film. The presence of C atoms inside the hole can cause a non-permanent, high resistance (tens of MΩ) short circuit. The MSE becomes unusable only when a low resistance short circuit (kΩ and less) is generated due to metal deposition inside the hole.

## 7.3. Discussions

As expected for a DC discharge, strong erosion of the cathode was observed. Erosion can be defined as a sputtering process where a large amount of material is removed. Sputtering is a mechanism in which the kinetic energy of a bombarding ion or atom is transferred in a collision to one or a few surface atoms of the cathode material, which are then repelled into the gas by the asymmetric potential at the surface. The sputtering coefficient has a threshold in respect to the momentum of the incoming particle. The sputtered material either diffuses out of the discharge area or the metal atoms are ionized and return to the cathode surface as positive ions contributing to further sputtering of the cathode [Sch-90].

The specific discharge geometry plays also an important role. The sputtering rate in hollow cathode discharges is larger than in the normal glow discharges, being a direct consequence of the higher current density [Mus-62]. For cathodes made of materials with high sputtering coefficient the erosion of the cathode can change the geometry until the cathode approaches a stable configuration. Experimentally was observed that the MSE discharge becomes more stable and the sustaining voltage gradually decreases after a given time of operation, depending on the working gas and discharge power.

Regarding the modification of the dielectric spacer, in the case of polyimide not only the surface is deteriorated but a large amount of material is removed, and the inside shape of the hole drastically change. It is rather difficult to separate the effects of diverse agents because inside the hole both ions and fast neutrals as well as UV radiation are simultaneously present. For a ceramic substrate however, the sputtering effect is much lower and the discharge configuration is not visible influenced. As well using materials with low sputtering rates for the electrodes, the erosion of the cathode can be strongly reduced and the lifetime of the MSE significantly increased.

# CHAPTER 8
# SUMMARY AND OUTLOOK

This work was devoted to the investigation of Micro-Structured Electrode (MSE) sustained discharges. Using MSE arrays the discharge gap is scaled down to the sub-millimetric range and accordingly the working pressure could be increased at low power consumption up to atmospheric.

Different discharge configurations using various electrode materials and substrates, with different hole diameters from 100 μm to 300 μm were DC operated in the glow discharge regime. The optical appearance shows a stable, homogeneous discharge for pressures ranging from 10 to 1000 mbar. Adjacent to the cathode the microdischarge presents the luminous and dark layer known from low-pressure discharges and their behavior with the pressure sustain the hypothesis that the MSE sustained discharge is a glow discharge. At relatively low pressures the discharge develops between the electrodes and expands out of the hole at the cathode side. The increase of the pressure determines its constriction inside the MSE hole, which results in an increased power density in the discharge volume. The MSE sustained discharge can be considered as a normal glow discharge whereby the excitation/ionization efficiency is increased by the specific discharge configuration (hollow cathode geometry).

Parallel operation of up to 200 microdischarges without individual ballast was proven in rare gases and gas mixtures for pressures up to 300 mbar. Furthermore, arrays of resistively decoupled microdischarges were successfully operated up to atmospheric pressure. Current densities from 0,5 to 120 A/cm$^2$, respectively power densities of about 0,1 to 25 kW/cm$^2$ have been reached.

Different spectral methods have been applied to investigate the intrinsic plasma parameters of the MSE sustained discharges. Emission spectroscopy and diode laser atomic absorption spectroscopy, were used for estimating the gas and electron temperature, as well as the number density of excited atoms and electrons.

The investigations have revealed the presence of a large number density of metastable atoms and energetic electrons. In the MSE sustained discharge the density of

excited atoms in metastable and resonance levels is on the order of $10^{13}$ $cm^{-3}$. By rising the pressure, the absolute number density of excited atoms is slightly increasing.

The gas temperature inside the MSE hole, derived from Doppler broadening of the Ar transitions at 800.838 nm and 801.699 nm, was found to increase linearly with the pressure from 380 K at 50 mbar to 1100K at 400 mbar. Although the plasma confined inside the hole may reach gas temperatures up to 1000 K, the ambient gas temperature immediately above the microstructure exceeds only slightly the room temperature.

The electron number density was calculated from the Stark broadening (shift) after extracting the collision broadening from the total pressure broadening and is increasing from $9 \cdot 10^{14}$ $cm^{-3}$ to $5 \cdot 10^{15}$ $cm^{-3}$ in the pressure range investigated. An advantage of this method upon emission spectroscopy is that it provides information about the electron number density in the dense plasma confined inside the hole. When using emission spectroscopy for electron temperature and density measurements it may happen that the detected light comes from the outermost regions of the discharge, which are colder and have a lower electron density. Therefore such measurements may not reflect the real electron number density in the discharge.

By using He as filling gas a lower gas temperature could be achieved but the electron density decreases too. Investigations at atmospheric pressure have shown that the gas temperature may rise up to 2000 K, while the electron number density increases to almost $10^{16}$ $cm^{-3}$.

These measurements have demonstrated that due to the high number density of metastable atoms produced in the microdischarge, diode laser atomic absorption spectroscopy could be implemented for the study of small size plasmas. It should be mentioned that this technique is an innovative approach for investigating sub-millimetric discharges.

The MSE sustained discharge provides non-equilibrium plasma in high-pressure gases and offers the premises for efficient plasma processing under non-thermal conditions. The reactivity of the microdischarge was proven in respect to waste gas decomposition and surface treatment. Since the free radical chemistry at high pressure is very fast, high production and destruction rates as well as high-speed treatment of surfaces could be achieved. The results obtained up to now are very promising but for applications on industrial scale the lifetime of the MSE has to be improved.

Surface treatment on industrial scale requires usually large area uniform discharges. In the case of MSE, large area could be achieved by running a large number of microdischarges in parallel (with or without resistive decoupling) to build a plasma module. Homogenous plasma could be obtained by increasing the density of holes to about 500 holes/cm$^2$. Another approach is to use the MSE discharge as "plasma cathode" for a high-pressure glow discharge created between the microstructure and an additional electrode. If the substrate to be treated is metallic can play itself the role of the additional electrode.

For special applications, when local and directed surface activation is desired a single-hole discharge can be operated under static conditions or as a plasma jet. Furthermore, the MSE plasma source is an ideal device for surface treatment, because it can be individually adapted even to curved or less accessible surfaces, if the electrode system is bonded to a flexible substrate.

Concerning waste gas decomposition and plasma chemistry, it was demonstrated that the MSE arrays could be implemented as a versatile gas filter at atmospheric pressure. An increased efficiency could be achieved by switching on more microdischarges successively.

Systematic studies concerning different applications have to be further performed and if required, the conditions optimized in laboratory experiments have to be scaled to industrial applications. The discharge reproducibility and long time stability, as well as the lifetime of the MSE under specific working conditions have to be investigated.

To conclude, the MSE sustained discharges are combining a non-thermal character with the advantage of high pressure, which recommends them for plasma assisted surface processing, plasma chemistry and generation of UV and VUV radiation.

# APPENDIX A

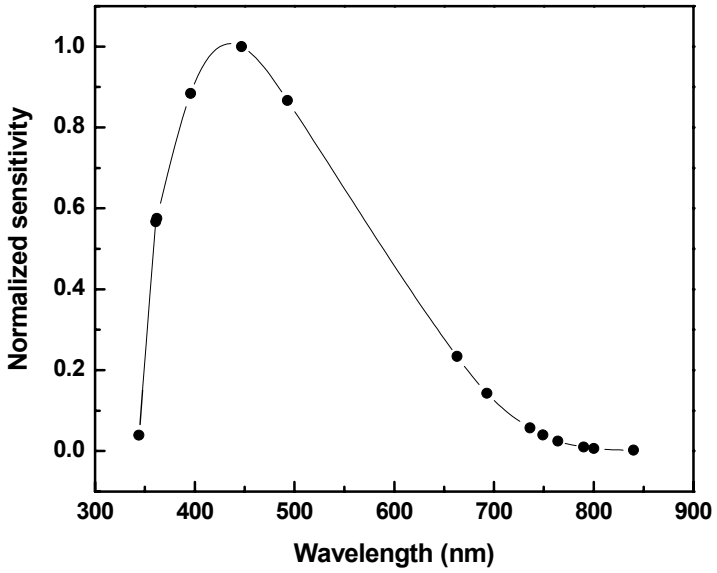


**Figure A.1:** Relative spectral response of the system OMA-spectrometer used in section 3.2.

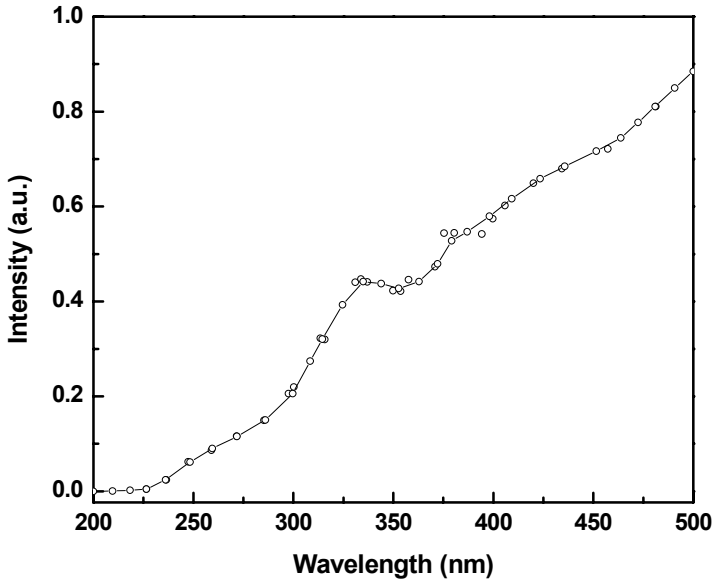


**Figure A.2:** Spectral response of the system spectrograph-CCD camera used in section 3.6.

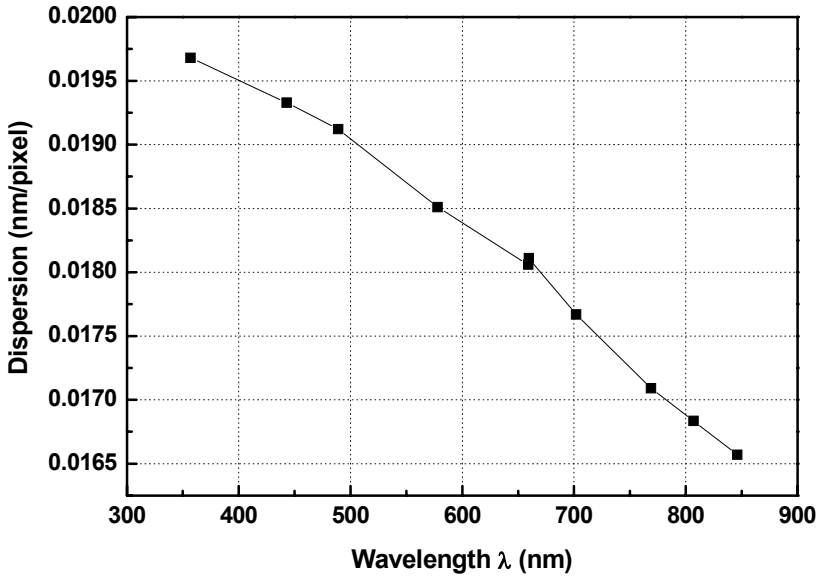


**Figure A.3:** Dispersion of the spectrometer Ortec BM100.

# APPENDIX B

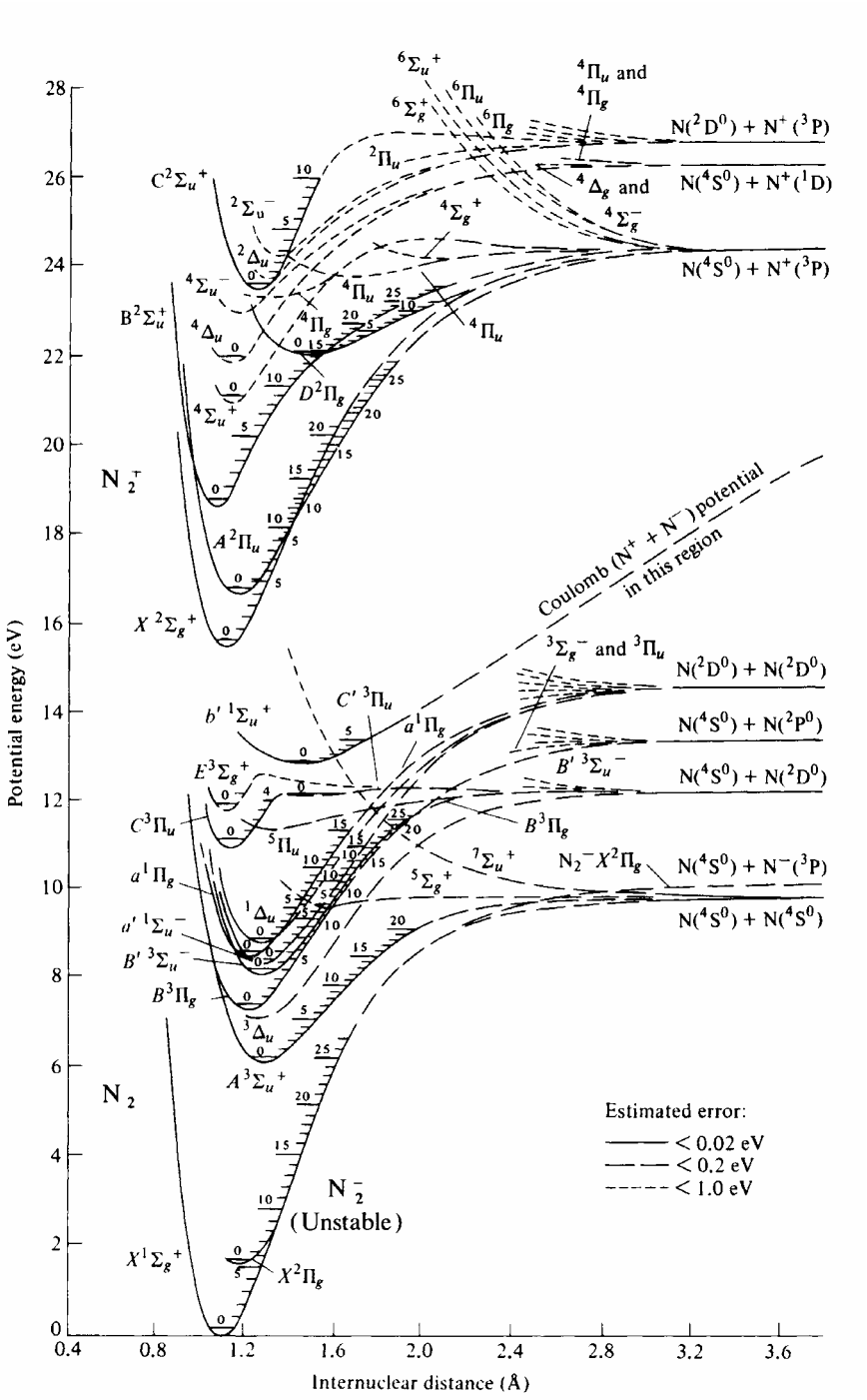


**Figure B.1:** Potential energy diagram for nitrogen from [Ste-85].

# BIBLIOGRAPHY


[Abr-66] L. Yu. Abramovich, B. N. Klyarfel'd, Yu. N. Nastich, "Superdense hollow cathode glow discharge", Sov. Phys. Techn. Phys. **11**, 4, pp. 528-532 (1966).

[Bal-01] A. T. Balaban, "Relevance of chemical kinetics for medicine: the case of nitric oxide", J. Chem. Ed., submitted (2001).

[Băd-58] E. Bădărău, I. Popescu, "Research on the double cathode effect", J. Electr. Contr. **4**, pp. 503-514 (1958).

[Bib-87] L. M. Biberman, G. E. Norman, K. N. Ulyanov, *"Kinetics of non-equilibrium low-temperature plasmas"*, Consultants Bureau, New York (1987).

[Bib-01a] N. K. Bibinov, A. A. Fateev, K. Wiesemann, "On the influence of metastable reactions on rotational temperatures in dielectric barrier discharges in He-$N_2$ mixtures", J. Phys. D: Appl. Phys. **34**, pp. 1819-1826 (2001).

[Bib-01b] N. K. Bibinov, A. A. Fateev, K. Wiesemann, "Variations of the gas temperature in He/$N_2$ barrier discharges", Plasma Sources Sci. Technol. **10**, pp. 579-588 (2001).

[Bil-00] A. M. Bilgic, U. Engel, E. Voges, M. Kückelheim, J. A. C. Brockaert, „A new low power microwave plasma source using microstrip technology for atomic emission spectrometry", Plasma Sources Sci. Technol. **9**, 1, pp. 1-4 (2000).

[Bog-95] A. Bogaerts, R. Gijbels, "Modelling of metastable argon atoms in a direct-current glow discharge", Phys. Rev. A **52,** 5, pp. 3743-3751 (1995).

[Bom-92] D. S. Bomse, A. C. Stanton, and J. A. Silver, „Frequency modulation and wavelength modulation spectroscopy: comparison of experimental methods using a lead-salt diode laser", Appl. Opt. **31,** pp. 718-731 (1992).

[Bor-66] V. S. Borodin, Yu. M. Kagan, "Investigation of hollow cathode discharge. I. Comparison of the electrical characteristics of a hollow cathode and a positive column" Sov. Phys.-Tech. Phys. **11**, pp. 131-134 (1966).

[Brä-00] A. Bräuning-Demian, L. Spielberger, C.Penache, H. Schmidt-Böcking, „ A source of large-area atmospheric pressure discharges: characterisation, electrical properties and spatially resolved photon emission„, Proc. of the XIII Int. Conf. on Gas Discharges and their Applications, Glasgow, pp. 426-429 (2000).

[Bro-59] S.C. Brown, *"Basic data in plasma physics"*, MIT Press, Cambridge (1959).

[Bus-01] R. Bussiahn, H. Lange, "Laser atom absorption spectroscopy on micro hollow cathode discharges in xenon", Proc. of the APP Spring Meeting "Diagnostics of Non-Equilibrium High Pressure Plasmas", Bad Honnef, pp.175-178 (2001).

[Cam-85] J.C. Camparo, "The diode laser in atomic physics", Contemp. Phys. **26**, 5, pp. 443-477 (1985).

[Cas-78] H. C. Casey, M. B. Panish, "Heterostructure Lasers Part A: Fundamental Principles", Academic Press, New York (1978).

[Cer-01] http://www.ceramtec.com

[Cli-78] M. A. A. Clyne, P. B. Monkhouse, D.W. Setser, "Energy transfer in collisions of $Ar(^3P_{0,2})$ metastable atoms with $H(^2S)$ atoms. Total rate constants and mechanism", Chem. Phys. **28**, pp. 447-454 (1978).

[Cst-01] http://www.cst.de

[Dra-65] H. W. Drawin, P. Feelenbock, *"Data for plasmas in local thermodynamic equilibrium"*, Gauthier-Villars, Paris (1965).

[Dra-69] H. W. Drawin, "Validity conditions for local thermodynamic equilibrium", Z. Physik **228**, pp. 99-119 (1969).

[Dem-96] W. Demtröder, „*Laser spectroscopy"*, Springer Verlag, Berlin (1996).

[Dup-01] http://www.dupont.com

[ElH-00] A. El-Habachi, W. Shi, M. Moselhy, R. H. Stark, K. H. Schoenbach, „Series operation of direct current xenon chloride excimer sources", J. Appl. Phys. **88**, 6, pp. 3220-3224 (2000).

[Eng-33] A. von Engel, R. Seelinger, M. Steenbeck, „Über die Glimmentladung bei hohen Drucken“, Z. Phys. **85**, pp. 144-160 (1933).

[Eng-65] A. von Engel, *„Ionized gases“*, Clarendon Press, Oxford (1965).

[Eng-83] A. von Engel, *„Electric plasmas: their nature and uses”*, Taylor and Francis Ltd., London and New York (1983).

[Ern-01] U. Ernst, “Emissionsspektroscopische Charakterisierung von Hochdruck-Mikrohohlkathodenentladungen”, PhD Thesis, Friedrich-Alexander University, Erlangen-Nürnberg (2001).

[Fat-00] A. A. Fateev, K. Wiesemann, “Rotational temperatures of different molecules in dielectric barrier discharges”, Proc. of Hakone VII, Greifswald, pp. 209-213 (2000).

[Fil-00] D.M. Filipovic, B.P. Marinkovic, V. Pejcev, L. Vuskovic, “Electron impact excitation of argon: the lowest resonance $4s[3/2]_1$ and metastable $4s[3/2]_2$ and $4s'[1/2]_0$ states“, J. Phys. D: At. Molec. Opt. Phys. **33**, pp. 2081-2094 (2000).

[Fra-93] J. Franzke, A. Schnell, K. Niemax, “Spectroscopic properties of commercial laser diodes”, Spectrochimica Acta Rev. **15**, 5, pp. 379-395 (1993).

[Fra-97] J. W. Frame, D. J. Wheeler, T. A. DeTemple, J. G. Eden, “Microdischarge devices fabricated in silicon”, Appl. Phys. Lett. **71**, 9, pp. 1165-1167 (1997).

[Ger-96] K.-H. Gericke, H. Schmidt-Böcking, „Vorrichtung zur Erzeugung mehrerer Mikroplasmen bei Umgebungstemperatur und Verwendung einer derartigen Vorrichtung“, German patent DE 196 05 226 C2 (1996).

[Gew-65] J. W. Gewartowski, H. A. Watson, „Principles of electron tubes”, Van Nostrand, Princeton (1965).

[Gil-77] P. Gill, C. E. Webb, „Electron energy distribution in the negative glow and their relevance to hollow cathode lasers“, J. Phys. D: Appl. Phys. **10**, pp. 299-311 (1977).

[Gol-78] M. Goldman, T. Goldman, *“Corona discharges in Gaseous Electronics 1, Electrical discharges”,* Academic Press, New York (1978).

[Gor-56] F. Gordon, Encycolpedia of Physics, Vol. XXII, *„Gas Discharges II“*, Springer Verlag, Berlin-Göttingen-Heidelberg (1956).

[Gri-62] H. Griem, "Stark broadening of isolated spectral lines from heavy elements in a plasma", Phys. Rev. **128**, 2, pp. 515-521 (1962).

[Gri-64] H. R. Griem, *"Plasma spectroscopy"*, MsGraw-Hill Book Company, New York (1964).

[Gri-97] H. R. Griem, *„Principles of plasma spectroscopy"*, Cambridge University Press, Cambridge (1997).

[Gün-23] A. Güntherschulze, „Die Stromdichte des normalen Kathodenfalles", Z. Phys. **19**, pp. 313-332 (1923).

[Her-50] G. Herzberg, *"Molecular spectra and molecular structure. Part I: Spectra of diatomic molecules"*, Van Nostrand Reinhold Company, New York (1950).

[Her-99] J. T. Herron, "Evaluated chemical kinetics data for reactions of $N(^2D)$, $N(^2P)$, and $N_2(A^3\Sigma_u^+)$ in the gas phase", J. Phys. Chem. Ref. Data, **28**, 5, pp. 1453-1483 (1999).

[Hoc-98] M. Hoch, "Development of fast tracking detectors: micro strip gas chamber and gas electron multiplier", PhD Thesis, CERN, Geneva (1998).

[Hol-68] W. Lochte-Holtgreven, *"Plasma diagnostics"*, North-Holland Publishing Company, Amsterdam (1968).

[Hud-65] R. Huddlestone, S. Leonard, "*Plasma diagnostic techniques"*, Academic Press New York London (1965).

[Hut-87] I. H. Hutchinson, *„Principles of plasma diagnostics"*, Cambridge University Press, New York (1987).

[Kog-91] U. Kogelschatz, B. Eliasson, H. Esrom, "Industrial applications of excimer ultraviolet sources", Materials and Design, **12**, 5, pp. 251-258 (1991).

[Kog-97] U. Kogelschatz, B. Elliason, W. Egli, "Dielectric barrier discharges: Principles and applications" Proc. of the XXIII-th ICPIG, Toulouse, pp. C4-47 (1997).

[Kun-01] K. Kunze, M. Miclea, G. Musa, J. Franzke, C. Vadla, K Niemax, "Diode laser-aided diagnostics of a low-pressure dielectric barrier discharge applied in element selective detection of molecular species", Spectrochimica Acta Part B, in print (2001).

[Kur-99] P. Kurunczi, H. Shah, K. Becker, „Hydrogen Lyman-α and Lyman-β emissions from high-pressure microhollow cathode discharges in Ne-$H_2$ mixtures", J. Appl. Phys. B: At. Mol. Opt. Phys. **32**, pp. 656-658 (1999).

[Lau-92] C. O. Laux, C. H. Kruger, "Arrays of radiative transitions probabilities for the $N_2$ first and second positive, NO beta and gamma, $N_2^+$ first negative and $O_2$ Schumann-Runge band systems", J. Quant. Spectrosc. Radiat. Transfer **48,** 1, pp. 9-24 (1992).

[Lau-93] C. O. Laux, „Optical diagnostics and radiative emission of air plasmas", PhD Thesis, Stanford University, Stanford (1993).

[Lei-00] F. Leipold, R. H. Stark, A. El-Habachi, K. H. Schoenbach, „Electron density measurements in an atmospheric pressure air plasma by means of infrared heterodyne interferometry", J. Phys. D: Appl. Phys. **33**, pp. 1-6 (2000).

[Lie-94] M. A. Lieberman, A. J. Lichtenberg, „Principles of plasma discahrges and materials processing", John Wiley & Sons, New York (1994).

[Lit-54] P. F. Little, A. von Engel, "The hollow cathode effect and the theory of glow discharges", Proc. Roy. Soc. A **224**, pp. 209-227 (1954).

[Lof-77] A. Lofthus, P. H. Krupenie, "The spectrum of molecular nitrogen". J. Phys. Chem. Ref. Data **6**, 1, pp. 113-307 (1977).

[Mas-98] F. Massines, A. Rabehi, P. Decomps, R. B. Gadri, P. Segur, C. Mayoux, "Experimental and theoretical study of a glow discharge at atmospheric pressure controlled by dielectric barrier", J. Appl. Phys. **83**, pp. 2950-2957 (1998).

[Mik-01] http://www.mikroglas.com

[Mil-99] M. Mildner, D. Korzec, J. Engemann, "13.56 MHz hollow cathode jet matrix plasma source for large area surface coating", Surface and Coatings Technol. **112**, pp. 366-372 (1999).

[Mit-71] A. Mitchell, M. Zemansky, „*Resonance Radiation and Excited Atoms"*, Cambridge University Press, pp. 95-96 (1971).

[Mos-01] M. Moselhy, R. H. Stark, K. H. Schoenbach, U. Kogelschatz, „Resonant energy transfer from argon dimers to atomic oxygen in micro hollow cathode discharges", Appl. Phys. Lett. **78**, 7, pp. 880-882 (2001).

[Mou-87] P.S. Moussounda, P. Ranson, “Pressure broadening of argon lines emitted by a high pressure microwave discharge (Surfatron)”, J. Phys. B: At. Mol. Phys **20**, pp. 946-961 (1987).

[Mus-62] T. Musha, “Cathode sputtering in hollow cathode discharges”, J. Phys. Soc. Japan **17**, pp. 1440-1446 (1962).

[Oka-93] S. Okazaki, M. Kogoma, M. Uehara, Y. Kimura, “Appearance of stable glow discharge in air, argon, oxygen and nitrogen at atmospheric pressure using a 50 Hz source”, J. Phys. D: Appl. Phys. **26**, pp. 889-892, 1993.

[Oed-88] A. Oed, „ Position-sensitive detectors with microstrip anode for electron multiplication with gases“, Nucl. Instr. Meth. A **236**, pp. 263-266 (1988).

[Pan-98] S. V. Pancheshnyi, S. M. Starikovskaia, A. Yu. Starikovskii, „Measurements of rate constants of the $N_2(C^3\Pi_u$ , v’ = 0) and $N_2^+(B^2\Sigma_u^+$, v’ = 0) deactivation by $N_2$, $O_2$, $H_2$, CO and $H_2O$ molecules in afterglow of the nanosecond discharge”, Chem. Phys. Lett. **294**, pp. 523-527 (1998).

[Pen-00] C. Penache, A. Bräuning-Demian, L. Spielberger, and H. Schmidt-Böcking, “Experimental study of high pressure glow discharges based on MSE arrays “, Proc. of Hakone VII, Greifswald, **2**, pp. 501-505 (2000).

[Pen-01] C. Penache, L. Spielberger, A. Bräuning-Demian, D. Penache, O. Hohn, H. Schmidt-Böcking, “Optical investigations of high pressure glow discharges based on MSE arrays”, Proc. of the APP Spring Meeting “Diagnostics of Non-Equilibrium High Pressure Plasmas”, Bad Honnef, pp. 151-154 (2001).

[Pet-97] G. M. Petrov, C. M. Ferreira, “Numerical modeling of Ar glow discharge at intermediate and high pressures”, Int. Rep. CFP 10/97, Lisbon Technical University (1997).

[Pet-01] I. Petzenhauser, U. Ernst, W. Hartmann, K. Frank, “Spectroscopic investigations of high-pressure microhollow cathode discharges”, Proc. of the APP Spring Meeting “Diagnostics of Non-Equilibrium High Pressure Plasmas”, Bad Honnef, pp.217-220 (2001).

[Pou-82] J. M. Pouvesle, A. Bouchoule, J. Stevefelt, "Modeling of the charge transfer afterglow excited by intense electrical discharges in high pressure helium nitrogen mixtures", J. Chem. Phys. 77, 2, pp. 817-825 (1982).

[Ptb-88] Physikalisch Technische Bundesanstalt, calibration certificate 3001 PTB 88 (1988).

[Rai-97] Yu. P. Raizer, „*Gas discharge physics"*, Springer Verlag, Berlin (1997).

[Rho-84] C. K. Rhodes, *"Excimer lasers"*, Springer Verlag, Berlin (1984).

[Rom-75] R. Rompe, M. Steenbeck, *"Progress in plasmas and gas electronics"*, Akademie Verlag, Berlin (1975).

[Rot-95] J. Reece Roth, *"Industrial plasma engineering: Principles"*, Institute of Physics Publishing, Philadelphia (1995).

[Rot-98] M. Roth, T. Haas, M. Lock, K.-H. Gericke, A. Bräuning-Demian, L. Spielberger, H. Schmidt-Böcking, "Electrically steerable catalysts for chemical reactions in the gas phase", Proc. of 1st Int. Conf. on Microreaction Technology, Springer Verlag, Berlin, pp. 62-69 (1998).

[Rot-01] J. Reece Roth, "*Industrial plasma engineering: Applications to nonthermal plasma processing"*, Institute of Physics Publishing, Bristol (2001).

[Rou-93] F. Roux, F. Michand, M. Vervloet, "High-resolution Fourier spectrometry of $^{14}N_2$; violet emission spectrum: extensive analysis of the $C^3\Pi_u \rightarrow B^3\Pi_g$ system", J. of Mol. Spectrosc. **158**, pp. 270-277 (1993).

[Sau-96] F. Sauli, „ GEM-A new concept for electron amplification in gas detectors", Nucl. Instr. Meth. A **386**, pp. 531-534 (1996).

[Sch-90] G. Schaefer, K. H. Schoenbach, „Basic mechanisms contributing to the hollow cathode effect", *Physics and Applications of Pseudosparks*, Plenum Press, New York, pp. 55-76 (1990).

[Sch-00] K. H. Schoenbach, A. El-Habachi, M. M. Moselhy, W. Shi, R. H. Stark, "Microhollow cathode discharge excimer lamps", Phys. of Plasmas **7**, 5, pp. 2186-2191 (2000)

[Sch-01] P. Scheffler, "Mikroelektroden-Arrays als nicht termische Plasmaquelle für einen weiten Druckbereich bis 1000 mbar", PhD Thesis, Technischen Universität Carolo-Wilhemina, Braunschweig (2001).

[See-98] R. Seeböck, H. Esrom, " Surface modification of polyimide with dielectric barrier discharges and with dielectric barrier discharge driven excimer UV lamps", Proc. of Hakone VI, Cork, **2**, pp. 270-275 (1998).

[See-00] R. Seeböck, H. Esrom, M. Charbonnier, M. Romand, U. Kogelschatz, "Mechanisms of polyimide surface modification by direct exposure to barrier discharges", Proc. of Hakone VII, Greifswald, **2**, pp. 455-459 (2000).

[Set-01] D. W. Setser, "Quenching reactions of electronically excited atoms", Proc. of the APP Spring Meeting "Diagnostics of Non-Equilibrium High Pressure Plasmas", Bad Honnef, pp. 49-60 (2001).

[Sil-92] J. A. Silver, "Frequency-modulation spectroscopy for trace species detection: theory and comparison among experimental methods", Appl. Opt. **31**, pp. 707-717, 1992

[Smi-81] D. Smith, N. G. Adams, "Charge transfer reaction $Ar^+ + N_2 \leftrightarrow N_2^+ + Ar$ at thermal energies", Phys. Rev. A **23**, 5, pp. 2327-2330 (1981).

[Smi-99] P.L. Smith, C. Heise, J.R. Esmond, R.L. Kurucz, "Atomic spectral line database from CD-Rom 23 of R.L. Kurucz", http://cfa-www.harvard.edu/amdata/.

[Spi-62] L. Spitzer Jr., *„Physics of fully ionized plasmas"*, 2nd. Ed., Willey Interscience, New York (1962).

[Spi-97] L. Spielberger, A. Bräuning-Demian, C. Penache, P. Scheffler, M. Roth, K.-H. Gericke, H. Schmidt-Böcking, "Nutzung der Mikrostruktur-Elektroden (MSE) – Flächenplasmaquelle bei Atmosphärendruck", IKF Annual Report, p. 65 (1997).

[Sta-98] R. H. Stark, K. H. Schoenbach, „Direct current high-pressure glow discharges", J. Appl. Phys. **85**, 4, pp. 2075-2080 (1998).

[Ste-85] J. I. Steinfeld, *„Molecules and radiation: An introduction to modern molecular spectroscopy"*, 2nd Ed., MIT Press, Cambridge (1985).

[Stu-67] D. J. Sturges, H. J. Oskam, „A qualitative theory of the medium pressure hollow cathode effect", Physica **37**, pp. 457-466 (1967).

[Tac-82] K. Tachibana, H. Harima, Y. Urano, "Measurements of collisional broadening and the shift of argon spectral lines using a tunable diode laser", J. Phys. B: At. Mol. Phys **15**, pp. 3169-3178 (1982).

[Ten-01] http://www.tencor.com

[Whi-59] A. D. White, "New hollow cathode glow discharge", J. Appl. Phys **30**, pp. 711-719 (1959).

[Wie-91] C. Wieman, L. Hollberg, "Using diode lasers for atomic physics", Rev. Sci. Instruments **62**, 1, pp. 1-19 (1991).

[Yar-76] A. Yariv, "Introduction to Optical Electronics", Holt, Rhinehart and Winston, New York (1976).

[Yok-90] T. Yokoyama, M. Kogoma, T. Moriwaki, S. Okazaki, "The mechanism of the stabilization of glow plasma at atmospheric pressure", J. Phys. D: Appl. Phys. **23**, pp. 1125-1128 (1990).

[Zig-01] http://www.zygo.com

[Zyb-97] A. Zybin, K. Niemax, "Improvement of the wavelength tunability of the etalon-type laser diodes and mode recognition and stabilization in diode laser spectrometers", Spectrochimica Acta **B52**, pp. 1215-1221 (1998).

# ACKNOWLEDGEMENTS

I would like to express my thanks to all the people who more or less contributed to this work, in a direct or indirect way.

I am indebted to my supervisor Prof. Dr. Horst Schmidt-Böcking who had offered me the opportunity to start this thesis on such an interesting subject. His enthusiasm, his brilliant ideas (even if not always quite easy to be applied) and his unlimited energy would motivate even a stone.

My very special thanks are addressed to Prof. Dr. Karl-Heinz Gericke from Technische Universität Braunschweig for spontaneously accepting to review my work and for offering me precious advice.

Then, I would like to thank to my former colleagues Dr. Angela Bräuning-Demian from Gesellschaft für Schwerionenforschung GmbH, Darmstadt and Dr. Lutz Spielberger from Gesellschaft für Technische Zusammenarbeit GmbH, Eschborn for the fruitful discussions and the good and friendly work atmosphere.

As part of the experiments was done in other institutes, I am sincerely thanking to all the people who kindly offered me support. Especially, I would like to thank to Dr. Manuela Miclea from Institute for Spectrochemistry and Applied Spectroscopy, Dortmund, to Dr. Uwe Ernst from Universität Erlangen-Nürnberg and to Dr. Saswati Datta from The Procter & Gamble Company, West Chester, Ohio. Also I am thanking to Prof. Dr. Klaus Wiesemann, Dr. Nikita Bibinov and Dr. Alexander Fateev from Ruhr-University Bochum and Dr. Cordula Geßner from Technische Universität Braunschweig.

I am thankful to all my colleagues from the HBS group in Frankfurt for fruitful discussions and teamwork during these years. I do not give names because all of them helped me more or less directly. My thanks are addressed as well to the mechanical and electrical workshop crew, especially Mr. Erich Zanger, to the accelerator crew, especially Mr. Karl Schneider and target laboratory, especially Dr. Mathias Waldschmidt for technical support. Also I am thanking to Ms. Claudia Freudenberger and to the library and administration crew for their permanent support.

Last but not least I am thanking to my family, especially to my husband Dan Penache.

## Lebenslauf

| | |
|---|---|
| Name: | Penache, geb. Zoran |
| Vorname: | Maria Cristina |
| Geburtsdatum: | 18 Mai 1972 |
| Geburtsort: | Bukarest, Rumänien |
| Nationalität: | rumänisch |
| Eltern | Valeriu Iuliu Zoran, gest. 1997 |
| | Maria Zoran, geb. Dida |
| Familienstand: | verheiratet |

| | |
|---|---|
| 1978 - 1982: | Besuch der Dimitrie Bolintineanu Grundschule, Bukarest, Rumänien |
| 1982 - 1986: | Besuch des Gymnasiums Nr.141, Bukarest, Rumänien |
| 1986 - 1990: | Besuch des Gymnasiums für Mathematik und Physik Nr.4, Bukarest, Rumänien |
| Juni 1990: | Abitur |
| 1990 - 1995: | Studium der Physik an der Universität Bukarest, Rumänien |
| Juli 1995: | Lizenzdiplom |
| 1995 - 1997: | Wissenschaftliche Angestellte am National Institute for Laser, Plasma and Radiation Physics, Bukarest, Rumänien |
| 1997 - 1998: | Weiterbildung (DEA für Plasmaphysik) und Forschungs-Aufenthalt an der Universität Paris-Sud, Orsay, Frankreich |
| August 1998: | Aufnahme als Doktorandin am Institut für Kernphysik der Johann Wolfgang Goethe Universität, Frankfurt am Main |
| März 2002: | Termin der Disputation. |